

Technische Universität München
Institut für Energietechnik

Lehrstuhl für Thermodynamik

Performance Improvements of Humidification-Dehumidification Desalination Systems with Natural Convection

Burkhard Sebastian Seifert

Vollständiger Abdruck der von der Fakultät für Maschinenwesen der
Technischen Universität München zur Erlangung des akademischen Grades
eines

DOKTOR – INGENIEURS

genehmigten Dissertation.

Vorsitzender:

Prof. Dr.-Ing. Harald Klein

Prüfer der Dissertation:

1. Prof. Dr.-Ing. Thomas Sattelmayer
2. Prof. Dr. Philip A. Davies

Die Dissertation wurde am 02.05.2017 bei der Technischen Universität München eingereicht
und durch die Fakultät für Maschinenwesen am 24.07.2017 angenommen.

Acknowledgements

This thesis is the result of my work on humidification-dehumidification for sea water desalination done as research assistant at the Institute for Thermodynamics of the Technische Universität München, Germany.

I would like to thank Professor Dr.-Ing. Thomas Sattelmayer for giving me the opportunity to work on this fascinating topic. I thank him for the scientific supervision of this work, for his guidance and support. I thank Dr. Philip Davies, co-examiner of this thesis, for his support.

I owe a special debt of gratitude to Dr.-Ing. Markus Spinnler who initiated this research activity. I had the opportunity to work with him on lectures and tutorials in the area of solar engineering and desalination. He introduced me to the topic of desalination which has fascinated me ever since. I thank him for his support, advice and friendship.

My thanks go to my colleagues, especially Dr.-Ing. Abdel Hassabou with whom I had countless discussions on desalination. I want to thank Dipl.-Ing. Alexander Kroiss for the support during my last year as research assistant. I also send my gratitude to all students who completed their Bachelor or Master thesis under my supervision. My special thanks go to Dipl.-Ing. Cathy Frantz, Dipl.-Ing. Petra Dotzauer and Dipl.-Ing. Konstantin von Bischoffshausen. They have supported me greatly, especially with their work done during field tests and experimental investigations.

My parents and family have continuously supported me. I can't thank them enough. My deepest thanks go to my wife Andra. I thank her for her understanding, support and encouragement.

Adelaide, October 2016

Burkhard S. Seifert

Abstract

Humidification-dehumidification (HD) is a promising technology for small to medium sized desalination systems. It operates at low temperatures which makes it ideal to be powered by solar energy. HD systems applying natural convection require fewer components but seem to have limited performance. The main purpose of the presented work is to describe analytical and experimental methods to analyse these limitations and to systematically investigate potential measures to improve the performance of HD systems.

Two measures are part of the investigations: increasing the feed water inlet temperature by recovering heat from the exiting brine flow, and splitting the single-stage HD system into a two-stage setup.

A numerical model for the dimensioning and analysis of the system is developed to determine heat and mass transfer along the height of the humidifier and dehumidifier. This model forms the basis for the analysis of system performance. Results from experiments with a single-stage and two-stage configuration are evaluated. As dropwise condensation occurs in the applied experimental setup, an explanation for this surprising phenomenon is given and an adequate approach for the numerical model is introduced.

The application of the conventional performance ratio PR can result in misleading conclusions due to large measurement errors accruing when measuring the condensate mass flow of the relatively small HD system. Therefore, an adapted performance ratio PR_{HD} is introduced, which requires only temperature differences of the feed water flow. This leads to a sufficiently accurate and fast determination of the system performance. It is observed that the applied measures to improve the performance are not effective.

Limitations and opportunities to enhance the performance ratio are identified by means of combining numerical analysis, experiments and graphical visualization. With this concept the inherent disadvantage of natural convection is explained, resulting mainly from its inability to sufficiently adjust the gas flow rate along the height of the humidifier and the dehumidifier.

Contents

1	Overview	1
1.1	Introduction	1
1.2	Process Principles Humidification-Dehumidification	2
1.3	Objectives and Outline	5
2	Literature Overview	7
2.1	System Classifications	7
2.2	System Configurations	8
2.2.1	Closed-Air HD	8
2.2.2	Open-Air HD	12
2.3	Operation Modes	13
2.4	Energy Supply Modes	14
2.5	Improved Configurations	15
2.5.1	Air Extraction	15
2.5.2	Water Extraction	16
2.5.3	Multi-Staging	16
3	HD Processes	19
3.1	Humidification Process	19
3.1.1	Separation Process	19
3.1.2	Partial Pressure and Concentration Differences	20
3.1.3	Boiling Point Elevation	20
3.1.4	HD as Quasi-Multi-Pressure Configuration	21
3.2	Dehumidification Process	22
3.2.1	Principles of Condensation	23
3.2.2	Conditions for Film and Dropwise Condensation	26
3.2.3	Multi-Effect Energy Recovery and Performance Ratio	27

3.3	Natural Convection	28
3.3.1	General Remarks	29
3.3.2	Natural Convection in Closed-Air HD Systems	29
3.3.3	Driving Pressure Difference in Closed Air Loop in HD	30
3.3.4	Pressure Drop	32
4	Mathematical Modeling	35
4.1	Overview	35
4.2	Assumptions	35
4.3	Modeling of the Humidifier	36
4.3.1	Energy and Mass Balances	38
4.3.2	Determination of the Interface Temperature	41
4.3.3	Operating Line	44
4.4	Modeling of the Dehumidifier	46
4.4.1	Energy and Mass Balances	46
4.4.2	Differential Heat and Mass Balances	48
4.4.3	Replacement Film Thickness for Dropwise Condensation	50
4.5	Visualization of Heat and Mass Transfer Relations	54
4.5.1	Tie Line	54
4.5.2	Number of Transfer Units and Height of Transfer Unit	56
5	Experimental Investigations	61
5.1	Experimental Setup	61
5.1.1	Single and Two-Stage Configuration	61
5.1.2	External Heater	65
5.1.3	Humidifier	66
5.1.4	Dehumidifier	70
5.2	Measurement and Control	71
5.2.1	Temperature Measurement	71
5.2.2	Condensate Mass Flow Rate Measurement	72
5.2.3	System Control	73
5.3	Experimental Results and Observations	74
5.3.1	Dropwise Condensation	74
5.3.2	Data Transient and Steady-State Phases	77
5.3.3	Results from Experiments Steady-State Phase	82

6 Analysis	83
6.1 Adapted Performance Ratio PR_{HD}	83
6.1.1 Internally Transferred Heat Flow	84
6.1.2 Definition Adapted Performance Ratio PR_{HD}	85
6.1.3 Comparison PR and PR_{HD}	86
6.2 Application Performance Ratio PR_{HD}	87
6.3 Application Operating Lines	89
6.3.1 Generation of Operating Lines	89
6.3.2 Operating Lines for Single-Stage and Two-Stage HD . . .	90
6.3.3 Number of Transfer Units and Height of one Transfer Unit	96
6.4 Summary	99
7 Conclusions	103
Bibliography	105
List of Figures	113
Appendix	117
A Performance Ratio versus Gained Output Ratio	118
B Experimental Equipment	119
C Heat and Unidirectional Mass Transfer	120
C.1 Dimensionless Numbers	122
C.2 Lewis Factor for Unidirectional Transport	123
C.3 Correlations for β , β_u and σ_{evap}	124

Contents

Nomenclature

Latin Letters

A	exchange surface area for heat and mass transfer	m^2
a	thermal diffusivity	m^2/s
a	specific surface area	m^2/m^3
a^*	specific effective surface area	m^2/m^3
c	molar concentration	mol/m^3
c_p	specific heat capacity at constant pressure	$J/(kg \cdot K)$
\dot{C}_p	heat capacity flow rate	$J/(K \cdot s)$
D	diffusion coefficient	m^2/s
d	diameter	m
d_{pack}	characteristic diameter of packing element	m
E_T	Ackermann correction factor	-
\dot{G}	mass flow rate of carrier gas, i.e. dry air	kg/s
g	gravitational acceleration	m/s^2
\dot{H}	enthalpy flow rate	J/s
h	specific enthalpy	J/kg
h_A	specific enthalpy humid air related to dry air content	J/kg
Δh_v	heat of vaporization of water	J/kg
HTU_G	height of one transfer unit (gas phase)	m
\dot{L}	feed water mass flow rate	kg/s
l	characteristic length	m
K	wall factor	-
M	mass	kg
\dot{M}	mass flow rate	kg/s

Nomenclature

\tilde{M}	molar mass	kg/kmol
\dot{m}	mass flow density; mass flux	kg/(m ² · s)
N	number of tube rows, stages or trays	-
n	number tubes per row	-
\dot{n}	molar mass flow density	mol/(m ² · s)
P	power	W
p	pressure	N/m ²
\dot{Q}	heat flow rate	W
\dot{q}	heat flow density; heat flux	W/m ²
\tilde{R}	universal gas constant	kJ/(kmol · K)
S	salinity	kg/kg
s	specific entropy	J/(kg · K)
s	saturation ratio	-
T	absolute temperature	K
t	Celsius temperature	°C
u	velocity	m/s
V	volume	m ³
v	specific volume	m ³ /kg
X	absolute humidity (related to dry air mass)	kg/kg
y	y-coordinate	m
Z	total height of column	m
z	height (z-direction, vertical coordinate)	m

Greek Letters

α	heat transfer coefficient	$W/(m^2 \cdot K)$
β	mass transfer coefficient	m/s
β_u	unidirectional mass transfer coefficient	m/s
δ	thickness	m
ϵ	effectivity	-
ϵ	void fraction (relative free volume)	m^3/m^3
Θ	contact angle	rad
λ	thermal conductivity	$W/(m \cdot K)$
μ	dynamic viscosity	$kg/(m \cdot s)$
ν	kinematic viscosity	m^2/s
ξ	pressure loss coefficient	-
ρ	density	kg/m^3
$\tilde{\rho}$	molar density	$kmol/m^3$
σ_{evap}	evaporation coefficient	$kg/(m^2 \cdot s)$
σ	surface tension	N/m
τ	time	s
φ	relative humidity	%
ψ	resistance coefficient	-

Constants

g	gravitational acceleration	$9.81 m/s^2$
$\Delta h_{v,0}$	heat of vaporization of water at $0.01^\circ C$	$2500.9 kJ/kg$
$\Delta h_{v,PR}$	heat of vaporization defined for PR	$1000 BTU/lb$
\tilde{M}_W	molecular weight of water	$18.0153 kg/kmol$
\tilde{M}_G	molecular weight of dry air	$28.9654 kg/kmol$
\tilde{R}	universal gas constant	$8.314 kJ/(kmol \cdot K)$
R_W	gas constant of water vapor	$0.4615 kJ/(kg \cdot K)$
R_G	gas constant dry air	$0.2870 kJ/(kg \cdot K)$
σ	Stefan-Boltzmann constant	$5.67 \cdot 10^{-8} W/(m^2 \cdot K^4)$

Indices

1	dehumidifier bottom	L	liquid
2	dehumidifier top	loss	heat losses
3	humidifier top	MU	make-up water
4	humidifier bottom	m	mean
A	humid air	out	outlet; output
bot	bottom of column	pack	packing
comp	comparisons	pd	pressure drop
Cond	condensate	Rec	recycling water
col	collector	repl	replacement
cross	cross section	S	surface; solid
d	droplet	sat	saturation condition
deh	dehumidifier	stat	static
evap	evaporation	Steam	heating steam
ext	external	top	top of column
f	free cross section	total	total
G	carrier gas (dry air)	u	unidirectional
grav	gravitational	v	vaporization
hum	humidifier	V	water vapor
I	at interface	W	(saline) water
i	component i in mixture	α	heat transfer related
in	inlet; input	β	mass transfer related
int	internal	∞	in bulk; ambient air

Dimensionless Numbers

Gr	Grashof number	$Gr = \Delta\rho \cdot l^3 \cdot g / (\rho \cdot \nu^2)$
GOR	gained output ratio	$GOR = \dot{M}_{\text{Cond}} / \dot{M}_{\text{Steam}}$
Le	Lewis number	$Le = \lambda / (\rho \cdot c_p \cdot D) = a / D$
Le_f	Lewis factor	$Le_f = \alpha / (\sigma \cdot c_p)$
Me	Merkel number	$Me = \sigma \cdot A / \dot{G}$
Nu	Nusselt number	$Nu = \alpha \cdot l / \lambda$
NTU_G	number of transfer units (gas)	$NTU_G = \sigma \cdot A / \dot{G}$
PR	performance ratio	$PR = \dot{M}_{\text{Cond}} \cdot \Delta h_{v,PR} / \dot{Q}_{\text{ext}}$
PR_{HD}	performance ratio for HD	$PR_{\text{HD}} = \dot{H}_{\text{int}} / \dot{Q}_{\text{ext}}$
Pr	Prandtl number	$Pr = c_p \cdot \eta / \lambda = \nu / a$
Re	Reynolds number	$Re = u \cdot l / \nu$
Re_{pack}	Reynolds number for packing	$Re_{\text{pack}} = u_A \cdot d_{\text{pack}} \cdot K / (\nu_A \cdot (1 - \epsilon_{\text{pack}}))$
Sc	Schmidt number	$Sc = \nu / D$
Sh	Sherwood number	$Sh = \beta \cdot l / D$
Z	compressibility factor	$Z = p_i / (\rho_i \cdot R_i \cdot T)$

Abbreviations

AH	air-heated
BPE	boiling point elevation
CA	closed-air
HD	humidification-dehumidification
MED	multi-effect distillation
MSF	multi-stage flash
NCG	non-condensable gases
OA	open-air
OW	open-water
TAT	top air temperature
TBT	top brine temperature
WH	water-heated

1 Overview

1.1 Introduction

Access to drinking water is one of the biggest challenges for civilization today. Population growth, urbanization, climate change and their subsequent effects increase the pressure on water supply in many regions of the world. According to the Human Development Report 2015 (UNDP), more than 660 million people rely on "an unimproved source of drinking water" [51]. Availability and quality of water sources vary locally which require a multitude of endeavours for the provision of fresh water. A promising approach is sea water and brackish water desalination. An overview of large and small scale desalination technologies is given [14, 20, 52, 77].

One method of producing fresh water is to evaporate water from saline water and to condense the produced water vapor. This thermal process has been used in solar stills for centuries and continues to be used today to produce fresh water [96]. Talbert *et al.* [95] describe the developments of solar stills up until the 1970s in their extensive report. The evolution of solar stills paved the way for humidification-dehumidification (HD)¹ technology. This can be seen from a historical overview of the development of HD [90].

Humidification-dehumidification is a thermal separation technology, preferably used for the production of condensate from sea water or brackish water, commonly applied on a small scale. For industrial applications, e.g. in the oil and gas industry, HD technology is applicable for the concentration of process liquids.

The preferred energy source for HD is renewable energy, such as solar thermal or geothermal [70]. Also, 'waste heat' released from thermal processes can be used as the operational temperature level of HD systems is low.

¹In literature, this technology is also referred to as humidification-dehumidification HDH, humidification-dehumidification desalination HDD [73] or multi-effect humidification-dehumidification method MEH [32, 50, 71].

1.2 Process Principles Humidification-Dehumidification

HD systems consist of three essential components, namely humidifier, dehumidifier and external heater. Fig. 1.1 depicts these components for a closed-air configuration together with the water flow and the humid air flow. Air as the carrier gas circulates within the humidifier-dehumidifier setup. In case of natural convection the air flow is driven by gravitational forces from density differences. This thesis focuses on this HD configuration with natural convection.

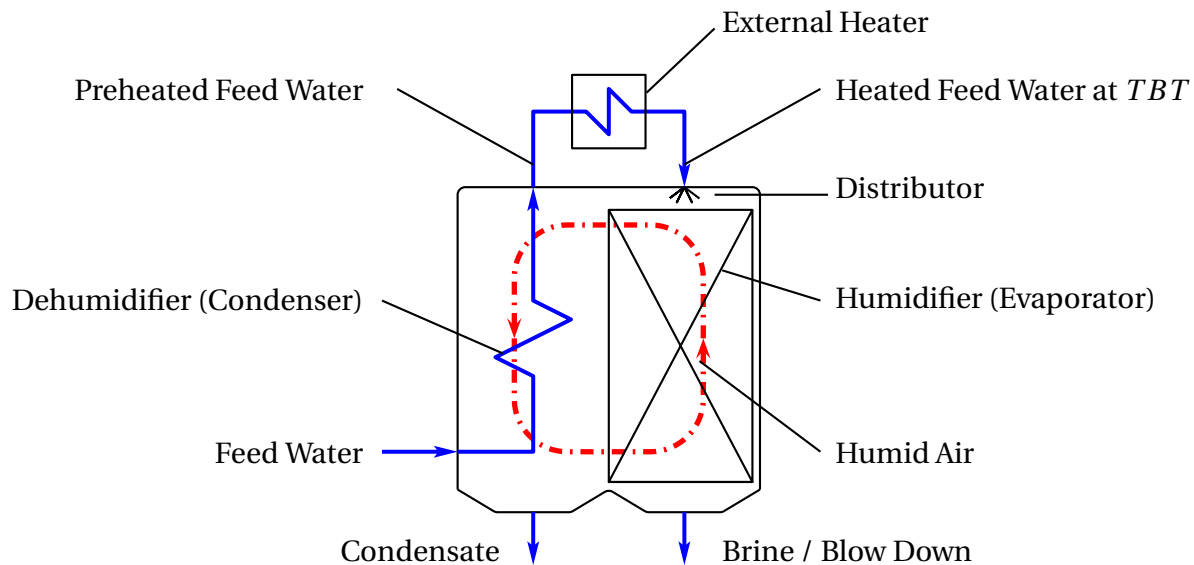


Figure 1.1: Schematic Setup of a Closed-Air Water-Heated (CA-WH) HD System

Hot saline water moves downwards in a packed column of the humidifier due to gravitation. In the humidifier the sensible heat of the down flowing water is used to evaporate (typically about three to eight percent) pure water and to heat the humid air. The heated and humidified air² enters the dehumidifier where pure water condenses on the heat exchanging surfaces. The released condensation enthalpy of the vapor (and to a small extent sensible heat of the air and the condensate) preheats the feed water, which passes the heat exchanger. The preheated feed water leaves the dehumidifier and is heated

² Each component within the feed water with a significant vapor pressure will be present in the generated vapor. As salt or other minerals have no significant vapor pressure, pure water vapor is produced when seawater is desalinated.

further in the external heater to the top brine temperature (TBT). The heated water is spread onto the packed column of the humidifier whilst the cooled and dehumidified air from the dehumidifier enters the humidifier. For natural convection, the air flow is driven by the density difference resulting from temperature and humidity differences. In forced convection systems, the air flow is enhanced by mechanical ventilation.

For steady-state conditions, i.e. conditions not depending on time, the condensate flow \dot{M}_{Cond} is a function of the constant mass flow \dot{G} of dry air and the difference in absolute humidity $X = M_W / M_G$ of the air at the air inlet (top) and outlet (bottom) of the dehumidifier:

$$\dot{M}_{\text{Cond}} = \dot{G} \cdot (X_{\text{in}} - X_{\text{out}}). \quad (1.1)$$

The partial pressure $p_{V,\text{sat}}$ of water vapor in saturated air and the corresponding absolute humidity X_{sat} of saturated humid air at temperature t at total pressure p increase significantly with increasing temperature [3, p. 292]:

$$X_{\text{sat}}(t, p) = \frac{M_{V,\text{sat}}}{M_G} = \frac{R_G}{R_W} \cdot \frac{p_{V,\text{sat}}(t)}{p - p_{V,\text{sat}}(t)}. \quad (1.2)$$

This sets the basis for the working principle of HD systems. Fig. 1.2 shows the absolute humidity X as a function of the temperature t_A for varying relative humidity values $\varphi = p_V(t_A) / p_{\text{sat}}(t_A)$. The density of saturated humid air ρ_A depends on the absolute temperature T , the partial pressure p_V , respectively the absolute humidity X , and the total static pressure p [35, p. 161]:

$$\rho_A(T, p, X) = \frac{M_A}{V} = \frac{p}{R_G \cdot T} - \left(\frac{1}{R_G} - \frac{1}{R_W} \right) \cdot \frac{p_V}{T} = \frac{p}{T} \cdot \frac{1 + X}{R_G + R_W \cdot X}. \quad (1.3)$$

The density difference results in a pressure difference Δp between the bottom and the top of a HD system. Further explanation of the driving pressure differences is given in chapter 3.3. The described working principle is also applicable for carrier gases other than air (e.g. helium as proposed by [75]) and liquids other than sea water (e.g. alkaline solutions).

However, for gases with $R_G > R_W$, as it is the case for helium, it has to be considered that the density increases with increasing vapor pressure, as evident from Eq. (1.3).

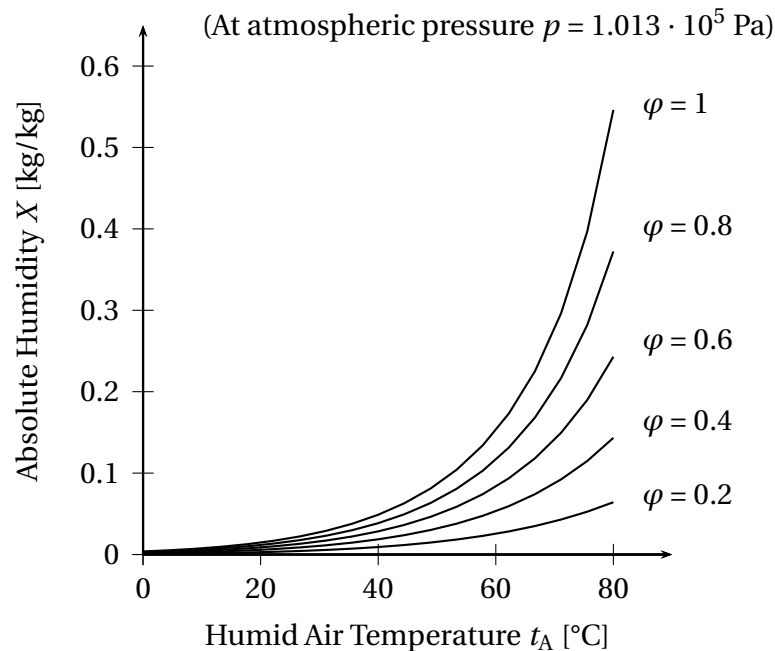


Figure 1.2: $t_A - X$ Diagram of Humid Air for Various Relative Humidity φ Values

The technical term ‘distillation’ respectively ‘distillate’, in relation to the humidification-dehumidification³ process is misleading: In a distillation process, the product component is vaporized and then condensed. In HD, the product component evaporates from the feed water (vaporization is not desired). Consequently, the term ‘condensate’ is used throughout this thesis when referring to the produced fresh water and not as ‘distillate’ as is commonly done. Being concise with these terms clearly differentiates HD from thermal desalination processes applying vaporization.

Low top brine temperatures (below 100 °C) and the operation of the system at ambient pressure (due to the presence of the inert carrier gas) permit the use of low cost materials. However, for the same reasons, heat and mass transfer within the system is low, resulting in large surface areas and space requirements. The aim of current and future developments is to reduce water production costs by improving process efficiency and optimizing system configurations.

³In German, HD is often referred to as ‘Feuchtluftdestillationsverfahren’. This directly translates to ‘humid air distillation process’. A more precise expression would be ‘Verdunstungs-Kondensations-Verfahren’ (evaporation-condensation process).

1.3 Objectives and Outline

The scope of this work is to analyse a closed-air water-heated HD system with natural convection using experimental and analytical investigations and to contribute towards the identification of its performance limitations. The following overview outlines the key findings of each chapter.

Chapter 1 introduces HD and describes the fundamental working principle and terminology of this technology. It appears that the condensation mass flow rate in HD systems with natural convection could be increased by increasing the mean humid air temperature within the dehumidifier.

Chapter 2 proposes an extended classification of HD technologies and relevant literature. Generally, low performance ratios are reported for systems with natural convection. Several improvement configurations proposed in the literature are mentioned. A common objective of these improvements is to adjust the ratio of feed water flow rate and air flow rate. For natural convection setups, this can be achieved with a multi-stage configuration, whereby the total humidifier and dehumidifier column height is segmented into several smaller systems. This method is further investigated in this work.

Chapter 3 describes the humidification and dehumidification processes and basic principles of natural convection. A focus is set on the physical characteristics within HD, such as uni-directional mass transfer. The dehumidification process covers indirect condensation in the presence of a carrier gas and the basics of film and dropwise condensation. Film condensation is commonly used to describe the dehumidification process in HD. Dropwise condensation is unexpectedly observed in the experiments; however, the very high heat transfer coefficients reported in literature cannot be achieved in HD due to the presence of non-condensable gases.

Chapter 4 summarizes the mathematical principles of the humidification and dehumidification process required for the 1-D numerical model. These relations are also essential to visualize heat and mass transfer, which are used to investigate the limitations of configurations with natural convection. The calculation of the interface temperature between humid air and water is of

special interest as it is a determining factor of the driving potential for heat and mass transfer.

Chapter 5 describes the experimental setups of the closed-air water-heated HD configurations. The experimental configurations were adapted and continuously improved over time. This included several single-stage and two-stage setups. Investigations were undertaken in the laboratory and additionally in two field tests in Greece and Dubai using solar collectors. They proved that the chosen control strategy results in an adequate performance. The developed and tested control method for the water flow is described. The advantages for transient heat input are presented, which is of particular interest for solar powered systems. The experimental investigations of the dehumidification process of humid air showed that dropwise condensation continuously occurs on the plastic heat exchanger. A simplified approach for the highly complex dropwise condensation process was established for HD to describe the condensation process in the presence of non-condensable gases.

Chapter 6 analyses the results from the experimental and numerical investigations. Since literature demonstrates no consensus about a favoured optimization figure [30, 71, 93], an adapted performance ratio PR_{HD} is introduced which takes into account temperature differences. The efficiency of a HD system is determined more accurately compared to the methods usually applied for HD wherein condensate mass flow rates are needed, which have potentially significant measurement errors for small-scale systems. The influence of increased water inlet temperature on both single- and two-stage HD configuration with natural convection is investigated. Through combining experimental data with numerical simulation and visualizing heat and mass transfer relations it is possible to identify the limitations of natural convection setups and describe influential factors.

Chapter 7 concludes that the HD system with natural convection has an advantageous system setup, but lacks an inherent ability to significantly increase the performance ratio. The described efforts to increase the performance show unsatisfactory results. This becomes apparent as soon as the more precise performance ratio PR_{HD} is applied. Based on these findings, measures to improve the performance of HD are recommended.

2 Literature Overview

This chapter proposes a HD classification and gives an overview of selected literature which is structured according to the classification.

2.1 System Classifications

HD systems configurations are usually classified by both air and water flow, whereby closed-air open-water (CAOW) and closed-water open-air (CWOA) configurations are commonly distinguished. Narayan [80] classified HD systems in three categories: energy source (e.g. solar or geothermal), cycle configuration (closed-water open-air and closed-air, both with natural or forced convection) and type of heating used (water and/or air heating).

Fig. 2.1 presents an extended classification for HD which diversifies its core elements: system configuration based on the air flow, operation mode and energy supply mode.

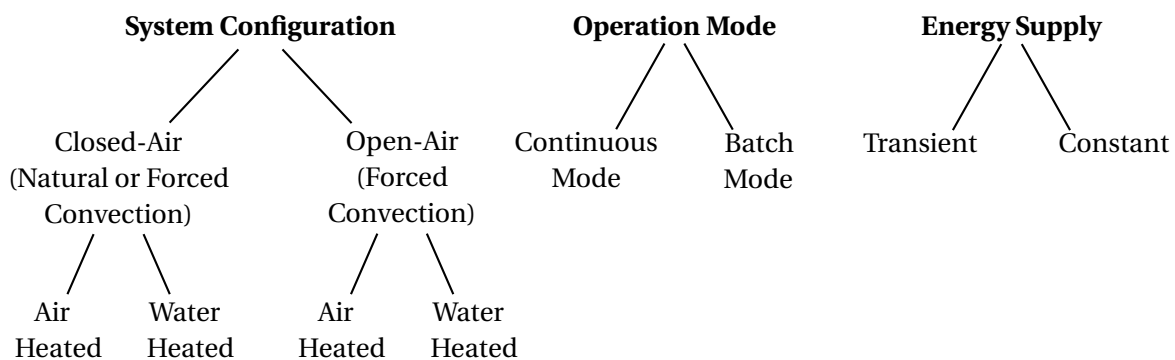


Figure 2.1: Proposed HD Classifications

The main distinction for system configurations is the air flow within the system: In a closed-air configuration (CA), humid air circulates in a closed loop where it is continuously humidified and dehumidified. In the open-air configuration (OA), air enters the system, is humidified and dehumidified and then leaves the system.

2.2 System Configurations

2.2.1 Closed-Air HD

Closed-air (CA) is the most common HD system configuration, presented in [39, 71, 80]. The air flow circulates through natural or forced convection. The external energy can be used to heat water (CAWH), air (CAAH) or both (CAWAH). Fig. 2.2 depicts the water (blue) and air flow (red) within a CAWH and a CAAH HD system.

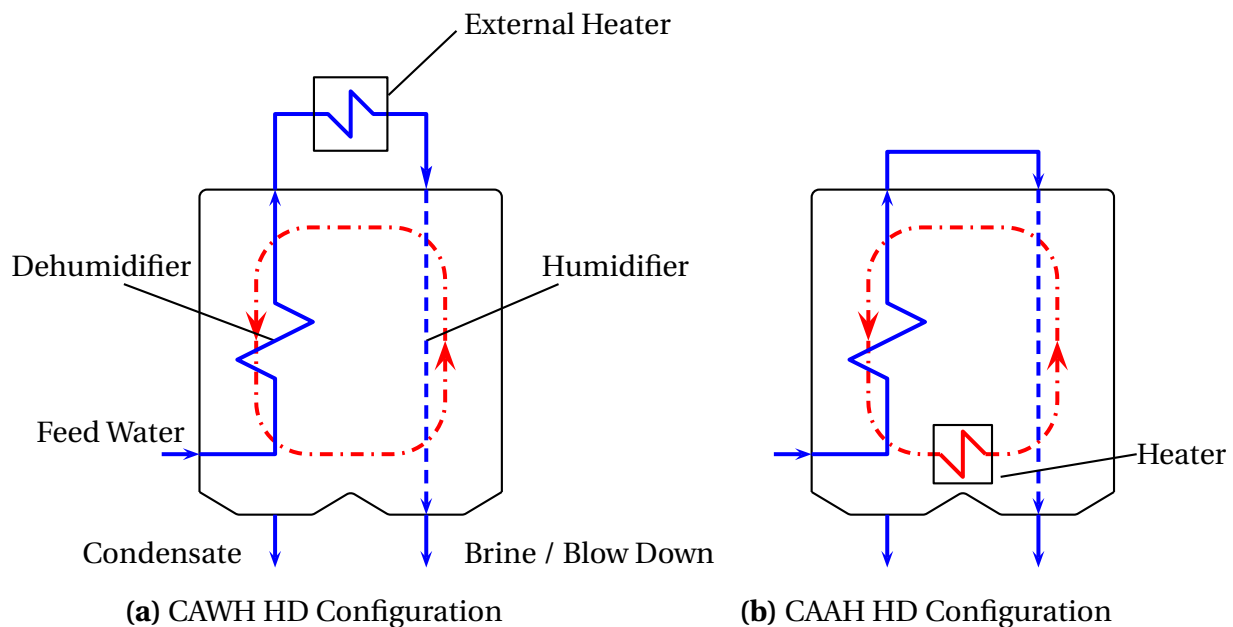


Figure 2.2: Closed-Air Water-Heated HD System Overview

Closed-Air Water-Heated (CAWH)

For water-heated (WH) configurations, the (saline) feed water is heated to top brine temperature (T_{BT}) of e.g. 85 °C using an external heater, after being preheated mainly by the heat of condensation in the dehumidifier. The top air temperature (T_{AT}) is obviously below T_{BT} e.g. 75 °C.

Müller-Holst [71] used natural convection flow for his investigations. He studied various possibilities to improve air flow, such as the removal of the separating wall between the humidifier and dehumidifier. He used TRNSYS[®] to model a closed-air water-heated HD system. Overall heat and

mass transfer equations were developed and validated with experiments for the characteristic water and air flow in a fleece humidifier and a flat plate dehumidifier. From the resulting data, an overall transfer coefficient was introduced which accounts for the heat transfer from the water in the humidifier to the water flowing in the dehumidifier. This simplification forms the basis for the numerical simulation tool.

Nawayseh *et al.* [83] described a simulation model with several simplifications to determine potentials for optimizations. They compared the results with experimental investigations from a closed-air water-heated HD configuration with natural and forced convection, described in [28]. In a subsequent publication [81], they used empirical heat and mass transfer correlations [39] and adjusted by correlations derived from experimental investigations.

Nawayseh and Farid [29, 82] used the previous findings to develop a simulation tool to investigate the influence of several parameters. They tested a closed-air HD unit with natural and forced convection and developed a calculation program to determine the performance of the desalination unit. The effect between the difference of air flow rate for natural or forced convection was found to be negligible. Investigations with constant energy input and constant air mass flow showed that increased feed water flow rates lowered the operating temperature in the solar collectors resulting in higher collector efficiencies but lower evaporation rates. Their model uses six equations derived from mass balances for the humidifier and dehumidifier and the external heater as well as equations for the heat and mass transfer, whereby logarithmic temperature and concentration differences are applied. According to the study, natural convection is preferred over forced convection. This conclusion is further investigated in chapter 4.5.2.

Al-Hallay [39] and Farid [28] continued the experimentation of Nawayseh [83] on natural and forced convection. They state that forced convection is optimal for low top brine temperatures (up to 50 °C) whereas a small performance increase was determined for natural convection for higher temperatures (70 °C and more). In a field test, two units were studied in Jordan and Malaysia [81]. A new design for the system in Malaysia included larger contact areas of both humidifier and dehumidifier, improving the productivity of the unit. It is men-

tioned that the effect of the air flow rate on the production rate is small. For this case it was concluded from experiments and numerical simulation that the water flow rate has greater influence on heat and mass transfer than the air flow rate.

In chapter 6 of this work, the influence of the mass flow ratios of water and air are analysed in detail. A HD system operated in forced convection can be equipped with a humidifier and dehumidifier with higher specific surface areas to compensate the pressure drop. As this is not possible in setups with natural convection, comparisons of natural and forced convection systems should acknowledge the different heat transfer areas.

Narayan *et al.* [79] studied the overall energy and mass balances for the humidifier, the dehumidifier and the external heater along with estimated component effectiveness and relative humidity at the exit of each component. Several plant configurations were numerically studied with an assumed effectiveness for humidifier and dehumidifier. Numerous parameter studies demonstrated the influence of selected parameters on the plant performance. Parameter studies are limited to the investigation of only few variable parameters and a larger number of constant parameters at a time. Since the effectiveness of each component is strongly dependent on the operation conditions and operating transfer potentials, parameter studies have not been pursued for this work.

Soufari *et al.* [93] modeled a HD process using governing equations with several simplifications gaining a heat balance for the interface between water and air for the humidifier and dehumidifier. It was identified that the water to air mass flow ratio for a setup with forced convection reaches an optimum. The reasons for this behaviour for single-stage systems are investigated in chapters 6 and 7. The recycling of brine from the humidifier into the feed water of the dehumidifier is described as a method to reduce specific energy consumption.

Bacha *et al.* [1] modeled the heat and mass transfer equations for steady-state operation. Investigations for solar powered HD systems followed [2] whereby hot water is produced and stored during times with high solar irradiation to be used during night time. This concept has also been described by [46].

This method which aims to increase the total water output per day depends on the available solar collector area and heat storage capacity. It avoids the disadvantages of the transient phases during heat up. This effect is discussed in subsection 5.3.2.

Hou *et al.* [49] investigated the pinch point method to optimize a HD system with constant ratio between the water \dot{L} and air \dot{G} mass flow rate. As the pinch point method aims to minimise the driving temperature difference between water and saturated air, the required products of transfer surfaces and coefficients become very large. It is shown that even for this case, the ratio between the recovered enthalpy flow and the (externally) added heat flow is limited to small values. The described method is not suitable to describe a system for which the ratio \dot{L}/\dot{G} can be adjusted along the column height.

Hassabou [40] established a 1-D simulation model. The governing equations were solved with Matlab[®]. The impact of the heat conductivity on the humidifier and dehumidifier for closed-air water-heated configuration with forced convection and direct heat exchange in the dehumidifier was simulated.

Various works are reported on water heated systems with *TBT* in the range between 50 °C and 90 °C. From 50 °C to 70 °C e.g. by [39], 60 °C e.g. [58], between 70 °C and 80 °C e.g. by [81] or from 80 °C to 90 °C e.g. by [72]. The effect on the mass transfer for low operating top brine temperatures (35 °C and 45 °C) was investigated [25].

Closed-Air Air-Heated (CAAH)

Dehumidified air is heated with an external heater before entering the humidifier, see Fig. 2.2 (b). This process can be repeated in multiple stages, as suggested e.g. by Chafik *et al.* [12]. Heating air instead of feed water significantly reduces the scale formation and corrosion potential. The small heat transfer coefficient in the air-heater and the low heat capacity of air are disadvantageous, resulting in low condensate water production and large heat exchanger surfaces.

Closed-Air Water- and Air-Heated (CAWAH)

For this configuration both water and air are externally heated. Nafey *et al.* [74] investigated the productivity of HD configurations using external heaters for both air and water. They used the resulting data for the validation of a numerical model to obtain a correlation for different operating conditions. The increase of the water and air temperature also increases the production rate of the system. The statement that lower cooling temperatures and higher flow rates also result in higher productivities is only valid for the described configuration.

2.2.2 Open-Air HD

Open-air configurations require forced convection [12, 16, 17, 103]. Forced convection is also recommended for higher plant sizes, increased pressure drop and higher static pressure difference. This pressure drop is compensated with mechanical ventilation. Dai *et al.* [16] performed a parametric analysis to optimize the unit performance of an open-air cycle system. A mathematical model was presented. Flow rates, temperatures of feed water, air and cooling water were studied for the parametric analysis.

Open-Air Water-Heated (OAWH)

Khedr [55] and Dai *et al.* [17] conducted experiments with open-air water-heated HD configurations and analyzed system performance. Water vapor from a boiler was used as a heat source. Several experiments were performed to find an optimum air mass flow rate for the increased condensate output of 85 °C and 65 °C for a constant feed water mass flow \dot{L} . Dai *et al.* report the very low thermal efficiency¹ of 0.85.

Open-Air Air-Heated (OAAH)

An advantage of air-heated systems is that air temperatures can be significantly higher than in water-heated systems allowing higher humidity ratios.

¹ Thermal efficiency is equivalent to performance ration PR which is explained in chapter 3.2.3.

Kolb [60] states that using solar air collectors with a air inlet temperature of 30 °C, an outlet temperature of 80 °C can only be achieved for air mass flow densities as low as 0.01 kg/(m²·s). Due to heat loss, the efficiency for solar flat plate collectors decreases with higher operation temperatures. The efficiency of the collector can be as low as 20% for such high air temperatures.

2.3 Operation Modes

A HD plant can be operated in a continuous or batch mode of the water supply. In batch mode, the system is operated with a set feed water amount. Batches of feed water are processed from water reservoirs. Batch mode is applied to concentrate feed waters during operation. The feed water can be recycled up to the limit whereby solved substances in the feed water crystallize lead to scale formation. The brine is replaced in one single step. The terminology ‘closed-water’ used in literature should be replaced by ‘batch operation’. The advantage of this mode is that a high portion of condensate can be extracted from the feed water.

HD processes in batch mode are applied for zero liquid discharge (ZLD) applications. Chehayeb *et al.* [13] investigated the effect of increased salinity on the performance of HD systems. It is reported that high salt concentrations reduce the performance ratio. Kiefer *et al.* [56] focused similar studies on salts with very high solubility and concluded that the performance ratio is significantly reduced for high salt concentrations.

In continuous mode, mass flows are generally in steady-state (not time dependent) equilibrium. Since evaporation rates are predominantly small, the concentration increase for continuous operation is small and consequently recirculation of brine is advisable.

The advantages of continuous mode operation is that large water storage facilities are not required. However, continuous operation requires an additional control for the feed and blow down periphery and a constant heat source or heat storage. Generally, large scale desalination plants operate in continuous mode.

2.4 Energy Supply Modes

The supply of thermal energy for the heater can be transient, meaning that the energy input fluctuates with time (e.g. in the case of solar energy supply), or it is constant (e.g. waste heat, geothermal heat). A HD system with a performance ratio² PR of 3 requires approximately 215 kWh of externally supplied thermal energy to produce 1 m³ of condensate. For natural convection setups, electrical power is required for the water pump and the control unit which only attribute to a small fraction of the total energy requirement. The electrical energy requirement for the discussed cases is not seen as a constraint for the operation.

The required thermal energy for a HD system can be provided at temperature levels below 100 °C. A variety of energy sources can be used. Waste heat from industrial applications (e.g. the cooling systems of diesel generators) can be further processed with HD. Geothermal energy is another constant energy supply. A. Mohamed and N. El-Minshawy [70] theoretically studied an OA configuration whereby water was heated with geothermal energy.

The coupling of HD plants with waste heat sources can be advantageous especially for the industrial sector to concentrate water. Waste heat from power plants can be attributed as constant heat sources. A HD process which uses waste heat from gas turbines is suggested by El-Dessouky [19]. In an open air configuration, the flue gas from a gas turbine is mixed with atmospheric air and enters the humidifier. For this case the specific capital investment can be considered to be lower than for other desalination processes.

Most renewable energy sources show transient behavior and therefore any production rate of a system powered by these energy sources cannot be operated in continuous mode unless energy storage is applied. For solar applications, seawater is either heated directly in the collector or with a heat exchanger with heating fluid that is circulating in the separate solar circuit. Corrosion resistant material has to be used when sea water is directly heated in the collector.

²The performance ratio is a dimensionless number to compare the efficiency of different thermal desalination systems as outlined in chapter 3.2.3.

When heat exchangers are used, additional thermal losses need to be considered along with additional technical efforts including plant control. Several research institutes developed systems for an efficient use of water desalination using solar energy [12, 16, 39, 43, 94, 96]. A reservoir of heated brine coming from the collector supports the continuous operation of the desalination plant during times without solar radiation [71]. This of course requires a larger collector area and an additional hot water storage capacity.

Rodriguez *et al.* [31] and Tzen *et al.* [98] provided a general overview of desalination systems powered by renewable energy, both of large and small scale. Parekh *et al.* [84] focused on system configurations using solar energy and outlined a detailed technical overview of existing systems.

Early investigations and tests using plastics for flat plate collectors started before 1978 [85]. Technical developments are described in [42, 87] for seawater applications. Flat plate collectors are mostly used for domestic water heating to temperatures of up to 60 °C. Thermal losses significantly increase with higher water outlet temperatures [23, p. 302]. Selective absorber material reduces thermal losses [53]. Evacuated tube collectors (heat pipes) reach higher operation temperatures and have, compared to flat plate collectors, significantly smaller heat losses [52, p. 131].

2.5 Improved Configurations

To increase the efficiency of HD systems, several improvements have been suggested in literature, in particular air extraction, water extraction and multi-staging.

2.5.1 Air Extraction

At lower temperature levels, high air flows need to circulate as the absolute humidity of saturated air decreases significantly with decreasing temperature. In the upper part of the humidifier, the air flow can be reduced.

The first large HD system was built in Puerto Peñasco (Mexico) in 1962. This closed-air water-heated HD plant with forced convection applied an air ex-

traction setup [47, 90]. Hodges *et. al* called these air extraction flows ‘bleed-offs’ [45]. By adjusting the air flows, the slope of the operating line³ is adjusted to the slope of the saturation line⁴. Air extraction is favourably applied in forced convection system configurations.

Müller-Holst [71] claims that by removing the separation wall between humidifier and dehumidifier the air mass flow is positively adjusted which means that the mass flow is higher at the lower part of the system compared to the upper part. He supposes that this is an automatically optimizing system.

2.5.2 Water Extraction

Instead of increasing the air mass flow in the lower part of the column, the slope of the operating line can be optimized through extracting water from the humidifier to recirculate it to the dehumidifier, as depicted in Fig. 5.1 (b). Brendel [9, 10] investigated the effects of the different heat capacity flows of water and air and suggests that instead of air flow, the water flow can be adjusted. At certain heights, a certain ratio of water flow from the dehumidifier is extracted and injected in the humidifier at the corresponding height.

Another way to recover heat is by injecting brine leaving the dehumidifier into the feed water entering the humidifier. This leads to an overall elevated temperature level of the system whereby for a given external energy input the mass flow rate can be increased. This is investigated in the presented work.

2.5.3 Multi-Staging

The concept of multi-staging is applied in conventional thermal desalination systems such as multi-stage flash (MSF) or multi-effect distillation (MED). The produced vapor from one stage flows to the subsequent stage where it is used to either preheat or vaporize feed water. Water vaporizes in each stage resulting in lower water temperatures in the subsequent stages. The individual stages in MSF and MED plants are operated at consecutively reduced pressure

³The operating line is a graphic indicator applied for the humidifier and dehumidifier to determine optimized water and air flow ratios. For the humidifier, cp. chapter 4.3.3 and for the dehumidifier, cp. chapter 4.4.1.

⁴The saturation line indicates the specific enthalpy of saturated humid air for a given air temperature. The driving potentials for heat and mass transfer vanishes when the operating line approaches the saturation line.

to vaporize water. As mentioned in chapter 3.1.4, this occurs automatically in HD as the partial pressure changes according to the temperature level.

For HD it can be advantageous to operate stages with different water or air mass flow. The concept of multi-stage setup with different air flows is depicted in Fig. 2.3. Water enters at the first stage of the dehumidifier and is then heated consecutively within each following stage by the condensing water vapor from the humidifier. For each stage an individual air mass flow rate can be set. Meinel *et al.* [67] refer to the first large-scale HD system [44] and add the idea of pressure-staging: The water vapor condenses in the dehumidifier at a higher pressure compared with the stage above. The recuperated heat of condensation from the stage below is used in the next stage.

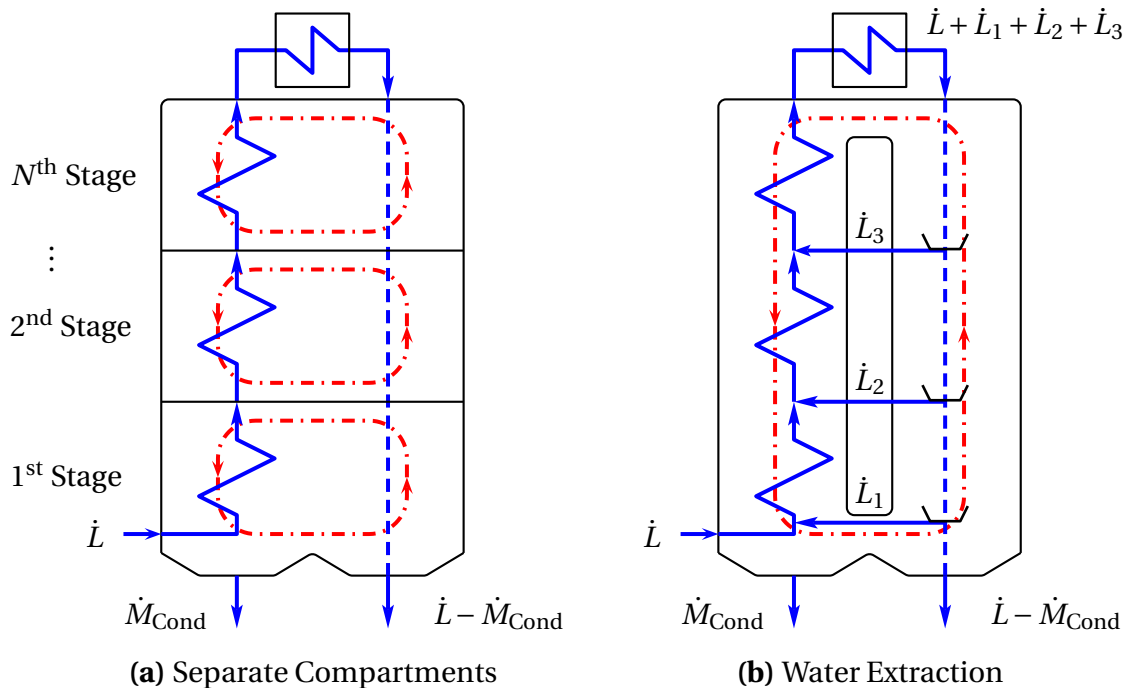


Figure 2.3: Multi-Stage Configurations of HD Systems

Hou [48] investigated a two-stage solar powered multi effect system using the pinch-point⁵ analysis and concludes, that this setup can achieve higher energy recovery rates than a single stage HD system. The concept of pinch-point analysis corresponds in HD to the concept of the operational lines,

⁵The pinch-point analysis is used to optimize process engineering processes in relation to the energy balance [99].

described in chapter 4.3.3. Zamen [104] worked on the improvement of solar powered HD using a multi-stage process and operated a 500 l/d unit in Iran whereby a 20% reduction of investment cost was reported compared to a single stage unit with the same capacity.

For closed-air water-heated HD systems, Chafik [12] suggest a stepwise loading of the air to increase the absolute humidity within the air. This concept was also adapted by Hassabou [40] whereby the humidifier consisting of a packed bed including phase change material releases heat through the dry patches (non-wetted surface area of humidifier) during operation to gain a similar effect.

Over the past years, several approaches have been published showing how to increase condensate output for HD systems, e.g. by [7, 49, 76, 80, 84, 93]. Limited research has been conducted on the improvement of the air flow within HD systems, especially natural convection and advanced HD designs.

3 HD Processes

3.1 Humidification Process

3.1.1 Separation Process

A characteristic of the operation of HD is that only components with a significant partial pressure are present in the gas phase. The dissolved components of sea water (the composition of standard seawater can be found in [100]) do not have a significant vapor pressure¹ [34].

Therefore, HD is a thermal separation process which can produce distilled water from saline water, also from water with very high salt concentrations². Salt water leaving the humidifier, the so called brine, has consequently a higher salt concentration of dissolved substances that do not evaporate. The dissolved ionic components are not transferred into the vapor, but in reality, sea water droplets or crystalline particles may be carried over by the gaseous flow to the dehumidifier.

Humidification of air corresponds to evaporative cooling that is used for many industrial applications with direct contact of water and air, such as in cooling towers for power plants. Wernicke [102] gives a detailed description of the theory of cooling towers. Distinct similarities between cooling towers and HD humidifiers, such as the active part of the cooling tower (packing) corresponds to the packing volume of the humidifier, offer the opportunity to transfer theoretical and technological cooling tower solutions to HD where suitable.

To generate a large interface surface between water and air, water runs through a packed bed (industrial filling material) which is one of the key elements to achieve increased heat and mass transfer in cooling towers and other evaporative cooling systems. Such highly sophisticated packing

¹Eucken [27] calculated exemplarily the ratio of the concentration c of salt ions in the solution to the concentration in the gas phase. This ratio is of many orders of magnitudes ($c_{\text{Solution}}/c_{\text{Gas}} \approx 10^{70}$).

²In contrast, the required operating pressure of reverse osmosis (RO) desalination systems is strongly dependent on the salinity of the water and consequently operation is limited to certain concentrations.

structures can be applied for humidifiers in HD systems for large exchange surfaces per column volume.

In cooling towers, the operating temperature range is significantly lower than in HD systems. Therefore, some simplifications applied for cooling towers, as introduced by Merkel [68], are not valid for HD systems. However, the elaborated methods for designing cooling towers are helpful for understanding the humidification processes and potential optimization approaches.

3.1.2 Partial Pressure and Concentration Differences

As the operating pressure in HD is low, the humid air can be considered as a mixture of ideal gases³. A partial pressure difference of vapor occurs during the evaporation process between the vapor pressure at the water-air interface and the vapor pressure in the bulk flow of humid air, as further explained in chapter 4.3. The corresponding concentration difference is the driving force for the transport of vapor into the air bulk flow. A commonly used definition of concentration c_i of a component in gases corresponds to a molar partial density $\tilde{\rho}_i$. For a component i (index i) of an ideal gas, the partial density ρ_i is $\rho_i = p_i / (R_i \cdot T)$. The molar partial density $\tilde{\rho}_i$ is calculated with the universal gas constant \tilde{R} instead of the specific gas constant $R_i = \tilde{R} / \tilde{M}_i$. The total pressure p of humid air is the sum of the partial pressure p_V of water vapor (index V) and partial pressure p_G of dry air (index G) according to Dalton's law [88, p. 52].

3.1.3 Boiling Point Elevation

The various states during the vaporization of saline water are depicted in Fig. 3.1. State (K) indicates the beginning of the vaporization process whereby the temperature t_W is maintained until the end of the vaporization process (L). The vapor released from saline water is superheated (M) because the saturation pressure of the released vapor corresponds to the lower temperature t_V of water. The temperature t_W is increased by *BPE* compared to t_V [69, p. 15]. The correlations for the determination of the enthalpy of the water vapor released from saline water is indicated in this figure. It has to be noted that the figure

³The compressibility factor Z differs only marginally from 1 for saturated water vapor ($Z = 0.9995$ at 0 °C and $Z = 0.9905$ at 80 °C) [34, p. 7-8, 88, p. 288 ff].

bined, a larger amount of water can evaporate and condense compared to a process in which only the external heating is used to evaporate water (compare also chapter 3.2.3 for the definition of the performance ratio PR). It is an inherent characteristic of the HD process that the partial pressure $p_{V,\infty}$ of the vapor in the bulk air and at the interface $p_{V,I}$ is also reduced along with the temperature, however the total pressure p_{total} remains constant. The difference to the total pressure is the partial pressure p_G of dry air. This resembles a multi-pressure configuration without the need of multiple separate stages or vessels. Therefore it is here suggested to introduce the term *quasi-multi-pressure* configuration for HD systems.

3.2 Dehumidification Process

Dehumidification in HD systems with indirect condensation is characterized by the condensation of water vapor via a solid heat exchanger surface in the presence of non-condensable gases (NCG).

Within the dehumidifier, condensable components within the humid air, here water vapor, precipitate on the heat exchanger surfaces. Additionally, the formed liquid condensate acts as a cooling surface. This dehumidification of humid air is like the previously described humidification process: a coupled heat and mass transfer phenomenon including phase change. Unidirectional mass transfer also has to be considered.

The heat of vaporization $\Delta h_V(t)$ is released during the dehumidification process forming the condensate. Condensation can occur when the cooling surface temperature is below the saturation temperature $t_{V,\text{sat}}$ of the vapor with partial pressure p_V . The presence of non-condensable gases (NCG) greatly influences heat and mass transfer. In HD, a dominant process for the dehumidification is the diffusion process in the gaseous phase⁴. For the condensation process, the effect of boiling point elevation is not relevant, as only pure water condenses in the dehumidifier.

⁴ Baehr and Stephan show that already for small concentrations of air, e.g. $p_G/p = 0.1$, the heat transfer is reduced to 16 % for natural convection [4, Fig. 4.10, p. 465].

3.2.1 Principles of Condensation

Condensation at cooling surfaces takes place in three steps [36, p. 284]. Firstly, vapor moves towards the cooling surface by molecular or molar transport whereby the presence of non-condensable gases and diffusion resistance can be high. Secondly, at the cooling surface, condensation of the water vapor takes place. In a third step, heat is removed from the interface by the cooling liquid, in this case feed water.

For a process in which pure vapor condenses (no presence of NCG), the thermal resistance in the gaseous phase (vapor) is usually neglected. This is also the case for Nusselt's water film theory [36, p. 285 ff.]. The thermal resistance is assumed to be only in the water film. This simplification is not valid for HD processes.

There are two basic principles for dehumidification: direct and indirect contact condensation. Both principles are applicable for HD.

Direct Condensation

With direct condensation, humid air is brought in direct contact with the cooling medium, e.g. cool pure water (liquid-liquid heat exchange). Direct condensation in humid air is essentially the reverse process of humidification of air because in this case heat removal occurs by enthalpy increase of cold (pure) water⁵, whereby for humidification the heat input occurs by enthalpy decrease of the hot seawater.

The correlations from the humidification process are transferred to describe heat and mass transfer processes for the dehumidification. The heat of condensation is recovered in an additional heat exchanger from the water leaving the dehumidifier [62]. A setup with one mixing water temperature can be considered as a single-stage unit without counter-current flow. Therefore PR is low.

Direct contact heat exchangers in HD are configured as bubble [78] or spray columns [18, 40, 46, 57, 62, 66]. Spray columns can be equipped with or with-

⁵ Also materials which are immiscible with and insoluble in water have been considered [47, p. 83].

out internals, such as a packing material. Distilled water or condensate is used as the cooling liquid and is sprayed into the hot humid air flow. The air flow can be in cocurrent or countercurrent direction to the spray. Cocurrent flow can avoid entrainment of fine particles in forced convection setups.

The advantage of direct condensation is that heat and mass transfer can be significantly increased compared to indirect condensers. The disadvantage is that an external liquid-liquid heat-exchanger and additional pumps are required to be able to recover the heat of condensation. A multi-effect configuration with countercurrent flow can only be achieved in a multi-stage setup.

Indirect Condensation

Indirect condensation requires a solid heat exchange surface. The condensation occurs on the solid surface and on the liquid which is formed on the surface⁶. For HD, the dehumidifier tube walls separate the cooling liquid from the condensate and the humid air flow. Additionally, condensation takes place on the adhering water surface of the condensate droplet or film. Indirect contact heat exchange allows compact plant design since no additional external heat exchanger is required and the control of the overall system can be simplified. Furthermore, this configuration allows a modular setup enabling possibilities for further plant optimizations and adaptations.

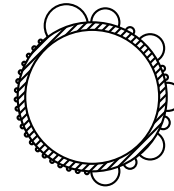
Preheated feed water can be extracted at virtually any point between inlet and outlet of the dehumidifier also enabling an advantageous multi-stage configuration. Results from experiments can be transferred to different tube diameters due to the reliable scalability as the heat-transfer surfaces are clearly defined. The temperature regions for operation are still relatively low so that low-cost material, such as polypropylene, can be applied. On the other hand, scaling inside the tubes needs to be considered.

There are three forms of condensation on solid surfaces: dropwise condensation, film condensation or a combination of both. When the condensate forms a continuous film on the heat exchanger surface, as shown in Fig. 3.2

⁶ Indirect contact heat exchanger in HD are built e.g. as arrangements of aluminium tubes with fins and seawater resistant in-liner [46], thin-wall plastic sheets made out of polypropylene [71] or polypropylene tube bundles [8, 91].



(a) Film Condensation



(b) Dropwise Condensation

Figure 3.2: Film and Dropwise Condensation on Tubes

(a), this phenomenon is called film condensation. The water film runs off as laminar or turbulent flow. In the case of incomplete wetting of the exchanger surface, the condensate forms droplets on the heat exchanger surface, shown in Fig. 3.2 (b). This case is called dropwise condensation, see [4, p. 450-451].

Literature usually focusses on condensation of pure vapor in the absence of NCG [4, p. 477 ff. 33, p. 673, 36, p. 309, 61, p. 100 ff. 99, p. Ja1 ff.]. Investigations on dropwise condensation started in 1930 by E. Schmidt [89]. Heat transfer with dropwise condensation in the absence of NCG can be very high compared with other convective heat transfer mechanisms as indicated in Table 3.1. Therefore, dropwise condensation is favored in industrial applications. Unfortunately, dropwise condensation can rarely be maintained for a longer time period on metal surfaces without additional technical efforts. These efforts include doting the vapor, coating the heat exchanger surface or ion-implementation [22, 54, 61, 86].

It has to be noted that surface conditions alter, e.g. due to corrosion effects, and due to the effect of impurities or additives. Therefore, maintaining the conditions for dropwise condensation for a long time is challenging. The vaporization and condensation rate strongly depends on the contact angle θ of the participating phases of the surface depicted in Fig. 3.4 [11].

Dropwise condensation in the absence of NCG usually occurs in short sequences. Krischer and Grigull, cited by Baehr and Stephan [4, p. 480], photographed Fig. 3.3 showing dropwise condensation on a vertical surface demonstrating that during a short period of time droplets grow, run off and leave a wiped surface behind. On this surface new droplets appear. During the

Table 3.1: Approximate Ranges of Heat Transfer Coefficient α for Convective Heat Transfer Mechanisms according to [61, 99]

Convective Heat Transfer Mechanism	$\alpha / \text{Wm}^{-2}\text{K}^{-1}$
Natural convection of air	2 - 15
Forced convection of air	30 - 200
Vaporization of water vapor	2.000 - 60.000
Film condensation of water vapor (in absence of NCG)	5.000 - 20.000
Dropwise condensation of water (in absence of NCG)	20.000 - 500.000

experiments with HD (chapter 5.3.1) dropwise condensation was observed; however, the sequences take a long time (minutes). This phenomenon is discussed in chapter 5.3.1.

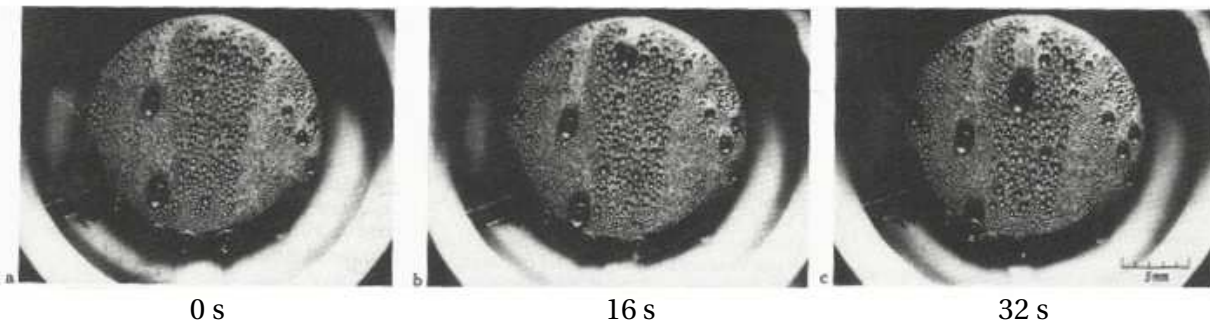


Figure 3.3: Dropwise Condensation in Absence of Non-Condensable Gases [4, p. 480]

3.2.2 Conditions for Film and Dropwise Condensation

Fig. 3.4 illustrates Young's equation [11]:

$$\sigma_{L,A} \cdot \cos\theta = \sigma_{S,A} - \sigma_{S,L}. \quad (3.1)$$

Young describes the correlation of surface tensions at point C at which the contact tension $\sigma_{S,A}$ between solid surface S and gas (humid air A), the surface tension $\sigma_{S,L}$, between surface and liquid (here water L) and the surface tension $\sigma_{L,A}$ between liquid and gas, are in balance. The contact angle θ is a measure for the wettability [11, p. 57]. The figure shows the case for a non-wetting liquid for which the criteria $90^\circ < \theta < 180^\circ$ applies.

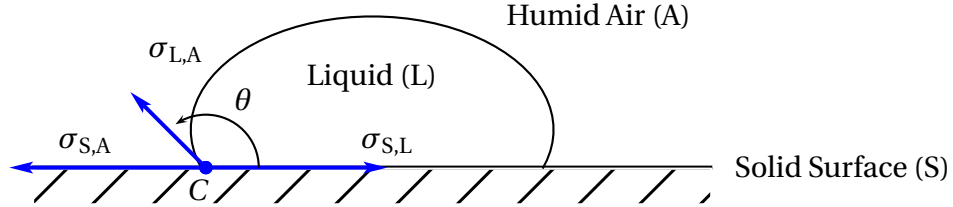


Figure 3.4: Contact Angle and Surface Tensions on a Liquid Droplet on Ideal Surface

In literature [11, p. 57, 36, p. 305, 86, p. 17] it is emphasized that a measured static contact angle θ is not a sufficient indicator to predict dropwise condensation as during the condensation process, heat and mass transfer influences the surface tensions. In technical applications, properties of surfaces are time dependent and deviate from ideal conditions. Additionally, hysteresis at the front and back of a moving droplet will affect dropwise condensation.

Emmons [24] describes the processes on a molecular level based on the kinetics of molecules. The wettability determines if dropwise or film condensation occurs on a surface. Here, the surface is considered as ideal when perfectly flat and smooth. Emmons emphasizes that the high volume reduction from water vapor to liquid water creates swirls accelerating the condensation process and therefore can explain very high heat transfer rates. Since this high volume reduction does not occur in the presence of NCG, this can explain that the high heat transfer rates cannot be achieved for setups with air as carrier gas, such as conventional HD systems.

3.2.3 Multi-Effect Energy Recovery and Performance Ratio

In a system without energy recovery, such as a conventional solar still, the external energy is used to heat the feed water, to evaporate the condensate and to compensate for heat losses. In such a system, the heat of condensation is not recovered, i.e. the internal energy transfer \dot{H}_{int} is zero as the heat of condensation is released to the ambient. In the 1950s, the concept of multi-effect humidification systems was applied to solar stills which then led to the development of the HD technology [38, 47, 63, 90].

In a multi-effect system the circulating air flow \dot{G} absorbs the evaporated water vapor in the humidifier and at steady-state conditions discharges the

same quantity to the dehumidifier. The enthalpy flow transferred in the dehumidifier consists predominantly of the heat of condensation Δh_v . Detailed calculations of the transferred heat and enthalpy flows are given in chapter 4.4.3.

The performance ratio PR is a widely used indicator in the desalination industry to compare thermal desalination systems regarding their multi-effectiveness. It is defined as the ratio of the heat of vaporization Δh_{PR} of the produced condensate \dot{M}_{Cond} to the externally provided energy \dot{Q}_{ext} :

$$PR \equiv \frac{\dot{M}_{\text{Cond}} \cdot \Delta h_{PR}}{\dot{Q}_{\text{ext}}}. \quad (3.2)$$

The specific heat of vaporization Δh_{PR} is set to the constant value 1000 BTU/lb which is equal to 2326 kJ/kg corresponding to a water vaporization temperature of 73 °C. A direct comparison of any thermal desalination plant is possible as the amount of produced condensate is related to the external energy input required to produce that amount. An accurate determination of relatively small condensate production rates is difficult for some system configurations.

A system, in which the energy for condensation of the produced condensate is larger than the externally added energy is defined as a ‘multi-effect’ system ($PR > 1$). For HD, performance ratios between 1.5 and 4.5 have been reported [72, 80].

3.3 Natural Convection

In contrast to forced convection with defined air velocities, natural convection requires an overall consideration of the conditions in the humidifier and dehumidifier to analyze the flow and is therefore a more complex process. For forced convection HD configurations, the air flow is adjustable by controlling the air blower, whereas in the case of natural convection the air flow is interdependent with heat and mass transfer in the humidifier and dehumidifier.

3.3.1 General Remarks

The driving force for the velocity of the circulating humid air in systems with natural convection results from density differences. An example is the heat transfer at a heated or cooled vertical surface which interacts with static ambient air. To describe the heat transfer coefficients for natural convection, the dimensionless Grashof number Gr is used instead of the Reynolds number Re . The Grashof number Gr uses the same characteristic length l but does not contain air velocity u , as in contrast to forced convection, the velocity is not initially known. Gr is defined as the product of the force of inertia and the buoyancy force, divided by the square of the viscosity force [33, p. 654]:

$$Gr \equiv \frac{\Delta\rho}{\rho} \cdot \frac{l^3 \cdot g}{\nu^2}. \quad (3.3)$$

In HD, a density difference emerges from temperature and humidity differences. The relative density difference $\Delta\rho/\rho$ in Eq. (3.3) resulting from temperature differences equals the negative relative temperature difference $\Delta T/T$. If density differences are created by concentration differences between two ideal gases, e.g. water vapor and dry air, the relative density difference $\Delta\rho$ is [33, p. 654, Eq. 9.17.11]:

$$\Delta\rho = \frac{\Delta p_1 \cdot (\tilde{M}_1 - \tilde{M}_2)}{\tilde{R} \cdot T}. \quad (3.4)$$

The following sections describe the created pressure differences which are the driving forces for natural convection in HD.

3.3.2 Natural Convection in Closed-Air HD Systems

For closed-air HD systems, the driving differences occur between humidifier and dehumidifier. The velocity of the air flow is determined by the driving density difference and the pressure loss in the system.

The approach using the Grashof number is therefore not advisable for HD. The velocity of the humid air can be determined from numerical simulation and validated with experiments together with known correlations for heat and mass transfer.

The air velocity of the bulk flow within a closed-air HD system in natural convection influences heat and mass transfer and consequently the condensate output. For an initial air velocity in the humidifier and dehumidifier, the driving pressure differences and the pressure losses can be calculated so that the velocity for natural convection can be iteratively determined.

3.3.3 Driving Pressure Difference in Closed Air Loop in HD

Density differences are created by the temperature and concentration difference within the humidifier and the dehumidifier. The pressure drop Δp_{pd} in steady-state closed systems with natural convection is equal to the gravitational pressure difference Δp_{grav} . Since the air velocity is small and the air flows in a closed loop, dynamic pressure differences are negligible.

For standard configurations where the humidifier and dehumidifier columns are connected at the top and bottom, the driving pressure difference Δp_{grav} is the difference between the gravitational pressure differences for the dehumidifier and humidifier in steady-state condition:

$$\Delta p_{grav} = g \cdot \left(\int_{z_{bot,deh}}^{z_{top,deh}} \rho_A(z) \cdot dz - \int_{z_{bot,hum}}^{z_{top,hum}} \rho_A(z) \cdot dz \right). \quad (3.5)$$

The density ρ_A of humid air, cp. Eq. (1.3), decreases with increasing temperature and absolute humidity, respectively partial pressure of water vapor p_V . In HD systems, the bulk humid air flow in the humidifier and in the dehumidifier can be assumed as a first approximation to be almost saturated at every location. To calculate the density of saturated humid air, the saturation pressure $p_{V,sat}$ of the water vapor is used.

Fig. 3.5 illustrates the density profile of humid air in the humidifier and the dehumidifier. The profile is derived from the numerical simulation (see chapter 4.3). The marked area equates to the integrals in Eq. (3.5) and is proportional to the driving pressure difference. The density differences result from lower temperatures and lower humidity in the dehumidifier. The higher heat and mass transfer in the upper part of the dehumidifier dominates the density profile.

For steady-state conditions, this pressure difference equals the pressure drop

Δp_{pd} in the air loop:

$$\Delta p_{grav} = \Delta p_{grav,deh} - \Delta p_{grav,hum} = \Delta p_{pd}. \quad (3.6)$$

The total pressure drop Δp_{pd} is the sum of the pressure drop in the humidifier $\Delta p_{pd,hum}$ and the dehumidifier $\Delta p_{pd,deh}$.

The densities of the humid air at the passage between humidifier and dehumidifier are identical as there is no heat transfer during the transition. In the dehumidifier, the density of the down flowing air increases during the dehumidification process rapidly and remains at a high level in the lower part of the dehumidifier.

The created overall density difference $\Delta \rho$ between humidifier and dehumidifier is proportional to the shaded area. Multiplied with gravitational acceleration g and height Z of the column, the shaded area represents the overall driving pressure difference of the system.

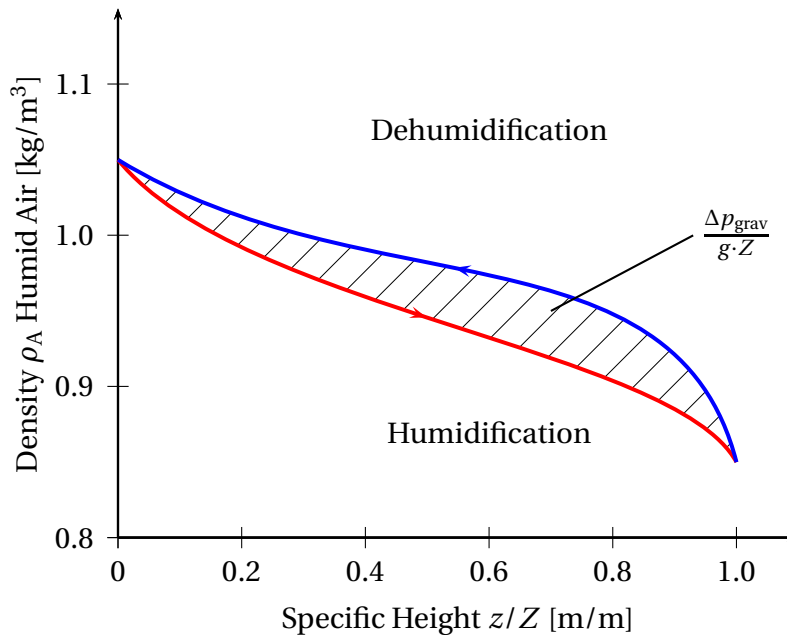


Figure 3.5: Characteristic Density Profile in HD

3.3.4 Pressure Drop

Pressure Drop in Humidifier

For the humidifier, the pressure drop in structured packings and filling material is described by Maćkowiak [64, 65].

The pressure drop depends on the velocity of water and air and the used packing material. Specific data can be obtained from the manufacturer or from literature. For conventional packing structures in process engineering applications, the pressure drop depends on the flooding point of the packing, respectively on the water mass flow, and the Reynolds numbers for water \dot{L} and air \dot{G} mass flow rate within a certain region. The flooding point of a column defines the point, whereby the air flow \dot{G} is so high that the down-flowing water flow \dot{L} is held up. In HD systems, the air flow \dot{G} is always far below the flooding point for standard configurations. Maćkowiak derived equations for the different conditions within packing columns. For typical HD configurations, i.e. laminar water flow $0.1 < Re_L < 2$ and any Reynolds number Re_A for the air flow, the pressure drop for a packed column with the total height Z can be calculated with [64, p. 271]:

$$\frac{\Delta p_{\text{hum}}}{Z} = \psi \cdot \frac{1 - \epsilon}{\epsilon^3} \cdot \frac{u_A^2 \cdot \rho_A}{d_{\text{pack}} \cdot K} \cdot \left(1 - \left(\frac{3}{g} \right)^{1/3} \cdot \frac{a^{2/3}}{\epsilon} \cdot (v_W \cdot u_L)^{1/3} \right)^{-5}. \quad (3.7)$$

The resistance coefficient (pressure loss) ψ for the gas flow through the packing, relative void fraction ϵ of the packing, diameter d_{pack} of one element of the packing, the wall factor K and the geometric surface area of packing per unit volume a are obtained from data sheets of the packing⁷. The gas velocity u_A is based on the cross-sectional area of an empty column. The term in brackets on the right side of the equation is approximately 1 for the small air velocities in HD systems. According to Ergun's [26] correlation using a friction factor⁸ accounting for viscous (i.e. laminar) and kinetic energy (i.e. turbulent) losses,

⁷ The wall factor K is 1 for structured packings.

⁸ In the original publication of Ergun [26], the friction factor f_V 'represents the ratio of pressure loss to viscous energy loss which is linear with the mass flow rate' and is defined as $f_V = 150 + 1.75 \cdot (N_{Re} / (1 - \epsilon))$. This friction factor with the usual definition of the Reynolds Number N_{Re} is considered in Eq. (3.7) and (3.8).

the resistance coefficient ψ is defined as [64, p. 118]:

$$\psi = \frac{150}{Re_{\text{pack}}} + 1.75. \quad (3.8)$$

For typical Reynolds numbers in HD Systems ($1 < Re_{\text{pack}} < 10$), the first term on the right side of Eq. (3.8) is dominant so that ψ becomes proportional to u_A^{-1} . Accordingly, the pressure drop in the humidifier becomes proportional to the velocity u_A of humid air ($\Delta p_{\text{hum}} \sim u_A^2 \cdot Re^{-1}$), as expected for a laminar flow regime, as described by Darcy's law [4, p. 394].

Pressure Drop in Dehumidifier

The pressure drop of the air flow in the dehumidifier depends on the used configuration of the condenser surface. In [99], the pressure drop for various configurations is given. For a tube bundle configuration in an aligned arrangement of tubes with N rows, the pressure drop is calculated according to [99, p. Lad 1-7]:

$$\frac{\Delta p_{\text{deh}}}{N} = \xi \cdot \frac{\rho_A \cdot u_A^2}{2}. \quad (3.9)$$

The pressure loss coefficient ξ depends on the geometric configuration of the tube arrangements and the Reynolds number Re . For laminar air flow the pressure loss coefficient ξ is proportional to Re^{-1} . For $Re \leq 10$, the temperature influence on the fluid properties and the influence of the larger number of tube rows ($N > 10$) is accounted through multiplication with a correction factor.

As air cools along the surface area, the change of the fluid properties, especially the density, needs to be accounted for. Additionally, the velocity $u_{A,f}$ of the free cross section at the top and the bottom of the dehumidifier are required for numerical investigations.

4 Mathematical Modeling

4.1 Overview

This chapter describes the approach used to analyse the processes of HD, focussing on one-dimensional (1-D) simulation of both humidifier and dehumidifier.

The observations on dropwise condensation within the dehumidifier, as observed in chapter 5.3.1, are anticipated in this chapter. An adapted simulation approach is introduced to account for dropwise condensation occurring instead of the expected film condensation.

This chapter also provides the fundamentals required to visualize heat and mass transfer relations using the concept of operating lines and tie lines. Further, the number of transfer units NTU and the height of one transfer unit HTU are discussed.

4.2 Assumptions

The humidifier and dehumidifier are investigated in the following sections with the numerical 1-D simulation tool Scilab[®] by applying adapted correlations for the combined heat and mass transfer outlined. Several assumptions are applied for the development of energy balances and heat and mass transfer rates:

1. The 1-D simulation investigates heat and mass transfer as a function of one length coordinate, the height z of the humidifier and dehumidifier column.
2. The system operates in steady-state.
3. The walls of the HD casing facing the surrounding are assumed to be ideally thermally insulated, i.e. adiabatic conditions.
4. Air and vapor are assumed as ideal gases. The validity of this assumption is shown in chapter 3.1.2.

5. Surface areas A_α for heat transfer and A_β for mass transfer are equal. The adapted approach for dropwise condensation is used for the dehumidifier simulation. For the humidifier simulation, the effective surface of the packing column $A_{\text{eff,pack}}$ is provided by the manufacturer (see also chapter 5.1.3) and used as a reference for the relevant calculations [69, p. 236].
6. Differences in potential and kinetic energy are neglected due to the small height of the system and the low velocities. This simplification relates to the energy balances but obviously not to the pressure difference which accounts for the natural convection flow of the circulating humid air.
7. The temperature of the packing t_{pack} is assumed to be equal to the bulk feed water temperature t_W . For the here investigated HD system, the packing material has a low heat capacity. It was not the aim to use the packing as heat storage¹.
8. Changes of the effective surface areas (e.g. due to scaling) are neglected.
9. Initial values for TBT , \dot{G} and \dot{L} are set in accordance with Fig. 4.4.
10. A replacement thickness of a water film is introduced to account for the prevailing complex dropwise condensation processes. This simple to use replacement model is explained in chapter 4.4.3.

4.3 Modeling of the Humidifier

Evaporation is the transfer of a substance from the liquid to the vapor state at temperatures below its boiling point². Humidification is the absorption of this vapor by a carrier gas.

In HD desalination systems, pure water vapor is transferred from the liquid phase, usually saline water (index W) to the gaseous phase, usually humid air (index A). \dot{L} refers to the mass flow rate of the liquid and \dot{G} to the mass flow rate of the carrier gas (dry air).

The specific enthalpy h_A of humid air³ for relative humidity $\varphi \leq 1$ is the sum

¹ Hassabou [40] investigates packings with high heat capacity and high thermal conductivity.

² Vaporization occurs at the boiling point of the liquid. Consequently, vaporization occurs also inside the liquid whereas evaporation only occurs at the surface of the liquid.

³ Assumption: Air and vapor are ideal gases with constant heat capacities for the regarded temperature regions.

of the enthalpy of dry air and of the enthalpy of the absolute humidity X at temperature t based on the mass of dry air [3, p. 295, 37, p. D25]:

$$h_A(t, X) = c_{p,G} \cdot t + X \cdot (\Delta h_{v,0} + c_{p,V} \cdot t). \quad (4.1)$$

Fig. 4.1 schematically illustrates a humidifier with countercurrent flow of liquid and gas. Fig. 4.1 (a) shows the temperature profile and (b) indicates the partial pressure p_V and p_G of vapor respectively of carrier gas in gaseous phase flow.

Water and air are assumed to be at thermodynamic equilibrium at the interface. This means equal temperatures $t_{W,I} = t_I = t_{A,I}$ and the partial pressure $p_{V,I}$ of the water vapor at the interface is equal to the saturation pressure $p_{\text{sat}}(t_I)$ for the interface temperature t_I [36, p. 284, 6, p. 20] when boiling point elevation is neglected (see also chapter 3.1.3).

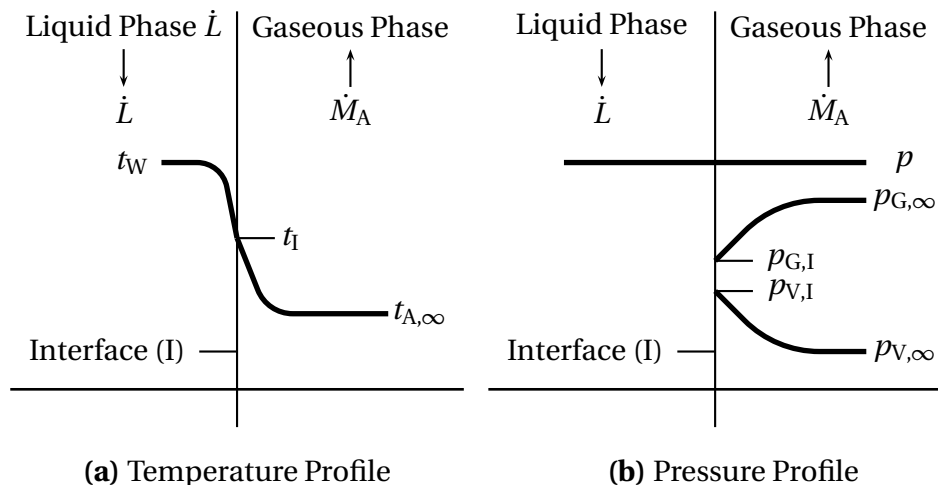


Figure 4.1: Evaporation Conditions of Water and Air Flow in Humidifier

The interface that separates the liquid and gaseous phase is characterized by its temperature t_I . This interface plays a decisive role for the heat and mass transfer. The interface temperature is unknown. Therefore it requires correlations which are based on measurable parameters in the bulk flow \dot{L} of water and the bulk flow \dot{M}_A of humid air, using assumptions as shown in the description of the 1-D simulation approach shown above.

The evaporation process comprises heat transfer due to temperature differences in the liquid phase and in the gaseous phase and mass transfer due to concentration differences of the water vapor in the gaseous phase between interface (index I) and the bulk gaseous flow (index ∞). The gaseous flow can be driven by natural or forced convection. Due to gravity forces, the liquid flows downwards in the humidifier as droplets and films on the packing so that irregular and constantly changing interfaces between the liquid and gaseous phase are created and the liquid is continuously mixed.

4.3.1 Energy and Mass Balances

Differential equations are formed according to the mass and energy flows as depicted in Fig. 4.2 and Fig. 4.3 to calculate process data within the humidifier over a certain differential height dz . The differential evaporated water mass flow $d\dot{L}$ is:

$$d\dot{L} = \dot{G} \cdot dX. \quad (4.2)$$

The evaporation coefficient⁴ σ_{evap} is defined according to Lewis, cp. [6, p. 22], as:

$$\sigma_{\text{evap}} \equiv \frac{\dot{m}_V}{X_I - X_\infty}. \quad (4.3)$$

Since non-condensable gases (NCG) are present during the humidification and dehumidification process in HD, the unidirectional mass transfer from the water surface to humid air is required. The relation of the coefficient β_u for unidirectional mass transfer and the evaporation coefficient σ_{evap} can be expressed as a function of β for equimolar mass flow and a correction factor.

This coefficient β can be determined from analogies between heat, mass and momentum transfer [36, p. 350 ff.]⁵:

$$\beta = \frac{\beta_u}{p} \cdot \frac{p_{V,I} - p_{V,\infty}}{\ln \frac{p - p_{V,\infty}}{p - p_{V,I}}} = \frac{\beta_u}{p} \cdot \frac{p_{G,\infty} - p_{G,I}}{\ln \frac{p_{G,\infty}}{p_{G,I}}}. \quad (4.4)$$

⁴ In some publications, such as the VDI Wärmearbeitsatlas [99], the evaporation coefficient σ_{evap} is referred to as β_X .

⁵ Grigull [36] labels β_h as the mass transfer coefficient for unidirectional diffusion at the semipermeable wall.

The logarithmic mean partial pressure of the carrier gas between interface and the bulk flow can be approximated for small pressure differences to $p_{V,I}$ [36, p. 354 ff.] leading to a simplified relation for the (unidirectional) evaporation coefficient σ_{evap} :

$$\beta \approx \beta_u \cdot \frac{p_{G,I}}{p} = \beta_u \cdot \left(1 - \frac{p_{V,I}}{p}\right). \quad (4.5)$$

$$\sigma_{\text{evap}} \approx \beta \cdot \frac{p}{R_G \cdot T_m} \cdot \left(1 - \frac{p_{V,\infty}}{p}\right). \quad (4.6)$$

Two control volumes are regarded according to Fig. 4.2 which is adapted from Bošnjaković [6, p. 22] for the differential description of the combined heat and mass transfer in an adiabatic setup. Water and air flow are separated by the interface I. With the horizontal cross section A_{cross} of the humidifier and the differential height dz of the packing column, the differential volume dV_{pack} of the packing is defined as:

$$dV_{\text{pack}} = A_{\text{cross}} \cdot dz. \quad (4.7)$$

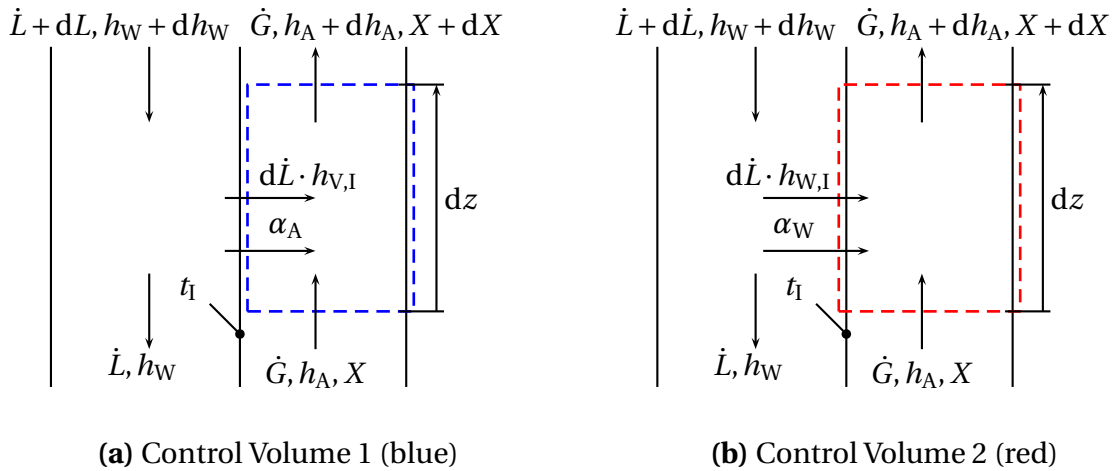


Figure 4.2: Control Volumes Without and With Adjacent Water Side at Interface I, adapted from [6, p. 22].

The differential heat and mass transfer surface dA_α and dA_β can be defined by the specific surface areas⁶ a_α respectively a_β :

$$dA_\alpha = a_\alpha \cdot dV_{\text{pack}} = a_\alpha \cdot A_{\text{cross}} \cdot dz \quad (4.8)$$

$$dA_\beta = a_\beta \cdot dV_{\text{pack}} = a_\beta \cdot A_{\text{cross}} \cdot dz. \quad (4.9)$$

Control volume 1 contains only humid air. The energy balance for control volume 1 is:

$$\dot{G} \cdot dh_A = \alpha_A \cdot (t_I - t_{A,\infty}) \cdot dA_\alpha + d\dot{L} \cdot h_{V,I}. \quad (4.10)$$

The enthalpy increase⁷ of humid air is the sum of the transferred heat $d\dot{Q}_A$ from the interface and the enthalpy of the evaporated water with the specific enthalpy $h_{V,I}$. In case of saline water, the enthalpy $h_{V,I}$ contains the supersaturation resulting from the boiling point elevation $c_{p,v} \cdot BPE$, as discussed in Fig. 3.1. Thus, the enthalpy of saturated vapor $h''(t_I)$ can be used, see also [97, p. 245].

The control volume 2 contains the humid air and is limited by a surface adjacent to the interface I at the water side. The energy balance of control volume 2 leads to the enthalpy change⁸ of the liquid which is equal to the transferred enthalpy from liquid to humid air:

$$\dot{G} \cdot dh_A = \dot{L} \cdot dh_W + d\dot{L} \cdot h_W = \alpha_W \cdot (t_W - t_I) \cdot dA_\alpha + d\dot{L} \cdot h_{W,I}. \quad (4.11)$$

The increase of enthalpy of humid air is equal to the sum of heat transferred to the interface and the enthalpy of the liquid water evaporating at the interface. Equation Eq. (4.10) and Eq. (4.11) correspond to the general energy equation for a two component (vapor and dry air) system in steady-state flow where kinetic energy differences and the effect of gravity and shear forces are neglected. Combining Eq. (4.10) and Eq. (4.11) leads to:

$$\alpha_W \cdot (t_W - t_I) \cdot dA_\alpha = \alpha_A \cdot (t_I - t_{W,\infty}) \cdot dA_\alpha + d\dot{L} \cdot (h_{V,I} - h_{W,I}). \quad (4.12)$$

Eq. (4.12) corresponds to Bošnjaković [6, p. 23, Eq. (58)] and is similar to the equation stated by Treybal [97, p. 245, Eq. (7-41)]⁹.

⁶ The so called effective interfacial area per unit volume a [34, p. 14-89] is also named as specific surface area (for packing columns).

⁷ Using Eq. (4.1) leads to: $dh_A = c_{p,G} \cdot dt + dX \cdot \Delta h_{V,0} + X \cdot c_{p,V} \cdot dt = (c_{p,G} + X \cdot c_{p,V}) \cdot dt + dX \cdot \Delta h_{V,0}$.

⁸ $d(\dot{L} \cdot h_W) = \dot{L} \cdot dh_W + d\dot{L} \cdot h_W$.

4.3.2 Determination of the Interface Temperature

Figure 4.3 illustrates three control volumes, the water film, the interphase and humid air. The interface is included as a separate control volume according to Wernicke [102, p. 4]. The interface is not shown separately when deriving heat, mass and energy balances along with other simplifications (evaporated water neglected) in a cooling tower or HD systems [80, 99, p. Mj6].

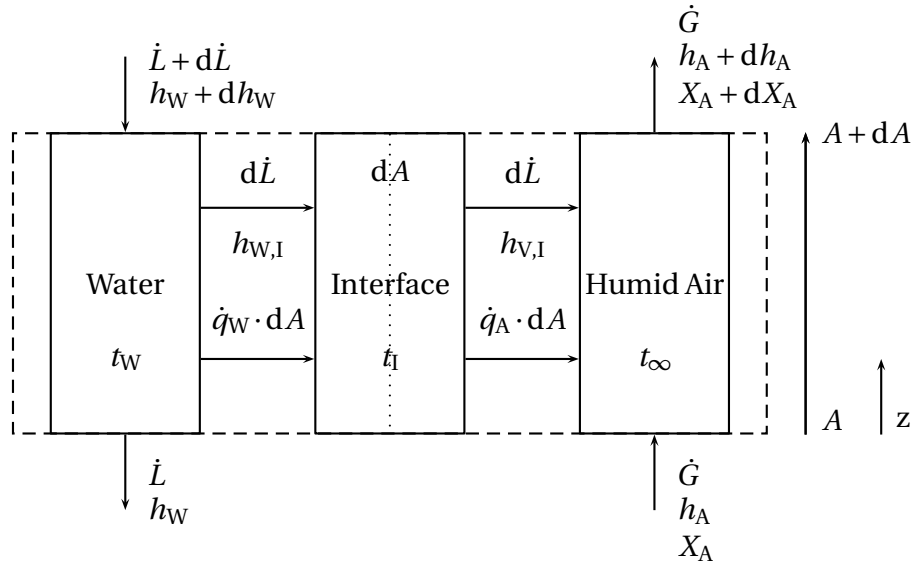


Figure 4.3: Control Volumes in Humidification, adapted from Wernicke [102]

The control volume of the interface distinguishes both water and air flow and accordingly, the heat and mass transfer can be described:

$$d\dot{L} \cdot (h_{W,I} - h_{V,I}) = (\dot{q}_W - \dot{q}_A) \cdot dA. \quad (4.13)$$

For evaporation of pure water, the enthalpy difference on the left side is the heat of vaporization at temperature t_I . It is assumed that at the interface both phases are in equilibrium, i.e. $h_{W,I}$ and $h_{V,I}$ are values at saturation. The interface temperature t_I is essential for the determination of the driving potentials for heat and mass transfer.

With the commonly used assumption, that the area for heat transfer equals the area for mass transfer $dA_\alpha = dA_\beta = dA$ and with the simplified Eq. (4.11)

⁹ Tribal's Equation [97, p. 245, Eq. 7-41] transformed to nomenclature used here:

$\dot{L} \cdot c_{p,W} \cdot dt_W = \dot{G} (c_{p,A} \cdot dt_A + [c_{p,V} \cdot (t_G - t_0) - c_{p,W} \cdot (t_W - t_0) + \Delta h_{v,0}] dX)$. The value in squared brackets is $\Delta h_V(t_I)$ which approximates to $h_{V,I} - h_{W,I}$.

for the sensible enthalpy change of the liquid:

$$\dot{L} \cdot c_{p,W} \cdot dt_W \approx \alpha_W \cdot (t_W - t_I) \cdot dA, \quad (4.14)$$

follows the temperature of the interface t_I from Eq. (4.12):

$$t_I = \frac{1}{1 + \frac{\alpha_A}{\alpha_W}} \cdot \left[t_W + \frac{\alpha_A}{\alpha_W} \cdot \left(t_{A,\infty} - (X_{A,I} - X_{A,\infty}) \cdot \frac{h_{V,I} - h_{W,I}}{Le_{f,u} \cdot c_{p,A}} \right) \right]. \quad (4.15)$$

This implicit equation is solved iteratively for differential heights of the humidifier. For each differential height of the humidifier or dehumidifier, the interface temperature $t_{I,i}$ is determined. Once the interface temperature is determined, the other parameters can be calculated stepwise as depicted in Fig. 4.4 where the simulation approach is depicted.

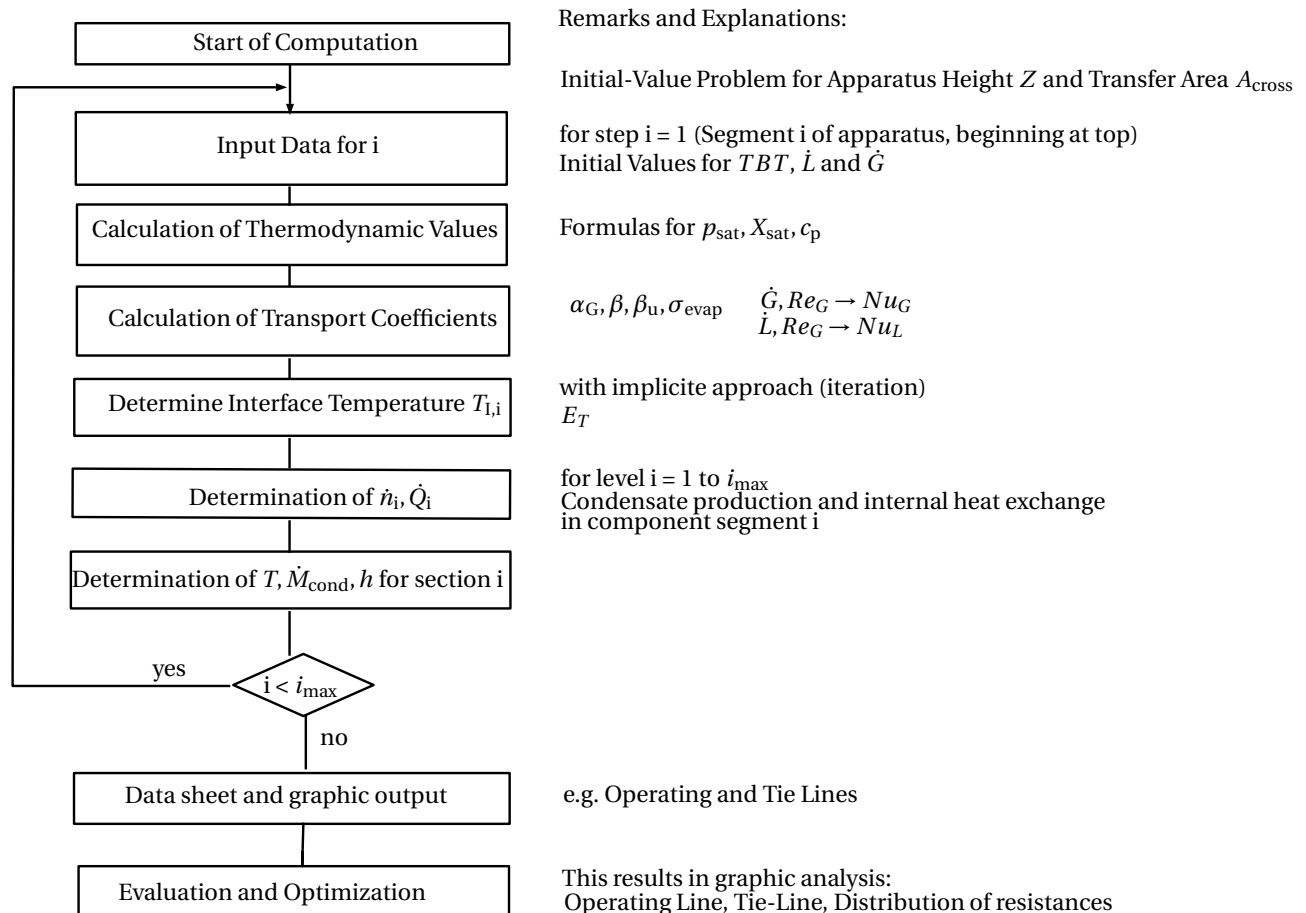


Figure 4.4: Computational Chart of 1-D Model for HD, cp. also [99, p. Jba 5]

The state of humid air or respectively water at the outlet of the humidifier can be calculated when the entry conditions for both air and water are known

($TBT, \dot{L}, t_{A,in}, \dot{G}, X_{A,in}$). The following parameters are essential: the total available area A for heat and mass transfer, the evaporation coefficient σ_{evap} , respectively $Le_{f,u}$, and the heat transfer coefficients for vapor into water α_W and vapor into air α_A . Several values for α_A/α_W are suggested in literature [41].

The molar density $\tilde{\rho}_A$ of humid air is the molar mass N_A of humid air per unit volume. After the implicit determination of t_I , further process data can be obtained from the equation which is transformed into difference equations for the numerical solution. Fig. 4.5 gives an example of temperature profiles in the humidifier. The interface temperature is shown in relation to the air and water temperatures. This gives an indication of the heat and mass transfer at each position. Also here, the differences at the top are higher due to the higher evaporation rates at higher temperatures.

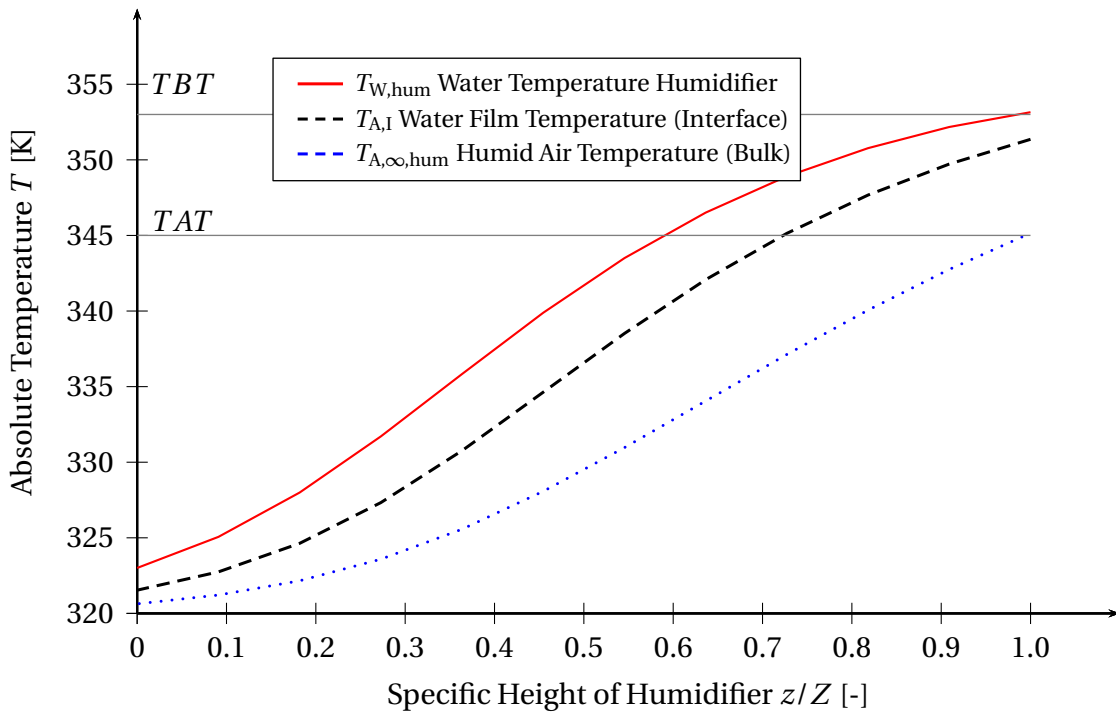


Figure 4.5: Example temperature profile of humidifier (1-D simulation) showing bulk water temperature $T_{W,hum}$ (80°C), water temperature $T_{A,I}$ at the interface between water and humid air and temperature $T_{A,\infty,hum}$ of the humid air. The height Z of the dehumidifier is 0.8 m.

4.3.3 Operating Line

The schematic of the vertical section of the humidifier in Fig. 4.6 describes conditions of water and air in the cross section at height z . An integral energy balance for steady-state conditions considers the cross section within the humidifier whereby a control volume is defined with an arbitrary height section of z of the column.

The enthalpy balance for the marked control volume of the column is:

$$\dot{L}_{in} \cdot h_{W,in} + \dot{G} \cdot h_A = \dot{L} \cdot h_W + \dot{G} \cdot h_{A,out} \quad (4.16)$$

Water inlet parameters are usually known and the mass flow \dot{G} of dry air remains constant. Therefore, mass related (specific) properties derived from extensive properties of humid air are as usual related to the dry air mass.

The water flow difference $\dot{L}_{in} - \dot{L}$ accounts for the evaporated water flow rate, which is a small percentage (< 10%) compared to the overall liquid mass flow rate \dot{L} and is neglected to simplify the graphical analysis using operating lines.

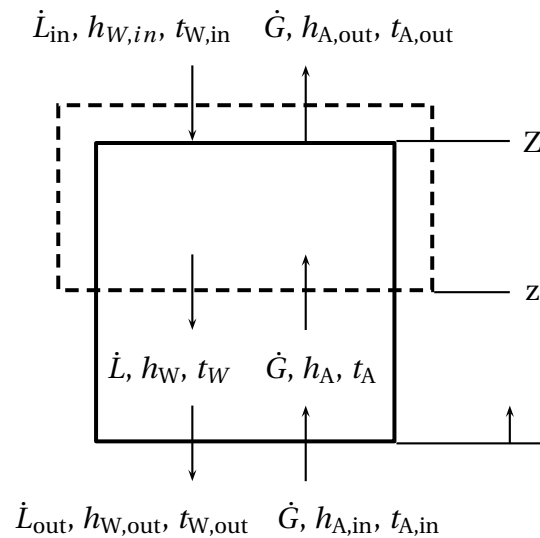


Figure 4.6: Schematic Humidifier for Integral Energy Balance

With the overall energy balance for the humidifier Eq. (4.16) and the simplification that the liquid mass flow \dot{L} in the humidifier is constant, the energy

balance is expressed as:

$$\dot{L} \cdot c_{p,w} \cdot (t_{W,in} - t_W) \approx \dot{G} \cdot (h_{A,out} - h_A). \quad (4.17)$$

This relation can be displayed in an enthalpy-temperature diagram, as shown in Fig. 4.7, which corresponds to the so-called operating line. The slope of the operating line in this diagram is proportional to the water and air mass flow:

$$\frac{dh_A}{dt_W} \approx \frac{\dot{L}}{\dot{G}} \cdot c_{p,w}. \quad (4.18)$$

The saturation line of humid air indicates the enthalpy of saturated humid air for a given temperature t . It is commonly assumed, that humid air is saturated at the interphase between water and air for a given interface temperature t_I . The application of both saturation line and operating line are described below and can be used to visualize the operating conditions of the system. The concept of an operating line is also applied for the dehumidification process. Additionally, the driving forces for heat and mass transfer are explained with tie lines. The required heat and mass transfer relations are derived in chapter 4.5.1.

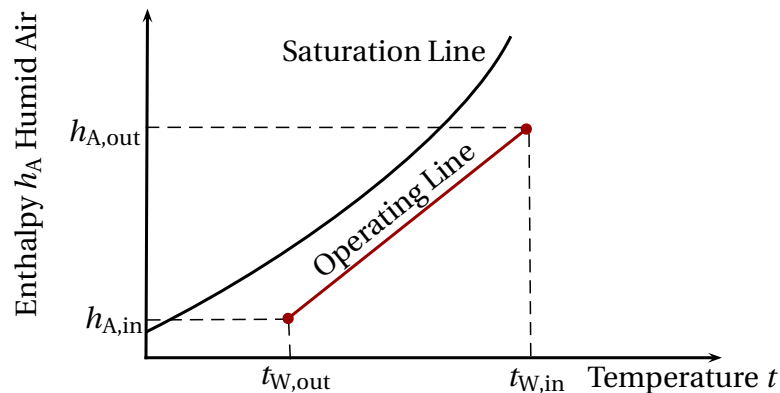


Figure 4.7: Operating Line for Humidifier, adapted from [97, p. 246]. The abscissa indicates the water temperature t_W for the Operating Line and the air temperature t_A for the Saturation Line.

This is an example used to predict the temperature profile of humid air and the water flow in the humidifier. The temperature differences between the downstream water bulk flow and the interface are mainly created by the transportation of the heat to the interface for the evaporation.

4.4 Modeling of the Dehumidifier

The suggested model for the description of dropwise condensation in the presence of NCG is based upon the application and adaptation of the film-theory [4, p. 98 ff, p. 487].

4.4.1 Energy and Mass Balances

The principles of the operating line, which were introduced for the humidification in chapter 4.3.3, can also be applied for the dehumidification process. The operating lines indicate for a given water temperature t_W at a specific height z of the apparatus, the corresponding enthalpy of the humid air at this height. Temperature differences on the abscissa correspond to enthalpy differences in the water flow because $c_{p,W}$ can be assumed to be constant.

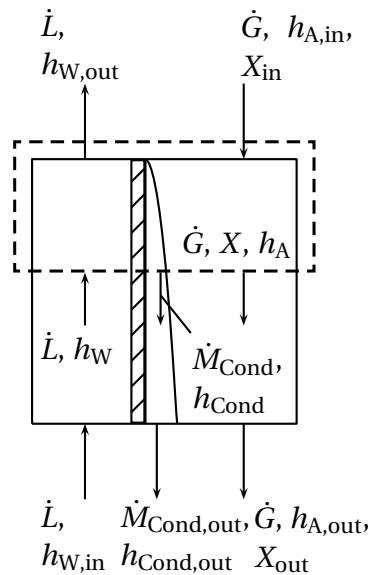


Figure 4.8: Schematic of Dehumidifier for Integral Energy and Mass Balance, adapted from [99, p. Jba 1]

Fig. 4.8 depicts the integral mass flows and their specific enthalpies for indirect dehumidification of humid air, cp. [99, p. Jba 1]. The mass flow rate \dot{G} of dry air and the mass flow rate \dot{L} of the feed water remains constant whereby the water content X in the humid air changes as vapor transforms into the

condensate mass flow \dot{M}_{Cond} . The energy balance can be formulated as:

$$\dot{G} \cdot h_{A,\text{in}} + \dot{L} \cdot h_{\text{W}} = \dot{G} \cdot h_{\text{A}} + \dot{L} \cdot h_{\text{W},\text{out}} + \dot{M}_{\text{Cond}} \cdot h_{\text{Cond}}. \quad (4.19)$$

The liquid \dot{L} is preheated by the released energy of the humid air, mainly the heat of vaporization of the condensate. The mass flow of the condensate produced in the dehumidifier results from the difference ΔX of the absolute humidity of the constant mass flow \dot{G} of dry air, as X is related to the dry air mass. The slope of the operating line is approximately the same as the slope for the humidifier, see also Eq. (4.18). The slope for the dehumidifier is derived from Eq. (4.19), which includes the specific heat capacity $c_{p,\text{W}}$ of (sea) water and neglects the sensible heat of the condensate as \dot{M}_{Cond} is small compared to the feed water mass flow \dot{L} :

$$\frac{dh_{\text{A}}}{dt_{\text{W}}} \approx \frac{\dot{L}}{\dot{G}} \cdot c_{p,\text{W}}. \quad (4.20)$$

Fig. 4.9 (b) depicts the enthalpy-temperature diagram for both humidifier and dehumidifier. The external heating provides the required gradient for the heat and mass transfer. The temperature difference Δt_{12} corresponds to the preheating of the feed water in the dehumidifier with the internal heat and enthalpy flow rate \dot{H}_{int} according to Eq. (4.21). Simplifications have been used (neglecting sensible heat of the condensate and changes of sensible heat of dry air) to illustrate the multiple recovery of evaporation enthalpy. The internally transferred enthalpy flow rate \dot{H}_{int} from the humidifier to the dehumidifier is defined as the enthalpy increase of the feed water mass flow \dot{L} in the dehumidifier which is approximately the released heat of vaporization of the condensate:

$$\dot{H}_{\text{int}} \equiv \dot{L} \cdot (h_{\text{W},2} - h_{\text{W},1}) = \dot{L} \cdot c_{p,\text{W}} \cdot \Delta t_{12} \approx \dot{M}_{\text{Cond}} \cdot \Delta h_{\text{v}}. \quad (4.21)$$

The internally transferred enthalpy flow rate \dot{H}_{int} follows from the temperature difference Δt_{12} . Fig. 4.9 (b) depicts the operating lines of the humidifier and the dehumidifier. The temperature difference Δt_{23} corresponds to the external energy \dot{Q}_{ext} ,

$$\dot{Q}_{\text{ext}} = \dot{L} \cdot c_{p,\text{W}} \cdot \Delta t_{23}, \quad (4.22)$$

whereby the heat capacity flow rate $\dot{C}_{\text{p}} = \dot{L} \cdot c_{p,\text{W}}$ is assumed as constant¹⁰.

¹⁰ The heat capacity $c_{p,\text{W}}$ of water increases by 0.3% when heated from 20 °C to 80 °C [4, p. 696]. The water mass flow \dot{L} is constant in the dehumidifier and the external heater for HD systems without water extraction.

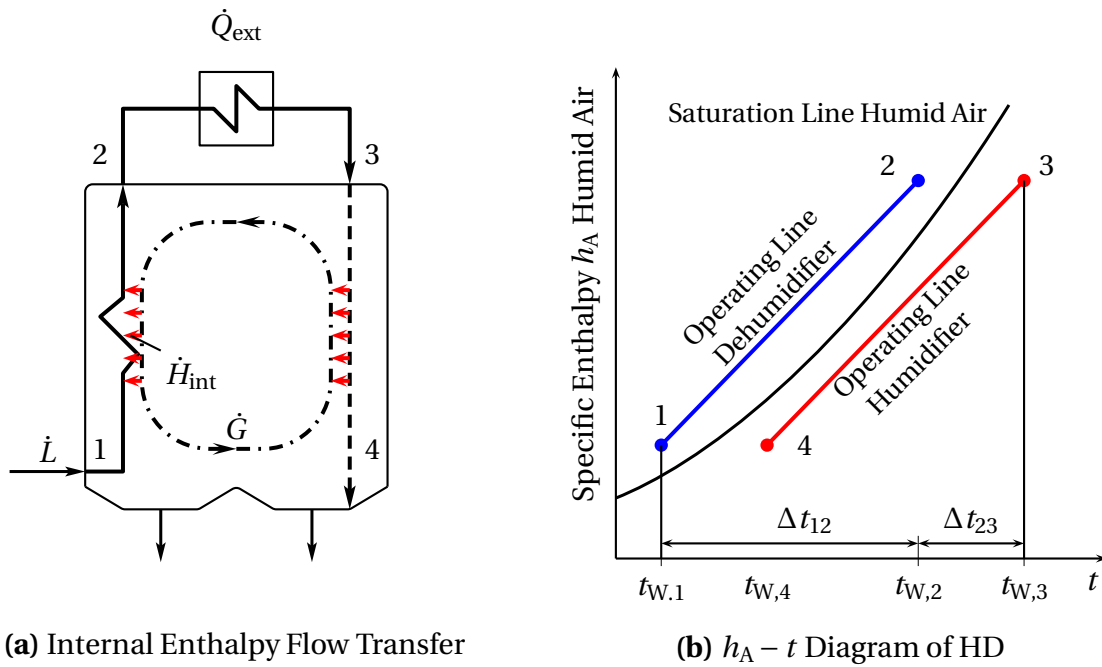


Figure 4.9: Schematic Overview Energy Transfer in HD

4.4.2 Differential Heat and Mass Balances

Fig. 4.10 depicts the control volume at the interface between the humid air flow and the condensate. The left side shows the mass flows of condensate and the cooling liquid (sea water), on the right side passes humid air.

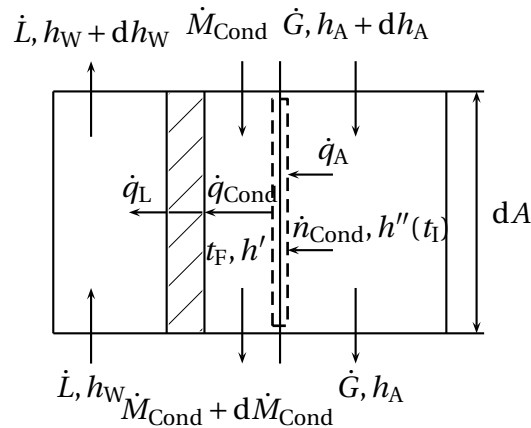


Figure 4.10: Differential Control Volume (dashed box) for Dehumidifier at Interface

The interface segment is included to determinate its temperature which is critical when non-condensable gases are present. The molar flow density

\dot{n}_{Cond} is commonly used to describe the condensation relations for the one-dimensional mass transfer of the differential vapor mass flow $d\dot{M}_{\text{Cond}}$, compare [4, Eq. (4.61)]:

$$|\dot{n}_{\text{Cond}}| = \left| \frac{d\dot{M}_{\text{Cond}}}{dA \cdot \tilde{M}_W} \right| = \beta_u \cdot \frac{p}{\tilde{R} \cdot T} \cdot \ln \left(\frac{\frac{p_{\text{sat}}(t_1)}{p} - 1}{\frac{p_{V,\infty}}{p} - 1} \right). \quad (4.23)$$

Fig. 4.11 depicts the control volumes to derive the differential equations similar to the previously discussed case for the humidifier. The velocity of humid air is very low due to the natural convection and therefore shear forces or kinetic energy are not to be considered in the energy balance.

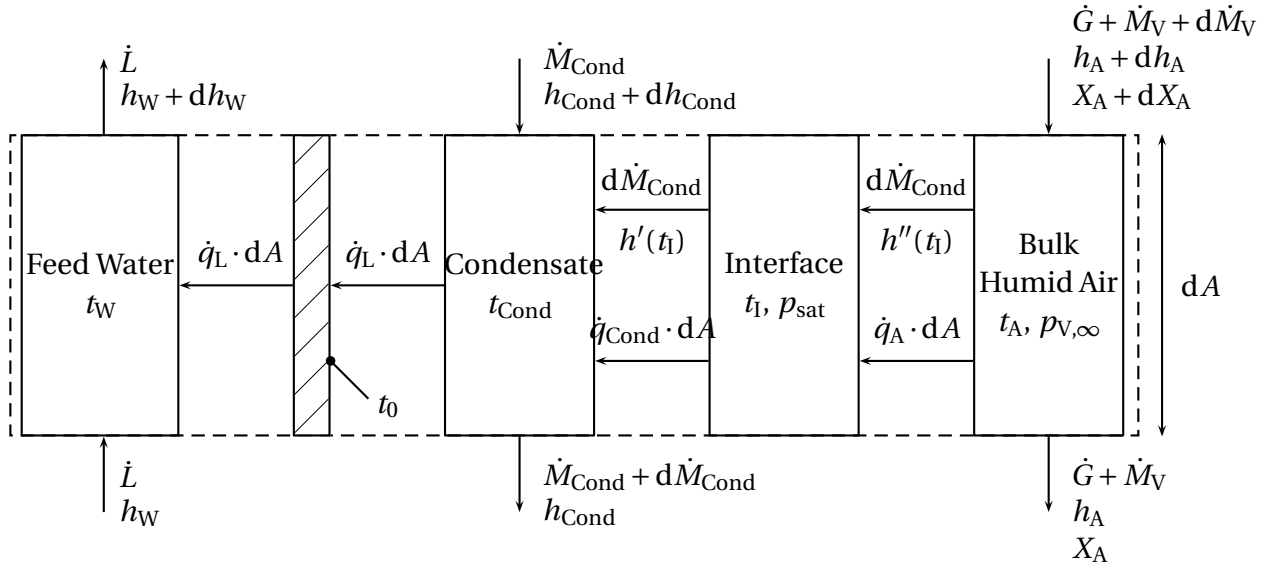


Figure 4.11: Heat and Mass Transfer for Dehumidification, adapted from Wernicke [102]

An energy balance including the two control volumes 'Condensate' and 'Interface' leads to Eq. (4.24):

$$\dot{q}_L = \dot{q}_A + d\dot{M}_{\text{Cond}} \cdot (h''(t_1) - h_{\text{Cond}}) + \dot{M}_{\text{Cond}} \cdot dh_{\text{Cond}}. \quad (4.24)$$

As previously noted the sensible heat of the condensate flow can be neglected which simplifies this equation to:

$$\dot{q}_L \approx \dot{q}_A + d\dot{M}_{\text{Cond}} \cdot \Delta h_V(t_1). \quad (4.25)$$

The transferred heat flux density \dot{q}_L defined in Eq. (4.25) can be written with k' as the heat conduction resistance at the separating wall including the heat

transfer from the wall to the cooling liquid and the conduction within the wall.

$$\dot{q}_L = \alpha_F \cdot (t_I - t_0) = k' \cdot (t_0 - t_W). \quad (4.26)$$

The heat transfer coefficient α_F describes the heat transfer between the interface and the separating wall. This value is derived in chapter 4.4.3. By elimination of the unknown wall temperature t_0 follows:

$$\dot{q}_L = \frac{\alpha_F}{\frac{\alpha_F}{k'} + 1} \cdot (t_I - t_W). \quad (4.27)$$

Due to the molar mass flow \dot{G} of humid air, the Ackermann correction factor E_T [99, p. Jba 2] on the heat transfer coefficient α_A for the energy transported by the vapor to the interface additional to the heat of vaporization (compare also [4, p. 463])¹¹ has to be considered:

$$\dot{q}_A = \alpha_A \cdot E_T \cdot (t_{A,\infty} - t_I). \quad (4.28)$$

The equation for the implicit determination of the temperature t_I at the interface with saturation conditions at the interface follows from Eq. 4.23 - 4.28:

$$\frac{\alpha_F}{\frac{\alpha_F}{k'} + 1} \cdot (t_I - t_W) = \alpha_A \cdot E_T \cdot (t_{A,\infty} - t_I) + \beta_u \cdot \tilde{\rho}_A \cdot \ln \left(\frac{\frac{p_{\text{sat}}(t_I)}{p} - 1}{\frac{p_{V,\infty}}{p} - 1} \right) \cdot \Delta h_V(t_I) \cdot \tilde{M}_W. \quad (4.29)$$

This equation corresponds to [4, Eq. (4.67)]. The interface temperature t_I is determined numerically. Therefore it can be proceeded as described for the humidifier.

4.4.3 Replacement Film Thickness for Dropwise Condensation

Film condensation without the presence of NCG has been described mathematically by Nusselt's water-film theory. The theory assumes that there is no resistance in the vapor phase, as shown in Fig. 4.12 (a).

The condensation produces a laminar film on a vertical or inclined wall with constant temperature. Shear forces are in equilibrium with gravity forces of

¹¹ In the mathematical model it is accounted for that the heat transfer occurs on a cylinder (tube), not on a plane surface (e.g. [4, p. 37]).

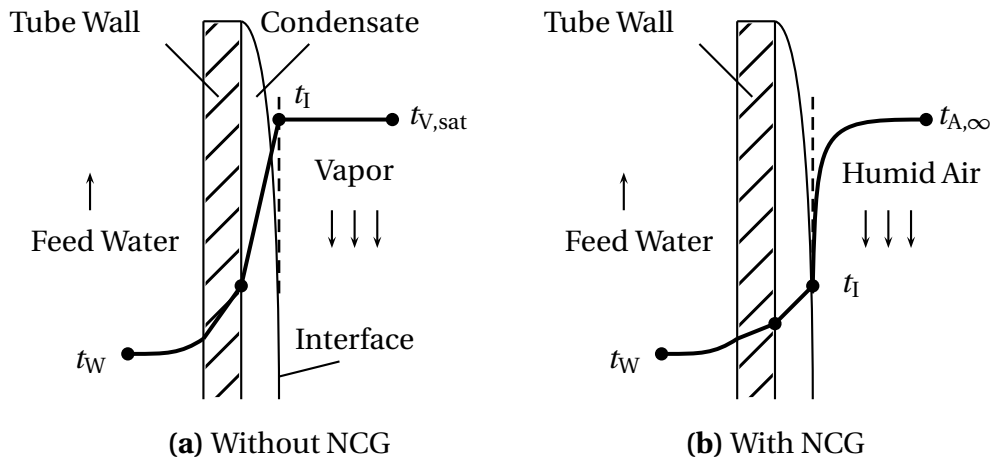


Figure 4.12: Film Condensation With and Without Presence of Non-Condensable Gases (NCG)

the film. The film thickness δ is calculated from the heat transfer necessary for condensation [4, p. 452 ff.].

Fig. 4.13 indicates the partial pressure p_v of the vapor for the condensation process. The interface temperature is referred to as a horizontal cross section of the water film. The presence of NCG is shown in Fig. 4.12 (b). A high thermal resistance is in the vapor phase. The temperature t_i of the interface of the film is the saturation temperature of the partial pressure of the vapor at the interface. This temperature cannot be determined explicitly as it is for the humidifier. In the following paragraph the relations for the determination of the interface temperature are presented.

The following explanations are partially new approaches since they are adjusted to dropwise condensation because of the presence of NCG and observations on the dehumidifier of the experimental setup.

As much as it is desirable to make a clear distinction between both transfer surfaces and to be able to determine both surface areas individually as exact as possible for numerical investigations, the complexity of dropwise condensation in presence of NCG requires a feasible approach. Fig. 4.14 indicates the heat and mass transfer surfaces for dropwise condensation.

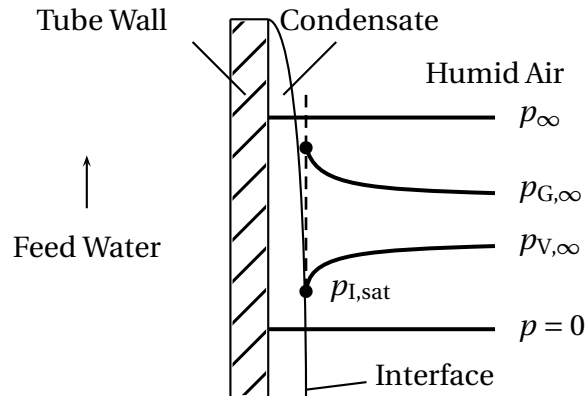


Figure 4.13: Pressure Profile in Dehumidifier (Humid Air Side)

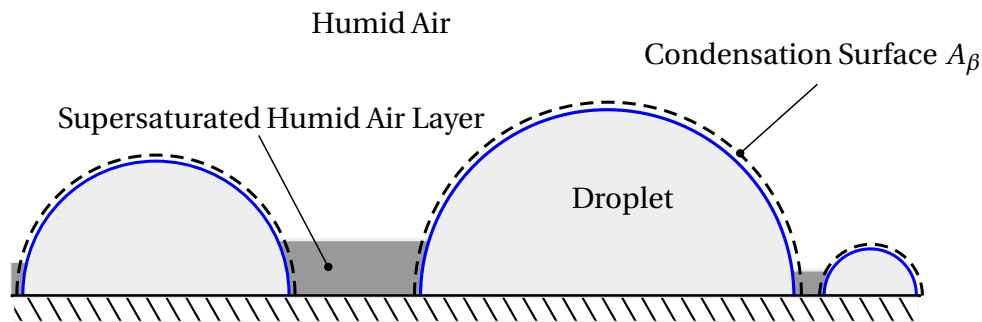


Figure 4.14: Heat and Mass Transfer Surfaces for Dropwise Condensation in Presence of NCG; Total Surface A Facing Humid Air (includes the Surface of the Supersaturated Humid Air Layer) may be attributed to A_α .

Cooling Surface for Heat Transfer

Cooling and sub-cooling of humid air occurs on both the droplet surfaces and the surfaces in-between the droplets. Dry areas between droplets cool the humid air without condensation. Humid air at the dry areas is therefore sub-cooled. There is no formation of fog. The required sub-cooling for homogenous nucleation is by far not reached. Thus, the whole surface (dry and liquid) is participating at the heat transfer process and can be referred to as A_α . A reason for high heat transfer coefficients in the case of dropwise condensation without NCG is the high convection flow generated by rapid volume decrease of vapor to the liquid state. This effect vanishes due to the presence of NCG. The temperature gradient between droplet and surface is necessary for the removal of the heat of condensation by the cooling liquid.

Condensation Surface for Mass Transfer

Condensation areas are only the surfaces of droplets. For large droplets, the condensing area may be concentrated on the cooler region of the droplet contacting the solid surface. There is no liquid film between the droplets but the influence on not fully participating surfaces may be neglected. The surface for mass transfer is referred to as A_β . Despite the separated surface areas for heat and mass transfer, an appropriate assumption is $A_\beta = A_\alpha = A$. Different feasible conclusions are hardly to justify due to the highly complex processes for dropwise condensation. Therefore a simple mathematical approach is suggested to assess the dehumidification process with dropwise condensation in the presence of NCG.

A precise mathematical description of dropwise condensation is hardly possible as emphasized in the literature [4, 11, 36]. Additionally, the conditions within a HD configuration make the simulation of dropwise condensation highly complex because of the changing droplet diameter distribution, the falling of drops from upper locations down to heat exchanger tubes situated below as well as changing the heat and mass transfer rates.

Fig. 4.15a shows an example of a tube with condensing droplets. On the left side, smaller droplets appear after the surface has been wiped by a down flowing large droplet. On the right side, large droplets are merging.



Figure 4.15: Modelling of Dropwise Condensation

Fig. 4.15b shows a layer with the replacement thickness δ_{repl} which is used to mathematically describe the irregular, inhomogeneous droplet coverage of the tube surface. The replacement thickness δ_{repl} of the water film influences heat conduction [4, p. 37] and is included in Eq. (4.29).

The layer of droplets remains on the tubes of the dehumidifier for a relatively long period which has a similar effect as a film. This approach seems to be evident from the undertaken experimental observations allowing a feasible numerical description. The phenomenon of dropwise condensation with its barrier for the heat transfer is similar. It also takes into account the relatively small effect of dropwise condensation on the complete dehumidification process for both heat and mass transfer.

The heat transfer coefficient α_F takes into account the water film thickness δ_{repl} for the determination of the heat transfer in the condensate film:

$$\alpha_F = \frac{\lambda_W}{\delta_{\text{repl}}}. \quad (4.30)$$

A stepwise solution of this initial-value-problem is required to calculate the driving forces and the transport coefficients for the determination of the required heat exchanger surface area. This 1-D approach corresponds to the described method for the dimensioning of the humidifier whereby known correlations for condensation in the presence of non-condensable gases are used. This can be done with an analysis of the condensation process and the introduction of adequate simplifications for the mathematical description.

4.5 Visualization of Heat and Mass Transfer Relations

This section describes a way to visualize the complex relations between the process parameters by way of applying some simplifications.

Operating lines (see chapter 4.3.3 for the humidifier and chapter 4.4.1 for the dehumidifier) are combined with tie lines as graphic visualization of the heat and mass transfer conditions in HD. The following description refers to the humidifier but can be transferred to the dehumidifier respectively the complete system.

4.5.1 Tie Line

Heat and mass transfer correlations are necessary together with mass and energy balances for dimensioning the packing column in the humidifier. The

driving difference between heat and mass transfer for the humidification process is graphically indicated with the tie line. Chapter 4.3.1 outlines the combination of Eq. (4.10) and Eq. (4.11) leading to Eq. (4.12) which is a correlation between the heat transfer in water and humid air and the energy balance of the interface.

The transferred evaporated water mass flow $d\dot{L}$ in the humidifier packing column can be described with the evaporation coefficient σ and the specific surface area a_β for mass transfer:

$$d\dot{L} = \dot{G} \cdot dX = \sigma_{\text{evap}} \cdot (X_I - X_\infty) \cdot a_\beta \cdot dV_{\text{pack}}. \quad (4.31)$$

Ignoring the sensible heat of the evaporated water according to [97, p. 246], Eq. (4.12) transforms to:

$$\alpha_W \cdot (t_W - t_I) \cdot a_\alpha = \alpha_A \cdot (t_I - t_{A,\infty}) \cdot a_\alpha + \Delta h_{v,0} \cdot \sigma_{\text{evap}} \cdot (X_I - X) \cdot a_\beta. \quad (4.32)$$

The following equation introduces the Lewis Factor Le_f according to Eq. (C.17):

$$\frac{\alpha_A}{\sigma_{\text{evap}} \cdot c_{p,A}} \cdot \frac{a_\alpha}{a_\beta} = Le_f \cdot \frac{a_\alpha}{a_\beta}. \quad (4.33)$$

Inserting Eq. (4.33) into Eq. (4.32) leads to [97, Eq. 7-48]:

$$\alpha_W \cdot (t_W - t_I) \cdot a_\alpha = \sigma_{\text{evap}} \cdot a_\beta \cdot \left[\left(c_{p,A} \cdot Le_f \cdot \frac{a_\alpha}{a_\beta} \cdot t_I + \Delta h_{v,0} \cdot X_I \right) - \left(c_{p,A} \cdot Le_f \cdot \frac{a_\alpha}{a_\beta} \cdot t_{A,\infty} + \Delta h_{v,0} \cdot X \right) \right]. \quad (4.34)$$

The common simplification for water vapor in air ($Le_f \cdot a_\alpha / a_\beta = 1$) and the assumption that both specific exchange surface areas are equal ($a_\alpha = a_\beta = a$) simplifies Eq. (4.34):

$$\alpha_W \cdot (t_W - t_I) \approx \sigma_{\text{evap}} \cdot (h_{A,I} - h_A). \quad (4.35)$$

From Eq. (4.35) follows that corresponding points on the operating line (for a given point with t_W and h_A on the operating line) and on the saturation line are connected with a tie line with the slope:

$$\frac{dh_A}{dt_W} \approx -\frac{\alpha_W}{\sigma_{\text{evap}}}. \quad (4.36)$$

Fig. 4.16 shows an exemplary point U on the operational line O-P and a triangle U-I-R. The tie line U-I connects the enthalpies of the humid air on the operating line for a given water temperature (corresponding to a given height z in the column) with the enthalpy of saturated humid air at the interface. The distance I-R corresponds to the enthalpy difference for point U at the operating line, as a measure for the driving force for the mass transfer in humid air. The distance U-R represents the temperature difference between bulk water (U) and interface (I), the driving force for the heat transfer.

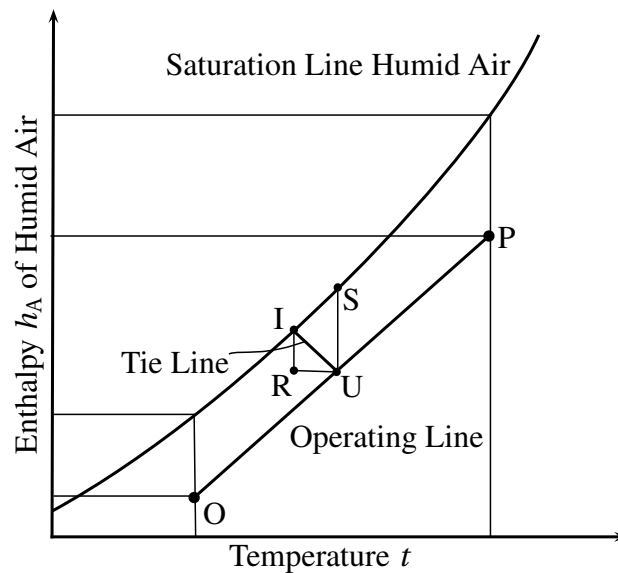


Figure 4.16: Schematic to explain Tie Line and Operating Line in the Humidifier. Diagram adapted from [97, p. 246].

Fig. 4.17 gives an example of a 1-D simulation result for the dehumidifier. Tie lines show that the driving forces in the lower part of the dehumidifier are not efficient due to the small driving differences, in relation to the upper segments. An optimized case should strive for an approximately 'parallel' position (i.e. same distance of the operating line to the saturation line) so that the approach of both lines is avoided.

4.5.2 Number of Transfer Units and Height of Transfer Unit

For the dimensioning of columns, the number of transfer units (NTU) and the height equivalent to one transfer unit (HTU) are commonly used.

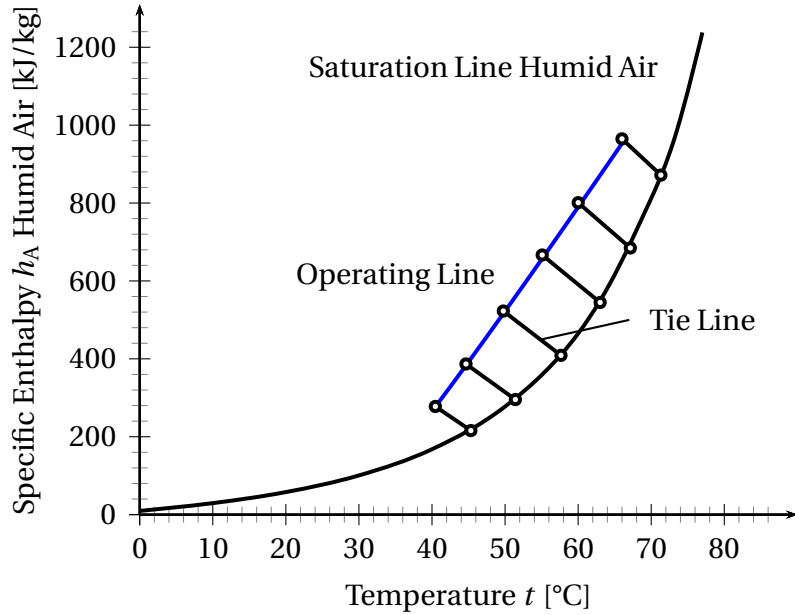


Figure 4.17: Example 1-D Simulation showing operating line of the dehumidifier (blue), saturation line of humid air and tie lines. The temperature t indicated on the x-axis refers to the interface temperature t_I when the saturation line is regarded and to the water temperature t_W at the corresponding cross section when the operating line is regarded.

The equation which is required to determine the number of transfer units (NTU) follows from Eq. (4.11) and Eq. (4.35) and by neglecting the sensible heat of the condensate:

$$\dot{G} \cdot dh_A = \alpha_W \cdot (t_W - t_I) \cdot dA_\alpha + d\dot{L} \cdot h_{W,I} = \sigma_{\text{evap}} \cdot (h_{A,I} - h_A) \cdot dA_\beta. \quad (4.37)$$

The NTU describes the ‘difficulty’ of the heat and mass transfer process [69].

Number of Transfer Units on the Gas Side

Assuming that both exchange surfaces are equal Eq. (4.37) transforms to:

$$dA = \frac{dh_A}{h_{A,I} - h_A} \cdot \frac{\dot{G}}{\sigma_{\text{evap}}}. \quad (4.38)$$

Integration of Eq. (4.37) leads to:

$$A = \int_{h_{\text{in}}}^{h_{\text{out}}} \left(\frac{1}{h_{A,I} - h_A} \cdot \frac{\dot{G}}{\sigma_{\text{evap}}} \right) \cdot dh_A. \quad (4.39)$$

If the heat transfer resistance $1/\alpha_W$ in the liquid phase is neglected¹², the tie line matches the distance S-U in Fig. 4.16. Consequently, this enthalpy difference is used. In this case, the integral is defined only with the vertical difference S-U (only gas side resistance). This integral is defined as the number of transfer units for the gas side NTU_G , also referred to as the Merkel number Me . The assumption that $\dot{G}/\sigma_{\text{evap}}$ is constant allows the transformation of the equation and to define the number of transfer units:

$$A = \frac{\dot{G}}{\sigma_{\text{evap}}} \cdot \underbrace{\int_{h_{A,\text{in}}}^{h_{A,\text{out}}} \frac{dh_A}{h_{A,S} - h_A}}_{NTU_G}, \quad (4.40)$$

$$NTU_G \equiv \int_{h_{A,\text{in}}}^{h_{A,\text{out}}} \frac{dh_A}{h_{A,S} - h_A}. \quad (4.41)$$

This simplification can also be applied if $1/\alpha_W$ can not be neglected. In this case, the transfer coefficient σ_{evap} is adjusted accordingly.

Height Equivalent to one Transfer Unit on the Gas Side

With $A = V \cdot a_{\text{pack}}$ and $V = A_{\text{cross}} \cdot Z$ leads to the equation for the height Z of the transfer column:

$$Z = \underbrace{\frac{1}{A_{\text{cross}} \cdot a_{\text{pack}}}}_{HTU_G} \cdot \frac{\dot{G}}{\sigma_{\text{evap}}} \cdot \int_{h_{A,\text{in}}}^{h_{A,\text{out}}} \frac{dh_A}{h_{A,S} - h_A} = HTU_G \cdot NTU_G. \quad (4.42)$$

The integral on the right side of Eq. (4.42) can be graphically analyzed [6, p. 64] to determine NTU_G . This equation defines the height HTU_G of one transfer unit. The volume V_{pack} of the column can therefore be calculated for a given cross section A_{cross} according to:

$$V_{\text{pack}} = Z \cdot A_{\text{cross}} = (HTU_G \cdot NTU_G) \cdot A_{\text{cross}}. \quad (4.43)$$

The simplification can lead to considerable deviations. Therefore a detailed numerical investigation of HTU is not recommended. But, the heat and mass

¹² The Merkel-approach uses this assumption [68].

transfer relations within the HD system are visualized and unfavourable conditions or dimensions are displayed by applying this concept.

Numerical HD models which are based on overall energy and mass balances for the top and the bottom of the columns are incapable to diagnose problematic heat and mass transfer conditions along the height of the column. The usage of logarithmic mean values to simplify computation [82] hides the fact that there may be segments of the columns in which NTU are very large.

The numerical approach outlined in this chapter considers the actual occurring driving force along the height of the humidifier and dehumidifier columns. They are based on the conditions at the interface between water and humid air.

Seifert [90, 91] reports the good agreement of the numerical simulation with experimental results. Chapter 6 applies the here described visualization approach for the interpretation of experimental results provided in the next chapter.

5 Experimental Investigations

The Institute for Thermodynamics at the Technische Universität München (Germany) started research on solar powered desalination in 2000 [94]. Experiments on humidification processes with forced convection followed in 2004. Investigations for the presented work started in 2007. Since then, several test rigs were designed, built, operated and optimized in the laboratory of the Institute. Additionally, field tests in Greece in 2010 and Dubai in 2012 were undertaken to demonstrate plant operation under real conditions. The experiments investigated the influence of selected operating parameters on the performance of single and two-stage HD systems. The applied temperature control method was also tested. These long-term experiments also revealed challenges and opportunities during setup, operation and maintenance.

5.1 Experimental Setup

5.1.1 Single and Two-Stage Configuration

Investigations on the system behavior of HD started with a single-stage closed-air water-heated HD system setup, shown in Fig. 5.1a. After several alterations and improvements on the system and the experimental test setup, a two-stage closed-air water-heated HD system setup was built and tested, as shown in Fig. 5.1b. The main parameters and ranges of operating parameters are given in Table 5.1. Annex B contains an overview of the used instrumentation.

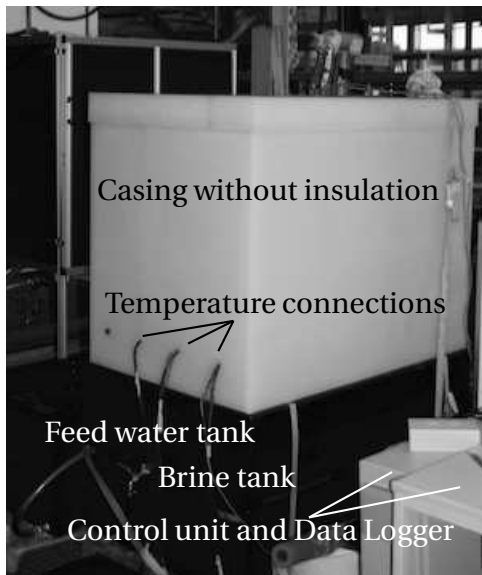
The two-stage closed-air water-heated configuration is depicted in Fig. 5.1b. The total exchange surfaces in humidifier and dehumidifier remained identical as for the single-stage setup. The testing equipment is shown in Fig. 5.2. The preheated feed water from the bottom stage dehumidifier entered the second stage.

The schematic of the experimental single-stage test setup is shown in Fig. 5.2a whereby the numbers refer to the elements exemplified in the legend.

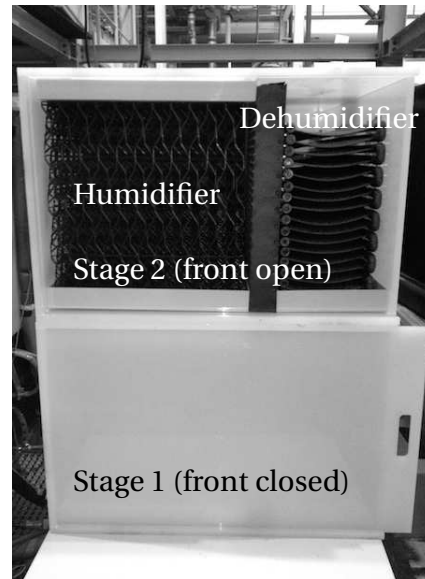
Humidifier (02) and dehumidifier (03) are placed within one casing (01). Heater (04), periphery and used measurement and control devices are shown and described in the following sections.

Table 5.1: Specifications of Experimental Setups. System Configuration: Single-Stage and Two-Stage Closed-Air Water-Heated HD Configuration with Natural Convection

Description	Indicator	Value / Range
Humidifier dimensions (single-stage)	length, width, Z	0.7 m x 1 m x 0.7 m
Dehumidifier dimensions (single-stage)	length, width, Z	0.3 m x 1 m x 0.7 m
Humidifier dimensions (two-stage)	length, width, Z	0.7 m x 1 m x 0.35 m
Dehumidifier dimensions (two-stage)	length, width, Z	0.3 m x 1 m x 0.35 m
Inlet temperature dehumidifier	TIR 03	15 ... 50 °C
Inlet temperature humidifier (<i>TBT</i>)	TIR 06	50 ... 90 °C
Water mass flow \dot{L}	FR 01	10 ... 350 kg/h
Electric heating power (laboratory) P_{el}	EC 01	0 ... 9 kW



(a) Single-Stage HD System

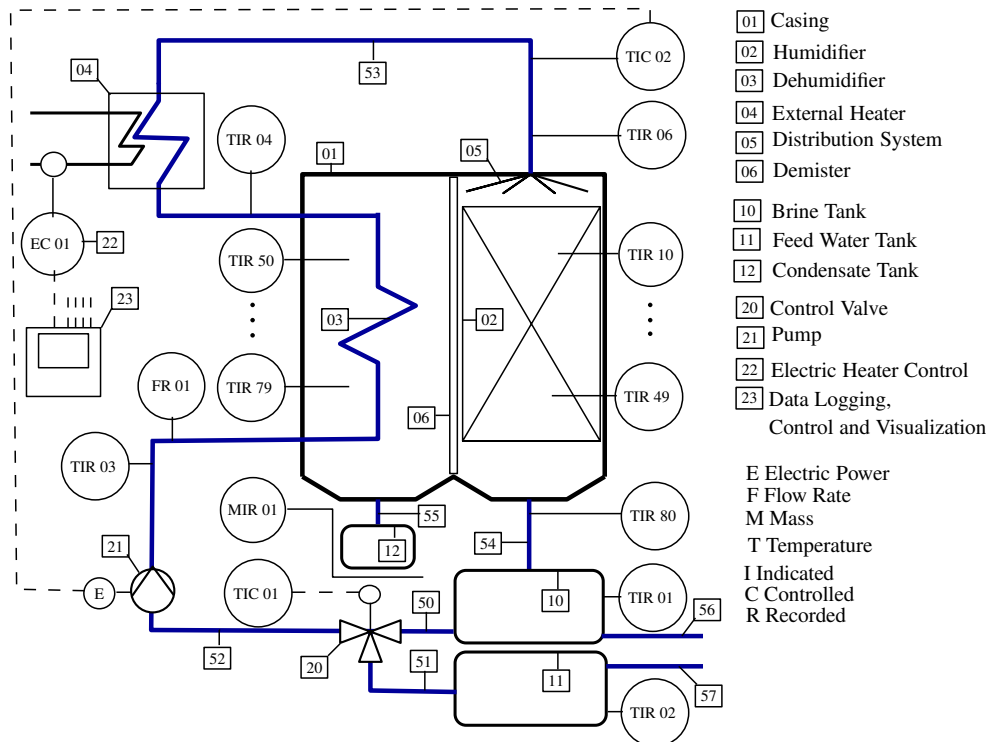


(b) Two-Stage HD System

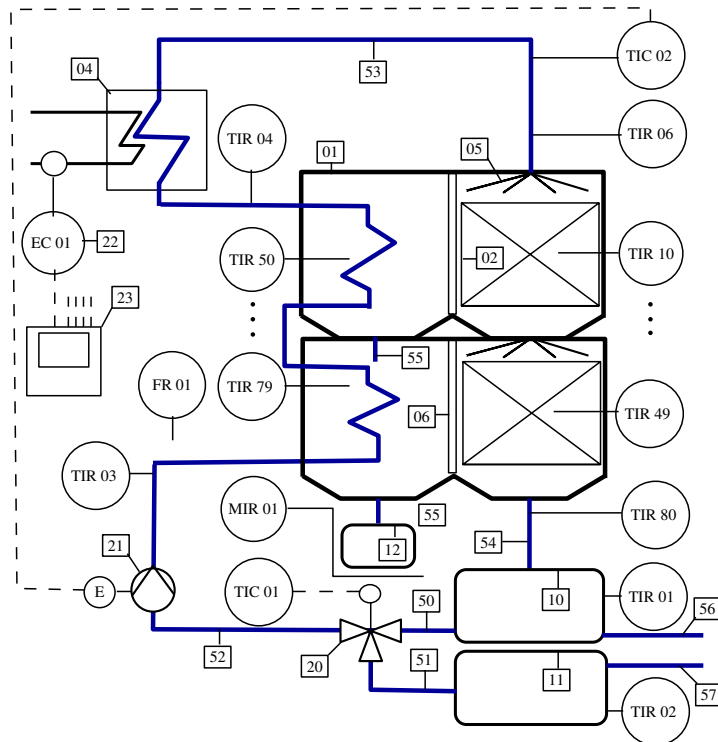
Figure 5.1: Experimental HD Setups at TUM

Material requirement considerations are essential for HD systems. Many experimental HD systems described in literature use plastic materials [8,

5.1 Experimental Setup



(a) Schematic of Single-Stage Closed-Air Water-Heater Experimental Setup



(b) Schematic of Two-Stage Closed-Air Water-Heater Experimental Setup

Figure 5.2: Overview Experimental HD Setups at the Institute of Thermodynamics, TUM

40, 71, 77]. Polypropylene (PP) was selected for the casing and a majority of the system components as it is durable, food-safe, cost effective, corrosion-resistant [21] and suitable for operating temperatures of up to 110 °C [5, p. E68]. In addition it is resistant against hot seawater; however, operating at high temperatures is limited by the increase of scaling and corrosion potential and needs to be considered when choosing the operation temperature range [101].

Water Flow

For experiments in the laboratory, tap-water was used instead of seawater to avoid corrosion on the electrical heating system. During the field tests, the system was run with local seawater. The system was operated as follows: the SHURflo (Type: 2088-313-145) diaphragm pump (21) feeds water into the tubing of the dehumidifier. The required 12 V DC voltage allows operation with photovoltaics. The water flows inside the tubes of the dehumidifier where it is preheated, passes the (electric or solar) heating device (04) and is spread with the distributor (05) onto the packing of the humidifier.

To prevent water droplets from entrainment into the dehumidifier, a demister (06) is placed between humidifier and dehumidifier. The condensate is released into the container (12). A digital scale (MIR 01) with registration and indication records the weight of the condensate.

The brine is collected in container (10). The storage tank (11) contains feed water. With a temperature- controlled valve (20) the mass flows of both tanks are mixed to preset set point temperature, i.e. feed water inlet temperature $t_{W,1}$, with control unit (TIC 01). The brine temperature in tank (10) increases during the startup phase. The transient phase is discussed and analyzed in section 5.3.2.

During this time, water is only taken from the brine container (10) until the set point temperature is reached. To keep this preset temperature, water from the cooler fresh water tank (11) is added. This measure reduces the time of the start-up phase and the influence of the inlet water temperature on the performance ratio is investigated.

Another temperature control is installed for the top brine temperature T_{BT} , which is controlled to a preset value with the PID-control unit (TIC 02). The control unit adjusts the frequency of the pump (21) and thus the mass flow \dot{L} of the feed water.

Air Flow

The HD experimental setup is designed for natural convection air flow at ambient pressure. As mentioned in chapter 5.1.1, a demister prevents droplet entrainment from the humidifier into the dehumidifier. According to Stoke's resistance law [37, p. B60], only very small droplets ($d_d < 0.1$ mm for $u_G = 0.2$ m/s) would be carried by natural convection air flow from the humidifier to the dehumidifier. Such small droplets may be produced when spray nozzles for water distribution in the humidifier are used.

The water distribution system is described in chapter 5.1.3. It creates droplets only by gravitational and surface tension forces so that entrainment by very small droplets is avoided.

Setups with and without a separation wall between humidifier and dehumidifier were investigated, as suggested by Müller-Holst [71].

5.1.2 External Heater

An electrical water heater is used as external heater (04) for the laboratory setup at the TUM. Solar collectors are used for field-tests in Greece and Dubai.

Electrical Water Heater

For investigations in the TUM laboratory, the test rig is equipped with a continuous-flow water heater, manufactured by DEW Dueblein. The electrical heating power of maximum 9 kW is controlled with a power-transformer by adjusting the voltage. The system is calibrated with water temperature and water mass flow measurements. The control system could also be configured to trigger time-dependent changes of power to simulate solar irradiation. The reference value for the external heating power \dot{Q}_{ext} is set as 4.7 kW for all of the here presented experimental data.

Solar Water Collectors

For experimental investigations using solar energy, two solar collector types were tested: flat plate collectors and vacuum heat pipe collectors. Earlier experimental investigations for the desalination systems included EPDM plastic swimming pool absorbers within a double glazed housing. Despite promising results and potentially low production costs, flat plate collectors are not suitable due to the low efficiency for the desired water outlet temperature of 85 °C. Therefore, vacuum heat pipe solar collectors were used for the field tests in Corfu, Greece (Type: Vacano-HPV-12-AL) and in Dubai, UAE (Type: Westec WT-B 58).

Thermal losses are low for heat pipe collectors due to vacuum insulation and the small heat transfer area at the collecting pipe at the upper end of the tube. An advantage of such a collector coupled with desalination systems is that only this collecting pipe is in contact with seawater. For the short experimental investigations standard collector pipes were used.

For future experimentation, the collecting pipe surface should be made of sea water resistant material, e.g. carbon or metal with resistant inliner. The setup tested in Greece is shown in Fig. 5.3. The fresh water production for this configuration reached up to 60 liters per day with a performance ratio PR ranging from 1.5 to 2.9.

5.1.3 Humidifier

The humidifier acts as a direct contact heat exchanger between water and air flow. It consists of a packed column with a distribution system situated on top. Seawater is distributed as droplets onto the packing as described below.

Packed Column

Packing material within the humidifier increases the contact area between water and air and reduces the velocity of the down flowing water droplets and water films. An optimized humidification process with small exergy losses requires large air-water interfacial contact areas along with high heat-transfer



Figure 5.3: Field Test of Solar Powered Single-Stage HD System in Corfu, Greece

and mass-transfer coefficients. This is supported by an advanced packing structure design¹.

Table 5.2: Manufacturing Data of Packing (Hewitech NC20)

Description	Parameters	Value / Range
Material		Polypropylene
Volume Humidifier	V_{hum}	0.4752 m^3
Channel Width	d_{pack}	20 mm
Relative Void Fraction	ϵ	$0.96 \text{ m}^3/\text{m}^3$
Specific Surface	a^*	$125 \text{ m}^2/\text{m}^3$
Geometric Packing Surface	$A_{\text{geo,pack}}$	47.5 m^2
Effective Packing Surface	$A_{\text{eff,pack}}$	59.4 m^2
Height of Humidifier	Z	700 mm

Packed columns, as used for process engineering applications, can contain random or structured packings. For the humidifier, both types were investigated. The following random packings, all made from polypropylene, were tested: Hiflowrings (type Rauschert, $d_{\text{pack}} = 28 \text{ mm}$, $a = 190 \text{ m}^2/\text{m}^3$,

¹ An overview of used materials for packings in HD humidifier reported in literature is summarized in [80].

$\epsilon = 0.92 \text{ m}^3/\text{m}^3$), Pall-Rings ($d_{\text{pack}} = 25 \text{ mm}$, $a = 220 \text{ m}^2/\text{m}^3$, $\epsilon = 0.92 \text{ m}^3/\text{m}^3$) and ENVIPAC spherical packing (type Envicon, $d_{\text{pack}} = 32 \text{ mm}$, $a = 138.9 \text{ m}^2/\text{m}^3$, $\epsilon = 0.936 \text{ m}^3/\text{m}^3$).

Packing structures can be defined by three parameters, provided by the manufacturers: the geometric surface area a of packing per unit volume, the effective surface area a^* of packing per unit volume and the void fraction or porosity ϵ [64]:

$$a = A_{\text{geo,pack}}/V_{\text{hum}}, \quad (5.1a)$$

$$a^* = A_{\text{eff,pack}}/V_{\text{hum}}, \quad (5.1b)$$

$$\epsilon = (V_{\text{hum}} - V_{\text{solid}})/V_{\text{hum}}. \quad (5.1c)$$

The effective surface $A_{\text{eff,pack}}$ of a packing can be significantly larger than the geometrically available surface $A_{\text{geo,pack}}$: Due to special design of the packing, water films can be created between the fins which increases the surface area for heat and mass transfer and can contribute to higher water production rates and higher performance ratio PR .

Apart from a large surface area and high porosity, the following criteria for the selection of packing material for HD with natural convection need to be considered: high wettability of the material, low flow resistance of humid air, high mechanical, thermal and chemical stability, low investment costs and simple maintenance.

Fig. 5.4 shows the structured packing Hewitech NC20 Module (polypropylene, channel width $d_{\text{pack}} = 20 \text{ mm}$, $a \approx 100 \text{ m}^2/\text{m}^3$, $\epsilon \approx 0.96 \text{ m}^3/\text{m}^3$) selected for the presented experiments. According to the data provided by the manufacturer, the effective specific surface is $a^* \approx 125 \text{ m}^2/\text{m}^3$. For systems with natural convection, the low pressure loss is of special importance, as described in chapter 3.3.4. The relative void fraction ϵ_{pack} dominates the pressure drop.

The factor $(1-\epsilon)/\epsilon^2$ in Eq. (3.7) is 0.0945 for Pall-Rings ($\epsilon = 0.92 \text{ m}^3/\text{m}^3$) and only 0.0434 for the Hewitech NC20 packing. Therefore, the structured packing was selected as the preferred humidifier filling for the experimental investigations despite the lower specific surface area which usually is the major selection criterion. Additionally, the high porosity ϵ_{pack} , which translates to a low mass,



Figure 5.4: Humidifier Packing (Hewitech NC20), Experimental Setup TUM

is advantageous for transient operation as described in chapter 5.3.2.

Scale formation is also of less relevance as cleaning of the packing involves little effort. The stable and compact structure simplifies the configuration, assembly and maintenance.

Distribution System

Significant effort and several development steps were required for the development of an advanced distribution system. Water needs to be distributed evenly across the whole cross section of the dehumidifier for varying low water flows without blocking and without creating fine droplets which would be carried by the air flow towards the dehumidifier [69, p. 267].

Various distribution systems, such as nozzles or shower heads, were tested with minor success, mainly because of scale formation and the appearance of fine droplets. Clogging of the outlet holes can occur due to scale formation when wet surfaces dry repeatedly. This leads to a disfunction of the complete system. Apart from scale formation in the dehumidifier, this is the main cause for system failure.

A promising design of the distribution system is shown in Fig. 5.5a. It uses a fleece situated on top of the openings for an even distribution, as shown in Fig. 5.5b, to ensure that openings in the distributor tray are continuously kept wet. The surfaces and openings don't dry and therefore scaling is avoided. Bio-fouling in the distributor is not expected due to the applied high temperatures.

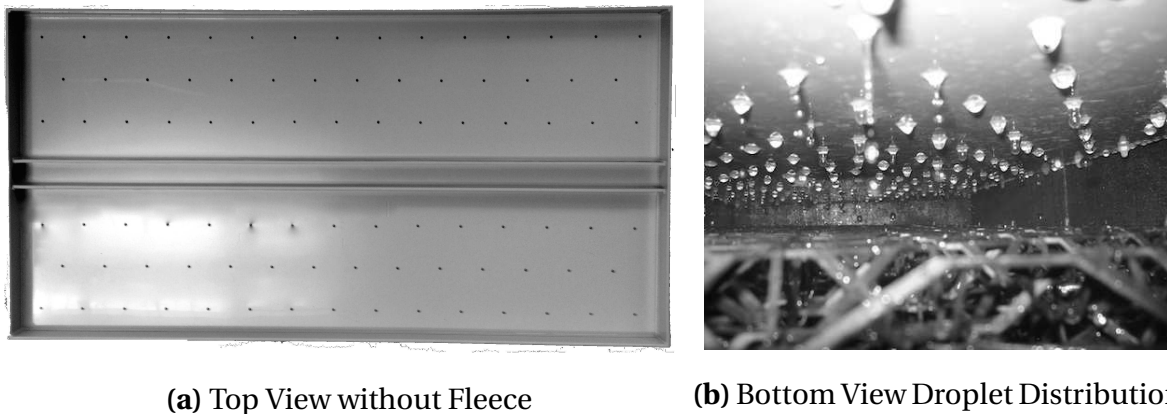


Figure 5.5: Distribution System and Droplet Distribution during Operation

5.1.4 Dehumidifier

For HD systems with indirect dehumidification, several dehumidifier designs and configurations are known from literature, e.g. plastic plates [71], tube mats [92] or aluminium tubes with fins [46]. Thermal conductivity of polypropylene plastic lies between 0.11 to 0.17 W/(m · K). In contrast, austenitic stainless steel has a thermal conductivity which is 15 W/(m · K), i.e. about 100 times higher [15, p. D-72]. Numerical simulation results described in chapter 4 show that for dehumidification, the thermal conductivity of the material does not play a dominating role. Practicality, costs and durability are in favour of the used plastic material.

Table 5.3: Data Overview Dehumidifier

Description	Parameters	Value / Range
Material		Polypropylene
Length of tubes	l	480 mm
Number of tubes per mat layer	N_t	48
Number of layers	N	18
Inner diameter	$d_{i,pack}$	3.5 mm
Outer diameter	$d_{a,pack}$	4.5 mm
Cross section	A_{cross}	0.3 m ²
Porosity (relative free volume)	ϵ_{pack}	0.5 m ³ /m ³
Total Surface	A	5.8 m ²
Height of Dehumidifier	Z	700 mm

The dehumidifier design developed at the institute changed significantly over

time. A special focus is set on material selection to ensure temperature resistance ($> 80\text{ }^{\circ}\text{C}$), qualified as food safe and low investment costs. The latest setup uses a polypropylene (PP) tube bundle heat exchanger as shown in Fig. 5.6. It consists of several stacked polypropylene tube mats with connecting pipes. The water flows from one mat into the other. Table 5.3 gives an overview of the humidifier data.



Figure 5.6: Dehumidifier for Singe-Stage Experimental HD Setup; Total Surface Area: 5.8 m^2

5.2 Measurement and Control

For the compilation of experimental data, an Agilent 349704A data logger with several Channel Generator Purpose Multiplexer Cards is used. The data logger is connected to a computer with a customized Labview© interface, developed to constantly measure and record data, to control the test setup and to oversee data and plant behavior. Data are stored in a text file which is then used for further data processing.

5.2.1 Temperature Measurement

Up to 80 thermocouples of K-type are used (TIR01 - TIC79) for the temperature measurements. A Kobold Type DPM-L3 (FIR 01) mass flow meter is used as measurement device for the feed water mass flow. The value is indicated on the Labview control panel and recorded. The PID control device also sends the pump frequency to the data logger.

During the field test, a solar pyranometer measures the solar irradiation. For the laboratory tests, the power control of the water heater allows the control

of the heat input and also the running of preset programs, e.g. to control the power which corresponds to the solar insolation during the day.

Water temperatures in connecting ducts can be determined with high precision ($t_{W,in}$, $t_{W,deh,out}$ and $t_{W,hum,in}$). Measuring the temperature of free flowing water within the humidifier, in particular $t_{W,hum,out}$, is challenging and is measured with far less precision. Errors also occur due to the transient behavior of the system. These errors can be reduced by reproducing experiments and averaging the results. For experimental results, a minimum of five experimental test runs have been obtained. The accuracy of single temperature measurements lies between ± 1 °C.

Measurements of the humid air temperature have a lower accuracy than the water temperatures because condensing water vapor falsifies the results. In their report Seifert *et al.* [91, p. 12, Fig. 6] published a deviation of ± 1.8 K between the measured temperatures of humid air and the temperatures from the simulation of the studied dehumidification. A temperature difference corresponds to a deviation of the saturation humidity X_{sat} . The mean slope $\Delta X_{sat}/\Delta t$ of the saturation line in the temperature region of 40.5 °C to 75 °C is 0.0123 1/K. Therefore a temperature error of ± 1.8 K results in a deviation of the absolute humidity of 0.022 kg/kg.

5.2.2 Condensate Mass Flow Rate Measurement

A digital scale is connected to the data logging unit to determine the condensate mass flow \dot{M}_{Cond} from the recording in the given time. The condensate mass flow and the external heat input \dot{Q}_{ext} are the necessary values for the determination of the Performance Ratio PR . It was initially assumed that the condensate mass flow can be determined with a satisfactory accuracy to interpret the measured data to draw conclusions regarding the overall effect of improvement measures. The water quality is determined manually with a conductivity measurement device (BC-Electronics, Model C135).

It became evident from the numerical investigations of the Performance Ratio PR , as shown in the next chapter, that the error is possibly in the range of 20% because the small amounts of water may not be detected correctly by the scale

within the selected time frame as any physical contact with the system causing vibration of the dehumidifier may have changed the liquid hold up.

A considerable margin of error needs to be applied to the water mass flow measurement data, as also shown in the next chapter where this error is further investigated by applying an adapted Performance Ratio PR_{HD} which is based on measurement values that can be determined with a greater certainty.

5.2.3 System Control

The aim of controlling the system is to maintain preset operating values during changing conditions, e.g. the start-up or when using solar energy. As the preferred control strategy, TBT is selected as the main controlled process variable with a constant set value, e.g. 85 °C.

The water mass flow is the actuating variable: the PID control unit sends a digital signal to the control unit of the pump to adjust the stroke frequency and the water mass flow respectively. The control unit (manufacturer: PMA, Model: ECO24) adjusts the system according to the solar radiation when operated with solar collectors. This control mechanism was found to be advantageous compared to the alternative, whereby the mass flow rate remains constant for a given external heat input, leading to changing TBT during operation. For significant change in irradiation, e.g. a moving cloud, the system would rapidly cool down resulting in a significant loss in production due to the additional starting-up phase in these time periods.

When coupling the system with a heat source with a constant temperature over a long period (e.g. waste heat from other processes) it may be advantageous to set the water mass flow to a constant value whereas for a transient heat input (solar power) the TBT may be set as a constant value.

The operation temperature region, at which humidification takes place, is dependent on the temperature $t_{W,in}$ (i.e. TIR 03 in Fig. 5.2) of the feed water flow into the dehumidifier. This temperature can be adjusted, given a constant sea water feed temperature, by mixing the cool sea water with brine. This of course is limited by the concentration and the scaling behavior.

With increased \dot{Q}_{ext} , the necessary heat and mass transfer surfaces can be reduced for a given condensate output as the driving temperature difference increases. This obviously reduces the performance ratio; however, investment cost can be reduced if \dot{Q}_{ext} is increased due to higher irradiation. $T_{W,\text{in}}$ is not a direct function of the external heat input but depends on the available feed water temperature and optional blending with available brine to recover available heat from the brine and reduce water input.

A system consisting of a water tank (10) for brine recirculation, a feed water tank (11) with cool water (may be replaced by a direct intake from the water source) in combination with a three-way temperature valve (20) for temperature regulation stabilizes the system's behavior. With the valve, the inlet temperature into the dehumidifier is controlled. Seifert *et al.* [91] describes this setup (with a similar recirculation approach) in the same year as Soufari *et al.* [93].

During the start-up phase, water is recirculated within the system, i.e. a close-air closed-water configuration where no water from the feed water tank (11) is used. As soon as the inlet water temperature t_{in} reaches the value set for TIC 01 the system changes to an open-water configuration, i.e. the control valve (20) opens and cooler water from the feed water tank (11) is mixed with water from the brine water tank (10). The pump (21) requires a certain water level within the brine tank (10), i.e. the inlet feed water t_{in} temperature is lower than the humidifier outlet temperature $t_{W,\text{hum},\text{out}}$. Therefore, the closed-water configuration during the start-up phases could not be used to its full potential due to technical limitations.

5.3 Experimental Results and Observations

5.3.1 Dropwise Condensation

The here distinguished condensation process considers the conditions within a closed-air HD setup with natural convection with a polypropylene tube bundle dehumidifier. The findings concerning dropwise condensation on plastic tubes (PP) may not be adaptable to other configurations or materials.

The common perception gained from literature attributed to dropwise condensation is that droplet growth and removal occurs with high rates (compare Fig. 3.3) and consequently high heat transfer rates are achievable. This perception is not valid in the presence of a considerable concentration of NCG. Due to the presence of NCG in HD systems, heat and mass transfer is highly reduced, especially for free convection. Droplets remain at their position on the surface for a long time. The main influence due to high volume contraction from the vapor to liquid phase [36, p. 307, 4, p. 478 ff] is diminished by the presence of NCG [4, p. 461 ff].



Figure 5.7: Dropwise Condensation on the Top Layer of the Tubular Polypropylene Heat Exchanger Surface of the HD Single-Stage Setup ($t_{A,deh,in} \approx 75\text{ °C}$, $t_{W,deh,out} = 68\text{ °C}$, $d_{tube} = 4.5\text{ mm}$)

Fig. 5.7 shows a photo of the condensation drops on the tubular heat exchanger surface within the experimental HD setup during operation. The illustrated experimental humidifier setup has been in use for several years. A transition to film condensation over time could not be observed.

The photo shows the top row of the dehumidifier heat exchanger which is covered by droplets. The droplet diameter varies widely. The photo is taken with a small waterproof endoscope camera. The camera lens was heated to humid air temperature ($> 70\text{ °C}$) to avoid condensation on the camera lens.

The following sequences of dropwise condensation on the plastic tube bundle

in the dehumidifier can be observed:

1. Rolling down of a large droplet with high velocity. This clearing process on a certain area occurs within a very short time (below one second).
2. On its way, the large droplet merges with other droplets and leaves behind a wiped trail.
3. On this trail, a high population density of small droplets appears shortly after.
4. Droplets grow due to condensation and due to merging with contacting droplets (the growth process lasts several minutes).
5. Areas between the droplets seem to be dry.
6. No additional droplets are created during the growth process. Merging leads to a reduction of the number of droplets.
7. During the growth process, droplets change their position only when merging or being captured by droplets moving down.
8. Some droplets become unstable, they flow down and the sequence starts again with the clearing process. If a droplet becomes unstable as it reaches a critical size or by vibrating surfaces or by merging with another droplet, it flows down the cooling surface.
9. Droplet motion during condensation in the dehumidifier of HD is very slow, except during the very short processes of clearing and merging.
10. Falling droplets clashing on the below tube clears a certain area. As this cleaning process continually occurs, the maximum droplet diameter is not reached for the affected droplets.

Micro droplets appear at the trail of the droplet with dry patches between the micro droplets. It can be assumed that heterogeneous nucleation immediately takes place at the wiped surface after passing of a large droplet. There is no more nucleation in the presence of neighbouring liquid surfaces for condensation at this temperature.

Droplets grow as condensate forms and by merging with smaller surrounding droplets. Vapor condenses at the droplet surfaces from sub-cooled humid air. Condensation takes place on the liquid surface. When droplets contact each other, the smaller droplet is incorporated by the larger droplets because droplets with a larger radius R have a lower inner pressure due to the surface

tension σ , according to $\Delta p = 2 \cdot \sigma / R$ [33, p. 355]. The droplet size on the tube surface depends on time, its position on the surface of the tube, and on the position of the tube within the tube bundle configuration.

These findings are an important element for the mathematical description of dropwise condensation in the HD system, as outlined in chapter 4.4.3.

5.3.2 Data Transient and Steady-State Phases

A large amount of experimental data is obtained from test runs with various system parameters. Fig. 5.8 shows results of a test run with a single-stage HD system and Fig. 5.9 a two-stage HD system with similar operating parameters. The figures indicate experimental results collected within 10,000 seconds after system start. The overall measurement time was usually chosen to be more than seven hours to validate that condensate water production rate remains constant over a longer time period. The considerable total operation time of the system gives an indication for maintenance requirements and component durability.

Four operating phases are distinguished: three transient phases (I-III) and a steady-state phase (IV). All phases are distinguished by temperature transitions which can be identified by sharp bends. This is the preferred method, especially for phase IV, during which the determination of the steady-state temperatures are difficult due to the marginal temperature changes.

The transition temperatures for each phase are highlighted in Fig. 5.8 (a) as points A, B and C. The condensate mass flow rate \dot{M}_{Cond} which was measured with the electronic scale is not shown as experimental results are captured over long time intervals. Measurable and meaningful results are determined during the steady-state phase. The condensate mass flow rate is evaluated in chapter 6 together with discussion of the performance ratio. The reference value of the external electrical heating power \dot{Q}_{ext} is set to 4.7 kW for all temperature profiles.

Pre-heat phase (I): The HD system is initialized during this phase. The water mass flow rate \dot{L} is low and unstable. The externally heated water predominantly preheats the interior of the humidifier and dehumidifier. This phase

takes a few minutes and ends as soon as the packing material is pre-heated and the temperature in the humidifier reaches a point in which substantial evaporation takes place. This is indicated by the change of the slope of the humidifier outlet temperature $t_{W,\text{hum},\text{out}}$ profile, marked as A in Fig. 5.8 (a).

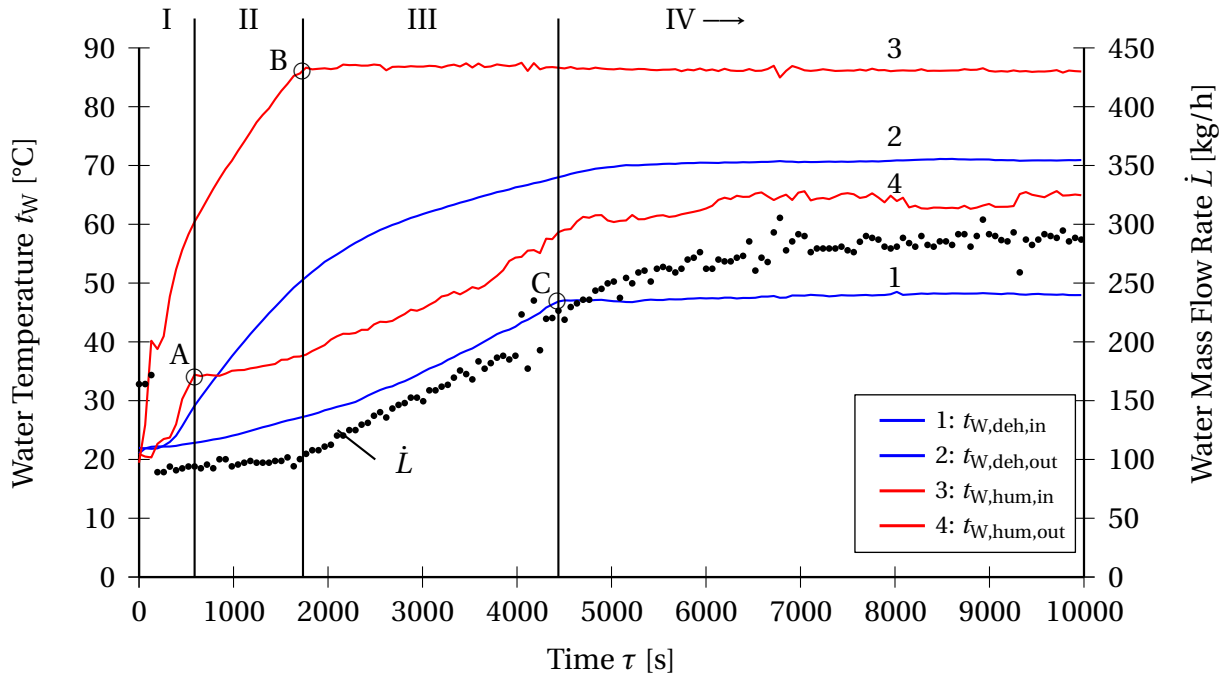
Heat-up phase (II): This phase ends as soon as $t_{W,\text{hum},\text{in}}$ reaches TBT , here 85 °C, marked as B in Fig. 5.8 (a). To decrease the duration of phase I to III, the feed water is taken from the brine tank (10), i.e. a closed-water mode, respectively batch mode. The water mass flow \dot{L} is low and remains almost constant during this phase.

Transition phase (III): The set target temperature $t_{W,\text{hum},\text{in}}$ (TBT) is reached (B) and remains constant by the controlled adjustment of the feed water mass flow \dot{L} . In this phase the dehumidifier water inlet temperature $t_{W,\text{in}}$ rises constantly until it reaches the set top inlet temperature. The evaporation rate increases, leading to a rising dehumidifier outlet temperature $t_{W,\text{deh},\text{out}}$.

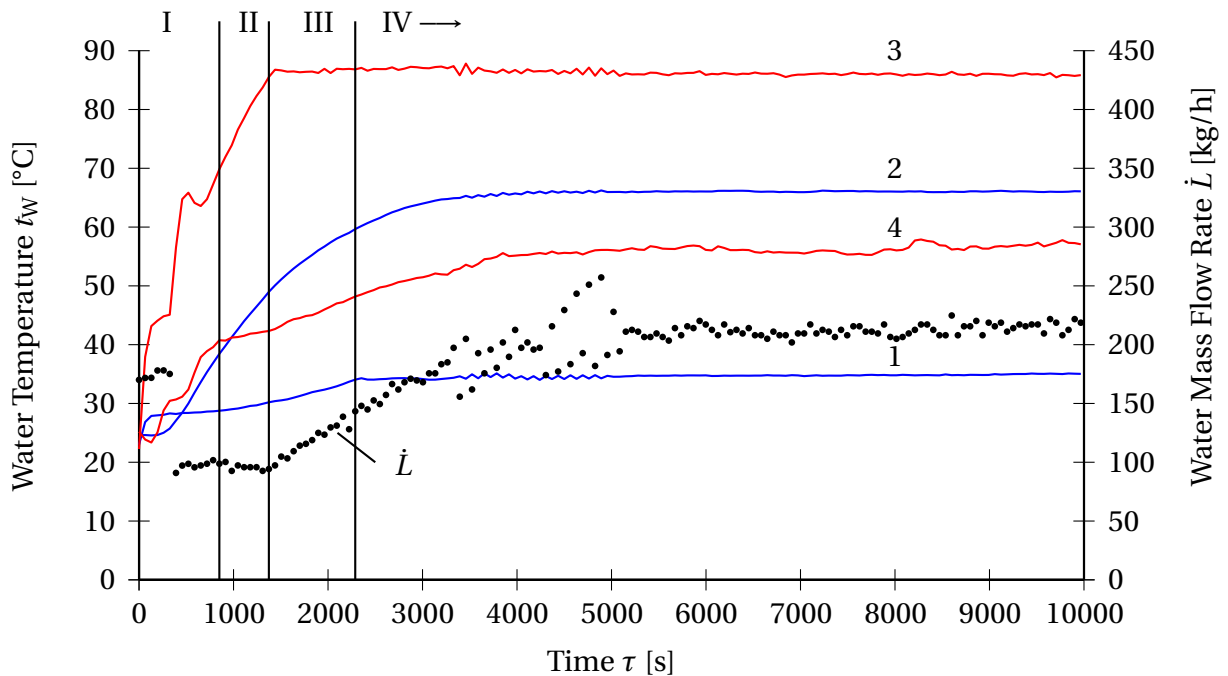
Steady-state phase (IV): In this phase the closed-water configuration changes to a continuous mode (open-water), i.e the feed water temperature $t_{W,\text{in}}$ reaches the set target value to stabilize all temperatures within the system. The set target value for $t_{W,\text{in}}$, marked as (C), is clearly distinguished; however, the steady-state conditions are reached some minutes later. This delay is negligible compared to the overall operation time (about seven hours). Table 5.4 gives an overview of data from measurements during the steady-state phase IV.

Fig. 5.8 and Fig. 5.9 show experimental results from a single-stage and two-stage HD system for set target values of 30 °C and 45 °C for the inlet water temperature and a target value of 85 °C for the top brine temperature. In all experimental test runs, the external heating \dot{Q}_{ext} is 4.7 kW. The inlet feed water temperature $t_{W,1}$ can be adjusted with a mixing valve. The following section discusses the transient phases I-III, whereas the analysis of the steady-state experimental results and the performance ratios is given in chapter 6.

Phase I and II represent startup transients for which the mass flow rates and temperature are similar in both cases. The duration of both phases are consequently very similar and quantitative interpretation not useful.

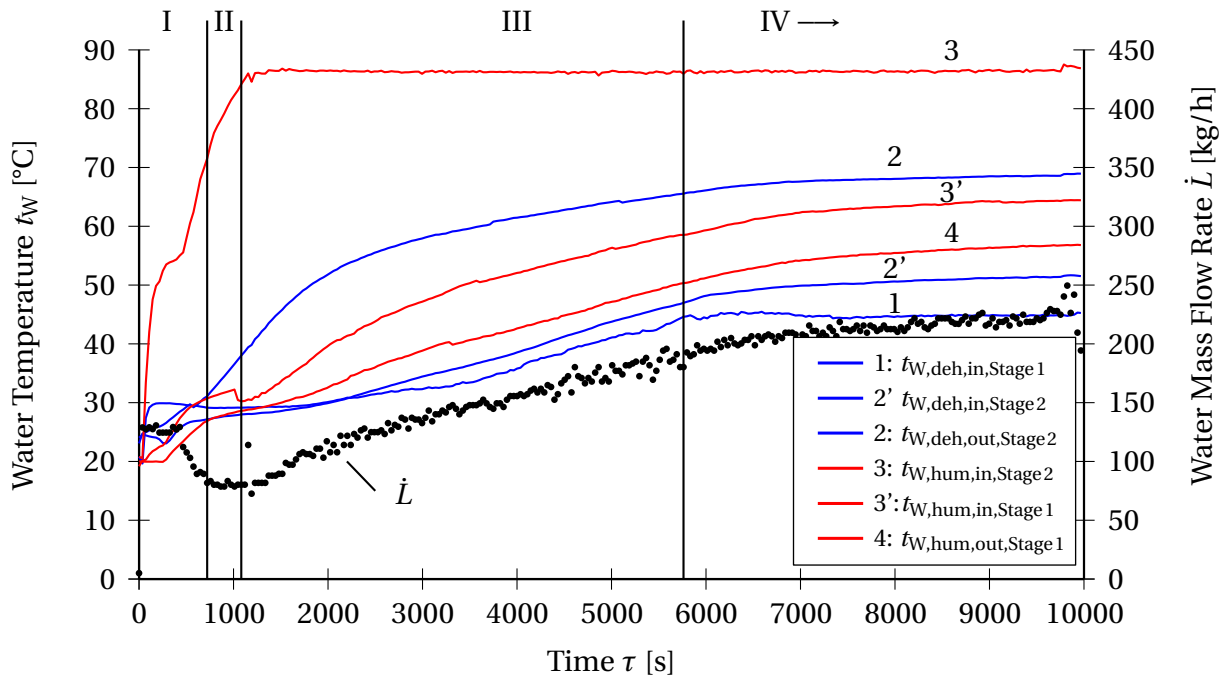


(a) Set Target Value (TIC 01) for Water Dehumidifier Inlet Temperature $t_{W,in} = 45\text{ }^{\circ}\text{C}$

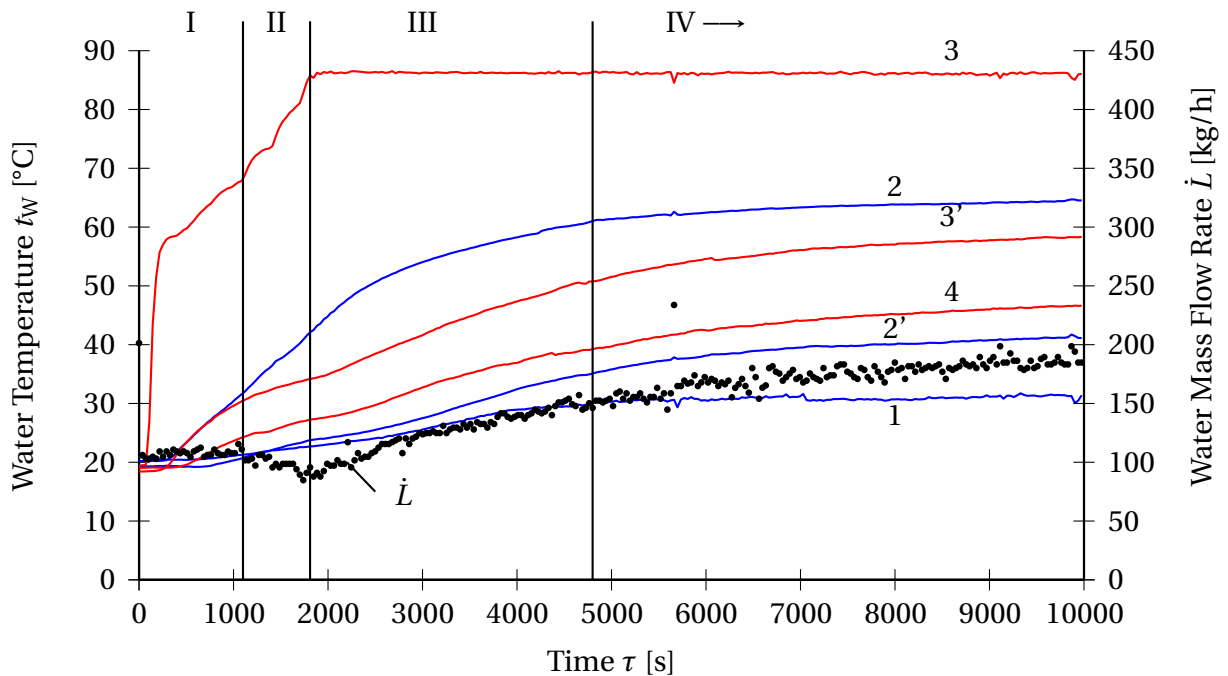


(b) Set Target Value (TIC 01) for Water Dehumidifier Inlet Temperature $t_{W,in} = 30\text{ }^{\circ}\text{C}$

Figure 5.8: Examples of Experimental Results with Single-Stage Closed-Air HD System for $t_{W,in} = 45\text{ }^{\circ}\text{C}$ and $30\text{ }^{\circ}\text{C}$. Operating Parameters: $\dot{Q}_{ext} = 4.7\text{ kW}$; Set $TBT = 85\text{ }^{\circ}\text{C}$ ($t_{W,hum,in}$ during Phase III and IV)



(a) Set Target Value (TIC 01) for Water Dehumidifier Inlet Temperature $t_{W,in} = 45\text{ }^{\circ}\text{C}$



(b) Set Target Value (TIC 01) for Water Dehumidifier Inlet Temperature $t_{W,in} = 30\text{ }^{\circ}\text{C}$

Figure 5.9: Examples of Experimental Results with Two-Stage Closed-Air HD System for $t_{W,in} = 45\text{ }^{\circ}\text{C}$ and $30\text{ }^{\circ}\text{C}$. Operating Parameters: $\dot{Q}_{ext} = 4.7\text{ kW}$; Set $TBT = 85\text{ }^{\circ}\text{C}$ ($t_{W,hum,in}$ during Phase III and IV)

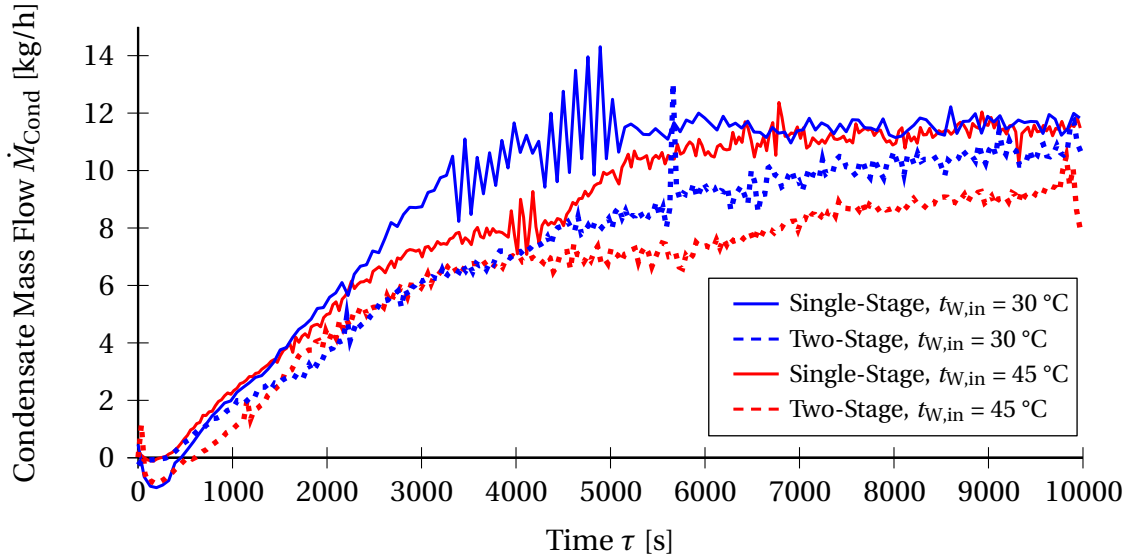


Figure 5.10: Condensate Mass Flow \dot{M}_{Cond} of Single-Stage and Two-Stage HD Setup. Total Experimental Duration: 30,000 s

For the single-stage HD setup (Fig. 5.8) the duration of the transition phase III is shorter for lower feed water inlet temperatures $t_{W,\text{in}}$ due to the lower feed water mass flow rate \dot{L} . This lower flow rate results from the higher water temperature difference between dehumidifier inlet and outlet and constant external heat input \dot{Q}_{ext} . The time for the transient phases can be further reduced by improving the system insulation and by recirculating hot brine produced during the previous day. Experimental results for a two-stage HD setup are shown in Fig. 5.9. The duration of the transient phase is also reduced with lower water inlet temperature $t_{W,\text{in}}$.

The condensate mass flow rate \dot{M}_{Cond} is indicated in Fig. 5.10 for the above mentioned cases. It is relatively stable or even declines for the combination of increasing water inlet temperature $t_{W,1}$ and increasing feed water mass flow rate \dot{L} . The condensate mass flow rate \dot{M}_{Cond} is calculated with the temperature difference Δt_{12} as per Eq. (4.21). It appears that the single stage configuration at lower inlet temperature achieves the highest condensate mass flow in initial phases. During the steady-state phase the condensate mass flow rates are similar for the single-stage configurations. The two-stage configurations show significant differences which are discussed in chapter 6.

5.3.3 Results from Experiments Steady-State Phase

The following experimental data sets in Tab. 5.4 represent data obtained for both single-stage and two-stage configurations with natural convection during the steady-state phase IV. The data show average values of at least five measurement test runs for each test setup. The target value for the feed water inlet temperature $t_{W,in}$ is set as a constant value for each test run. It was expected that increasing this parameter had a positive effect on the system performance.

Table 5.4: Overview Measurement Data of Experiments with Single-Stage (Numbers 1 – 6) and Two-Stage HD System (Numbers 7 – 12)

No.	$t_{W,in}$ °C	$t_{W,deh,out}$ °C	$t_{W,hum,in}$ °C	$t_{W,hum,out}$ °C	$t_{A,deh,in}$ °C	\dot{L} kg/h	\dot{M}_{Cond} kg/h	\dot{Q}_{ext} kW	PR -	
Single-Stage	1	26.6	63.8	86.4	48.4	68.1	181.9	10.3	4.7	1.39
	2	30.5	65.1	86.2	53.7	69.3	191.3	10.3	4.7	1.41
	3	35.0	66.1	85.9	57.2	70.2	209.8	10.3	4.7	1.38
	4	39.3	67.7	86.0	59.5	71.7	230.1	10.1	4.7	1.33
	5	43.4	69.4	86.0	62.7	73.6	254.3	10.4	4.7	1.36
	6	47.9	70.8	85.9	65.7	75.0	283.7	9.6	4.7	1.24
Two-Stage	7	25.5	62.0	86.2	42.6	78.9	163.1	10.4	4.7	1.47
	8	30.9	64.7	86.1	47.6	80.3	183.5	10.8	4.7	1.52
	9	36.1	66.3	86.1	51.1	81.0	199.3	11.2	4.7	1.58
	10	40.4	67.5	86.1	53.5	81.4	210.2	10.8	4.7	1.54
	11	45.4	69.3	86.3	57.6	82.1	231.6	10.7	4.7	1.51
	12	50.3	71.3	86.3	62.8	83.0	267.8	12.3	4.7	1.71

The displayed data are average values of experiments with the same target value for $t_{W,in}$, TBT and \dot{Q}_{ext} during steady-state conditions. The determined PR values are based on the condensate mass flow rate \dot{M}_{cond} . The PR values don't show a clear tendency with increasing water inlet temperature $t_{W,in}$ respectively with increasing feed water mass flow \dot{L} . As mentioned in chapter 5.2.1 the measurement error for condensate mass flow rates \dot{M}_{cond} is high. The next chapter introduces an adapted performance ratio which is dependent on temperature measurements and consequently applicable for a more precise analysis.

6 Analysis

This chapter analyzes the experimental data provided in chapter 5. An advantageous definition for the performance ratio is introduced to evaluate and analyse experimental results with adequate precision. Applying the conventional definition of the performance ratio is not recommended as it may lead to misinterpretation due to the high inaccuracy for the studied small system. The experimental data are used as input values for the 1-D numerical simulation to visualize heat and mass transfer relations described in chapter 4.3.

On this basis the limitations of the studied HD system with natural convection are identified. Suggestions to overcome these limitations are outlined in chapter 7.

6.1 Introduction Adapted Performance Ratio PR_{HD}

The conventional performance ratio PR , as defined in Eq. (3.2) is commonly used to determine the efficiency of a HD system or the Gained Output Ratio GOR which is further described in Appendix A. However, determination of the condensate mass flow \dot{M}_{Cond} is associated with high measurement errors due to the small quantity per time interval for systems, which have a low condensate mass flow and/or a high liquid hold-up from droplets adhering to the heat exchanger surface of the dehumidifier.

Because of these limitations, an advantageous performance ratio PR_{HD} is recommended to continuously determine the efficiency during operation with appropriate precision.

PR_{HD} is adapted from the conventional performance ratio PR to determine the multi-effectiveness of thermal desalination plants. It is particularly useful for small-scale systems and as optimization parameter during the operation.

The internally transferred heat flow \dot{H}_{int} is described in the next section as it is considered for the derivation of the definition of PR_{HD} .

6.1.1 Internally Transferred Heat Flow

Fig. 6.1 depicts the mass and heat flows in a HD system and the boundaries for the energy balances used to draw the similarity between the conventional PR and PR_{HD} .

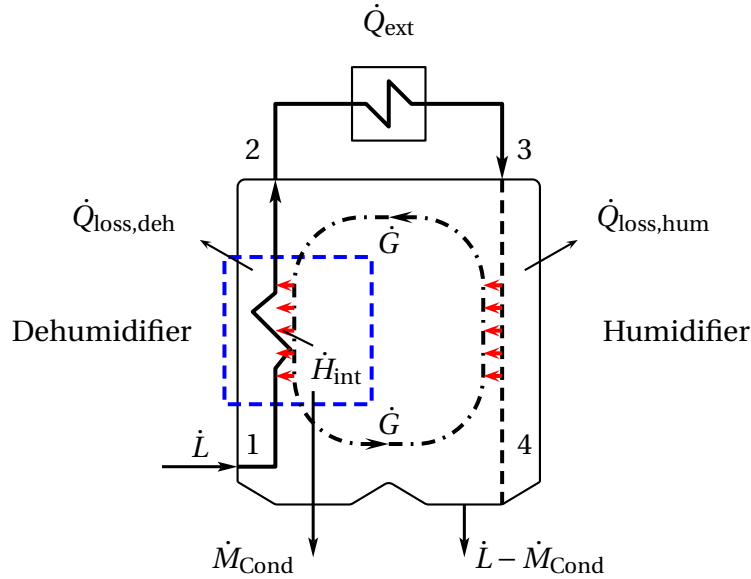


Figure 6.1: Overview Mass and Heat Flows in HD, System Boundaries Dehumidifier

The introduction of the internally transferred heat flow \dot{H}_{int} is the concept behind the adapted performance ratio PR_{HD} . The subscripts 1, 2, 3 and 4, which are part of the nomenclature of some parameters, refer to the location within the HD system, as indicated in Fig. 6.1.

The effectively transferred enthalpy \dot{H}_{int} preheats the feed water flow \dot{L} in the dehumidifier:

$$\dot{H}_{int} \equiv \dot{L} \cdot (h_{W,deh,out} - h_{W,deh,in}) = \dot{L} \cdot (h_{W,2} - h_{W,1}) \quad (6.1)$$

The energy balance of the dehumidifier is written in accordance with Eq. (4.19) and includes energy losses through heat transfer of the dehumidifier to the ambient:

$$\dot{G} \cdot h_{A,in} + \dot{L} \cdot h_{W,1} = \dot{G} \cdot h_{A,out} + \dot{L} \cdot h_{W,2} + \dot{M}_{Cond} \cdot h_{Cond} + \dot{Q}_{loss,deh} \cdot \quad (6.2)$$

6.1.2 Definition Adapted Performance Ratio PR_{HD}

The here proposed adapted performance ratio PR_{HD} relates the internally regained energy flow rate \dot{H}_{int} utilized for preheating the feed water in the dehumidifier to the external energy flow \dot{Q}_{ext} :

$$PR_{HD} \equiv \frac{\dot{H}_{int}}{\dot{Q}_{ext}}. \quad (6.3)$$

The multi-effect in HD is not created from multiple condensation processes (as it is applied for example in large-scale MED systems) but from the reduction of the external energy requirements.

For constant feed water mass flow rate \dot{L} , PR_{HD} can be approximated as the ratio of the temperature difference $t_{W,2} - t_{W,1}$ of feed water between inlet and outlet in the dehumidifier and the temperature difference $t_{W,3} - t_{W,2}$ of feed water between inlet and outlet in the external heater. This neglects small deviations of the specific heat $c_{p,W}$ of the feed water flow. Therefore the correlation corresponds to Eq. (4.21) and Eq. (3.2):

$$PR_{HD} = \frac{t_{W,2} - t_{W,1}}{t_{W,3} - t_{W,2}} = \frac{\Delta t_{12}}{\Delta t_{23}}. \quad (6.4)$$

This performance ratio only requires the measurement of three temperatures within the liquid water flow. Hodges *et al.* [46, p. 91] define this ratio as the ‘number of effects’ of the HD system. Meinel *et al.* [67, p. 556] express the grade of multi-effectiveness¹ for Hodges’ HD system as the ratio of the temperature differences $\Delta t_{13}/\Delta t_{23}$. This definition results in a dimensionless number, which is $(PR_{HD} + 1)$.

For the calculation of PR_{HD} it is sufficient to determine the water temperatures $t_{W,1}$, $t_{W,2}$ and $t_{W,3}$, as outlined in Eq. (6.4). As these temperatures can be measured with high accuracy, PR_{HD} can be determined with a relative error of less than 2%.

¹ Traditional solar stills don’t recover the heat of condensation to preheat the feed water, resulting in a $PR_{HD} = 0$, which strongly deviates from $PR = \dot{m}_{Dist} \cdot \Delta h_v / \dot{Q}_{in}$.

PR_{HD} offers a variety of advantages, especially for small-scale HD systems:

1. PR_{HD} requires only temperatures of the feed water within the system, which can be measured more accurately, with higher reproducibility and faster compared to measuring small water mass flow rates for the calculation of PR .
2. PR_{HD} can be constantly determined during the operation, whereas the conventional performance ratio PR requires the measurement of condensate within a certain period of time.
3. PR_{HD} uses the prevailing temperature differences, which correspond to the transferred heat, whereas PR normalizes Δh_v to 1000 BTU/lb.
4. The condensate mass flow rate \dot{M}_{Cond} can be constantly approximated during steady-state conditions with known external heat input: $\dot{M}_{Cond} \approx PR_{HD} \cdot \dot{Q}_{ext} / \Delta h_v$, as per Eq. (4.21) and Eq. (6.4). The heat of condensation Δh_v has to be chosen for a mean interface temperature.

6.1.3 Comparison PR and PR_{HD}

Inserting the correlation for the enthalpy of humid air according to Eq. (4.1) (for ideal gases) into Eq. (6.2) follows:

$$\begin{aligned} \dot{G} \cdot [c_{p,G} \cdot t_{A,in} + X_{A,in} \cdot (c_{p,V} \cdot t_{A,in} + \Delta h_{v,0})] + \dot{L} \cdot h_{W,1} = \dot{L} \cdot h_{W,2} + \dot{M}_{Cond} \cdot h_{Cond} \\ + \dot{G} \cdot [c_{p,G} \cdot t_{A,out} + X_{A,out} \cdot (c_{p,V} \cdot t_{A,out} + \Delta h_{v,0})] + \dot{Q}_{loss,deh}. \end{aligned} \quad (6.5)$$

This leads to an equation for \dot{H}_{int} expressed as the energy transport of the humid air in the dehumidifier, which is applied for the comparison with the conventional performance ratio:

$$\begin{aligned} \dot{H}_{int} = \dot{G} \cdot c_{p,G} \cdot (t_{A,in} - t_{A,out}) + \dot{G} \cdot [X_{A,in} \cdot c_{p,V} \cdot t_{A,in} - X_{A,out} \cdot c_{p,V} \cdot t_{A,out}] \\ + \dot{G} \cdot (X_{A,in} - X_{A,out}) \cdot \Delta h_{v,0} - \dot{M}_{Cond} \cdot h_{Cond} - \dot{Q}_{loss,deh}. \end{aligned} \quad (6.6)$$

This formula is translated into an equation for PR_{HD} according to Eq. (6.4). Eq. (6.6) is divided by the external heat input \dot{Q}_{ext} . The definition of PR as per

Eq. (3.2) and Eq. (1.1) is applied to calculate the condensation flow rate \dot{M}_{Cond} :

$$PR_{HD} = PR \cdot \frac{\Delta h_{v,0}}{\Delta h_{v,PR}} - \frac{\overbrace{\dot{M}_{Cond} \cdot h_{Cond}}^{\Delta PR1}}{\dot{Q}_{ext}} + \frac{\overbrace{\dot{G} \cdot c_{p,G} \cdot (t_{A,in} - t_{A,out})}^{\Delta PR2}}{\dot{Q}_{ext}} + \frac{\overbrace{\dot{G} \cdot c_{p,V} [X_{A,in} \cdot t_{A,in} - X_{A,out} \cdot t_{A,out}]}^{\Delta PR3}}{\dot{Q}_{ext}} - \frac{\overbrace{\dot{Q}_{loss,deh}}^{\Delta PR4}}{\dot{Q}_{ext}}. \quad (6.7)$$

With this formula the difference between PR and PR_{HD} is defined based on four deviations $\Delta PR1$ to $\Delta PR4$.

6.2 Application Performance Ratio PR_{HD}

The experiments were conducted to determine the influence of the feed water inlet temperature $t_{W,in}$ for a constant top brine temperature TBT on the performance ratio.

Table 6.1 gives an overview of PR and PR_{HD} using the experimental data obtained with the single-stage and two-stage setup. It is only possible to draw a conclusion with the more precise adapted performance ratio PR_{HD} .

Fig. 6.2 depicts the performance ratio PR_{HD} for the single-stage and two-stage configuration. The assumed improvement from the two-stage configuration can not be observed for this system with natural convection. The difference between the calculated performance ratio PR and the performance ratio PR_{HD} is caused by the inaccuracy of the determination of the condensate mass flow \dot{M}_{Cond} and the corresponding air mass flow rate \dot{G} .

Determining PR_{HD} with these experimental and analytical data shows that the performance decreases for the analyzed experiments and is low for all experimental investigations compared to thermal desalination processes with forced convection. The investigated measures did not result in the expected improvement. This conclusion can not be drawn from the conventional performance ratio because of its large error margin. This assessment shows that PR_{HD} is the preferred dimensionless number to evaluate the performance of small HD systems.

Table 6.1: Analysis and Comparison of PR , PR_{HD} and PR_{comp} from Experimental Results with a Single-Stage and Two-Stage HD System. Operation Parameters: $\dot{Q}_{ext} = 4.7$ kW, $TBT = 85$ °C; Detailed Experimental Results as per Tab. 5.4, page 82

No.	$t_{W,1}$ °C	\dot{L} kg/h	PR -	PR_{HD} -	$PR \frac{\Delta h_{v,0}}{\Delta h_{v,PR}}$ -	$\Delta PR1$ -	$\Delta PR2$ -	$\Delta PR3$ -	$\Delta PR4$ -	PR_{comp} -
Single-Stage	1	181.9	1.39	1.65	1.49	0.068	0.118	0.101	0.100	1.48
	2	191.3	1.41	1.64	1.52	0.078	0.095	0.089	0.100	1.52
	3	209.8	1.38	1.57	1.48	0.090	0.082	0.082	0.100	1.48
	4	230.1	1.33	1.55	1.43	0.098	0.071	0.080	0.100	1.49
	5	254.3	1.36	1.57	1.46	0.111	0.058	0.095	0.100	1.51
	6	283.7	1.24	1.52	1.29	0.113	0.047	0.089	0.100	1.49
Two-Stage	7	163.1	1.47	1.51	1.58	-0.072	0.108	0.072	0.100	1.39
	8	183.5	1.52	1.57	1.63	-0.091	0.093	0.089	0.100	1.47
	9	199.3	1.58	1.53	1.70	-0.107	0.080	0.082	0.100	1.47
	10	210.2	1.54	1.46	1.66	-0.116	0.067	0.085	0.100	1.42
	11	231.6	1.51	1.40	1.62	-0.130	0.058	0.048	0.100	1.38
	12	267.8	1.71	1.40	1.84	-0.148	0.048	0.107	0.100	1.39

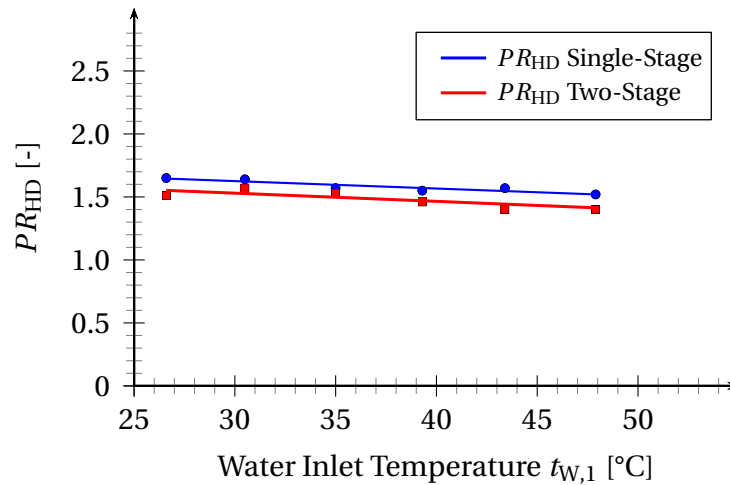


Figure 6.2: PR_{HD} for Increasing Inlet Temperatures $t_{W,1}$ and Feed Water Mass Flows \dot{L} for a Single-Stage and Two-Stage HD System, $TBT = 85$ °C, $\dot{Q}_{ext} = 4.7$ kW

Eq. (6.7) is solved for PR to explain the systematic deviations between PR and PR_{HD} . This expression is named PR_{comp} as it is comparable to the conventional performance ratio PR if the systematic deviations can be determined

accurately:

$$PR_{\text{comp}} = (PR_{\text{HD}} + \Delta PR1 - \Delta PR2 - \Delta PR3 + \Delta PR4) \cdot \frac{\Delta h_{\text{v,PR}}}{\Delta h_{\text{v,0}}}. \quad (6.8)$$

Since the deviations are determined from measurement data with relative high uncertainties ($t_{\text{A,in}}$) and assumptions (thermal losses), PR_{comp} can only be used as an indication to show that the deviations are small or partially compensate each other. The thermal losses of the dehumidifier $\Delta PR4$ are accounted for as 10% of the external energy.

Obviously the performance would increase by enlarging the available heat and mass transfer surfaces but these efforts are limited by the driving potentials analysed and visualized in the following section. Combining Eq. (4.21) and Eq. (4.22) proves that for a given external heat input \dot{Q}_{ext} the maximum condensate mass flow \dot{M}_{Cond} can be achieved if the performance ratio PR_{HD} is maximised.

6.3 Application Operating Lines

6.3.1 Generation of Operating Lines

Operating lines represent a simplified visualization of the conditions within the humidifier and dehumidifier. The principles of operating lines are described in chapter 4.3.3. Each point on the operating line marks the specific enthalpy h_{A} of bulk humid air flow as a function of the bulk water flow temperature at a column height. The diagrams include the saturation line of humid air whereby the x-axis is interpreted as the temperature of saturated humid air.

These values indicate the conditions of the saturated humid air at the interface between air and water in the humidifier and dehumidifier. Heat and mass transfer processes and the determination of the interface temperature are explained in chapter 4.3.2. The visualization of the driving potential with a tie line is detailed in chapter 4.5.1.

The operating lines for humidification and dehumidification are determined

from the energy and mass balances described in chapter 4.3.1 (humidifier) and chapter 4.4.1 (dehumidifier). The introduced simplifications lead to equal equations for the slope of the operating lines, refer Eq. (4.18) and Eq. (4.20).

The slope of the operating line $dh_A/dt_W \approx \dot{L}/\dot{G} \cdot c_{p,W}$ depends on the ratio of the flow rate \dot{L} of water and \dot{G} of air. The water flow rate \dot{L} is adjustable. Experimental values were used as input data for the 1-D simulation to calculate the air mass flow rate and to create the operating lines.

Fig. 6.3 shows an example of the operating lines for a single-stage and two-stage HD configuration. The enthalpy of humid air h_A at the top in (2) and (3) and the bottom (1) and (4) does not change as the air is only transferred from one column to the other.

The temperature $t_{W,in}$ of the feed water flow is depicted in point (1). The influence of this temperature is investigated in the following subsection for the studied single-stage and two-stage HD systems. The transferred enthalpy flow \dot{H}_{int} , cp. Eq. (4.21), preheats the feed water in the dehumidifier resulting in a proportional temperature difference Δt_{12} of the feed water, point (2).

Fig. 6.3b depicts the operating lines for each stage of the two-stage HD configuration. Stage 1 is indicated as (1) to (2') and Stage 2 as (3') and (4). The diagram also indicates the deviation of the operating lines to the theoretical slope of the operating line of the dehumidifier, i.e. parallel to the operating line of the dehumidifier. The water temperatures 3'a and 4a deviate from the measure temperatures 3' and 4. These deviations are due to the inaccurate measurement of the water temperatures and heat losses in the humidifier.

The brine outlet temperature $t_{W,4}$ is not required to determine PR_{HD} . For the determination of the specific enthalpy h_A of humid air at position 1 and 4 (y-axis), the mean temperatures measured at the exit of the dehumidifier and entry of the humidifier are used.

6.3.2 Operating Lines for Single-Stage and Two-Stage HD

Fig. 6.4 and Fig. 6.5 show the operating lines for the single-stage and two-stage experiments for various feed water inlet temperatures. The operating lines are

obtained from experimental data, summarized in Tab. 5.4, which are used as input values for the numerical 1-D simulation, outlined in chapter 4.3.3 and chapter 4.5.

The feed water inlet temperature $t_{W,in}$ is increased stepwise to investigate its influence on the performance, as shown in Fig. 6.4a to 6.4f. Fig. 6.4a shows the operating line for $t_{W,in}$ of 27 °C and a corresponding feed water mass flow \dot{L} of 181.9 kg/s to maintain a top brine temperature of 85 °C. The external heat input \dot{Q}_{ext} remains constant at 4.7 kW. The feed water mass flow rate \dot{L} is controlled to maintain the set top brine temperature of 85 °C. Increasing $t_{W,in}$ leads to an increase in the slope of the operating lines and a decrease in the temperature difference Δt_{23} .

The internally transferred enthalpy flow rate \dot{H}_{int} remains almost constant, as indicated by the very similar performance ratios for each case. The decreasing distance between the operating lines and the saturation line represents a decrease of the driving potential for heat and mass transfer, which is compensated for by an improvement of the transfer coefficient. Additionally, the transfer areas in the humidifier potentially increase as the water mass flow \dot{L} increases significantly from 180 kg/h to 283 kg/h. The ratio between the temperature differences Δt_{12} and Δt_{23} , i.e. the performance ratio PR_{HD} , remains almost constant as both temperature differences decrease in proportional relation.

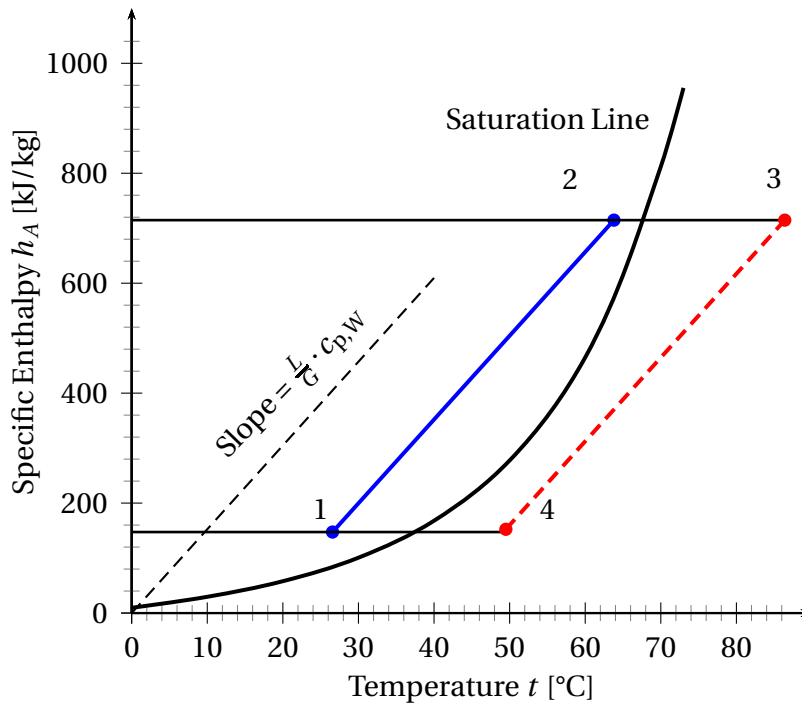
Both, single and two stage tests showed that with increasing inlet temperature, the performance ratio decreases. This can be explained, as the driving potential for natural convection increases in the cooler areas of the dehumidifier. Operating at higher temperatures can be recommended for forced convection only.

All operating lines of the single-stage configuration show that the performance ratio is limited to low values as otherwise the operating lines would approach the saturation line at singular positions.

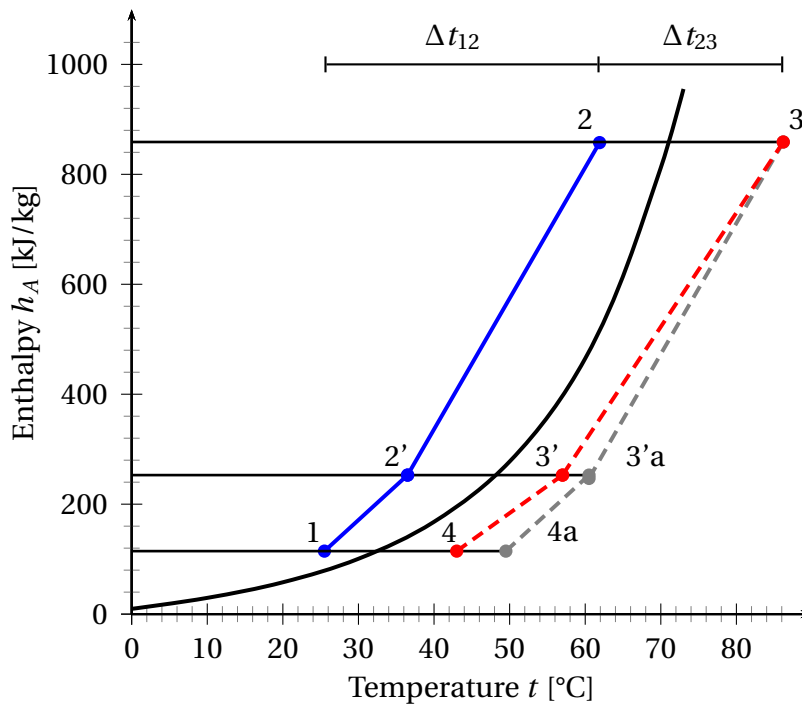
The comparison of cases 6, Fig. 6.5f, and 12, Fig. 6.4f, shows that the bottom stage contributes little to the internally transferred enthalpy \dot{H}_{int} for high inlet temperature (45 °C) and is small in the lower part of the column. It can also

be observed that for higher temperatures the upper part is more effective but the overall performance ratio is smaller because the smaller temperature differences reduce the natural convection flow.

In a multi-stage configuration, the operating lines could be adjusted to the saturation line if the air flow is adjusted (forced convection). All figures show that the ability to adjust the slope along the saturation line is desirable. HD setups with natural convection offer only limited opportunities compared to forced convection.



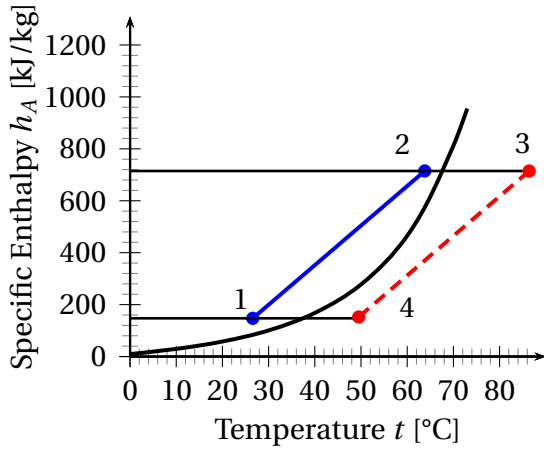
(a) Operating Line Single-Stage



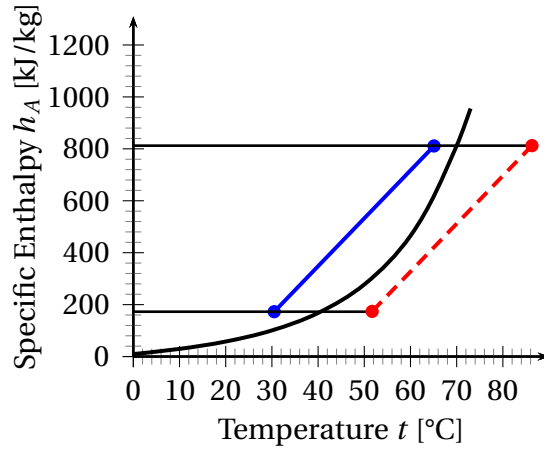
(b) Operating Two-Stage

Figure 6.3: $h_A - t$ Diagram with Operating Lines of Humidifier and Dehumidifier of Single-Stage and Two-Stage Closed-Air HD System

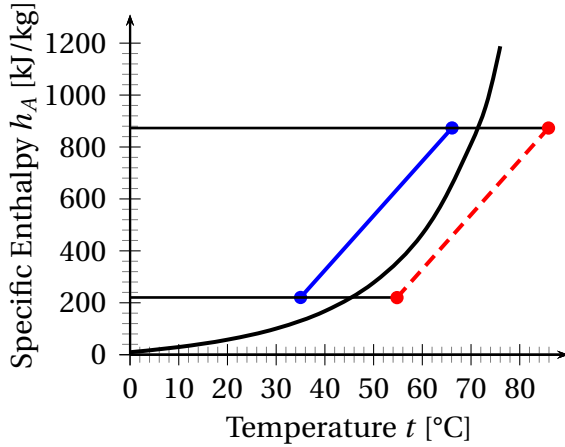
(a) No. 1: $t_{W,in} = 26.6\text{ }^\circ\text{C}$, $\dot{L} = 181.9\text{ kg/h}$



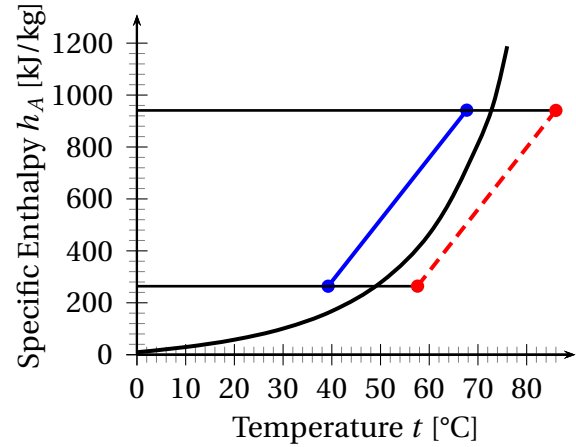
(b) No 2: $t_{W,in} = 30.5\text{ }^\circ\text{C}$, $\dot{L} = 191.3\text{ kg/h}$



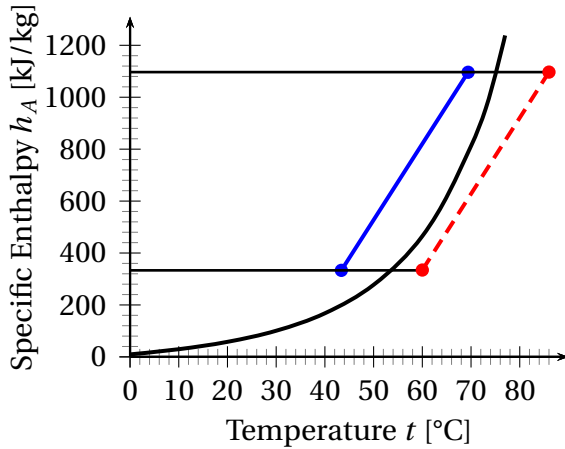
(c) No 3: $t_{W,in} = 35.0\text{ }^\circ\text{C}$, $\dot{L} = 209.8\text{ kg/h}$



(d) No 4: $t_{W,in} = 39.3\text{ }^\circ\text{C}$, $\dot{L} = 230.1\text{ kg/h}$



(e) No. 5: $t_{W,in} = 43.4\text{ }^\circ\text{C}$, $\dot{L} = 254.3\text{ kg/h}$



(f) No. 6: $t_{W,in} = 47.91\text{ }^\circ\text{C}$, $\dot{L} = 283.7\text{ kg/h}$

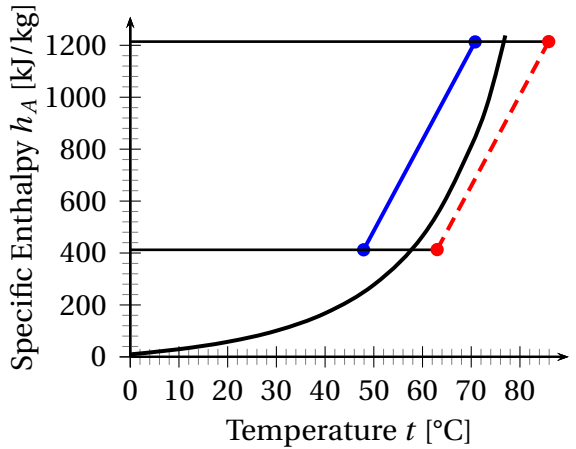
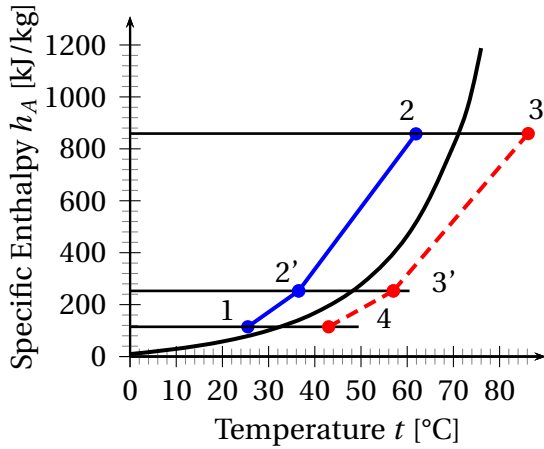
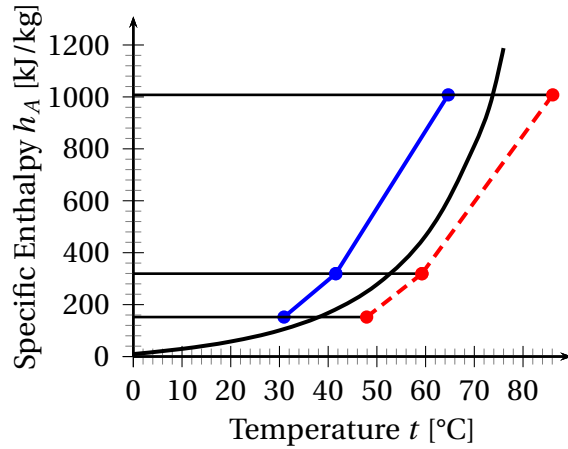


Figure 6.4: $h_A - t$ Diagram with Operating Lines of Humidifier and Dehumidifier of Single-Stage Closed-Air HD System, $\dot{Q}_{ext} = 4.7\text{ kW}$, $TBT_{set} = 85\text{ }^\circ\text{C}$, Overview of Measurement Data see Tab. 5.4, p. 82

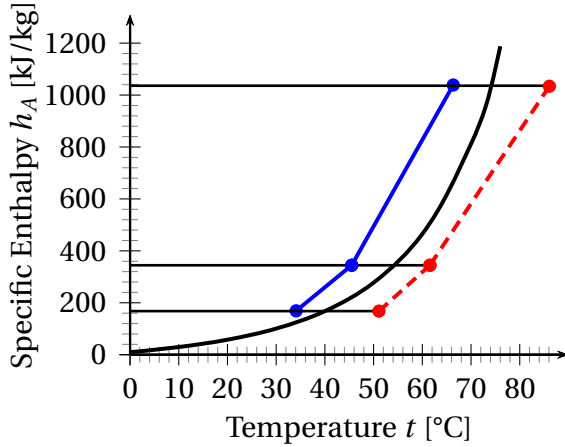
(a) No. 7: $t_{W,in} = 25.5\text{ }^\circ\text{C}$, $\dot{L} = 163.2\text{ kg/h}$



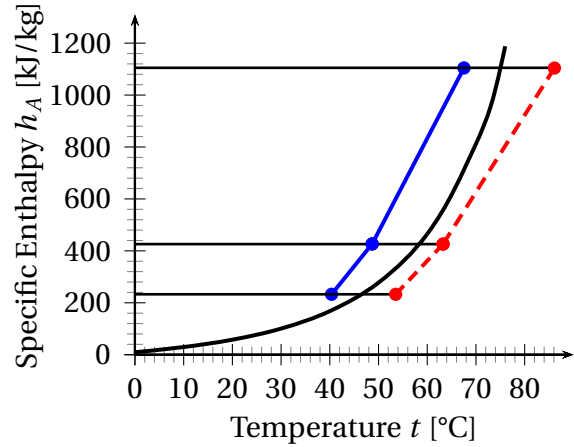
(b) No. 8: $t_{W,in} = 30.9\text{ }^\circ\text{C}$, $\dot{L} = 183.53\text{ kg/h}$



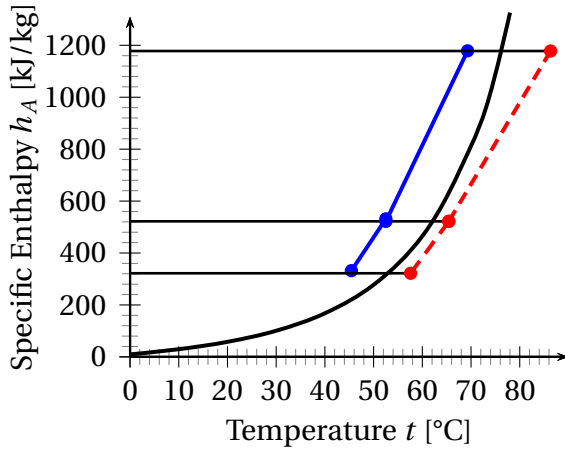
(c) No. 9: $t_{W,in} = 36.1\text{ }^\circ\text{C}$, $\dot{L} = 199.3\text{ kg/h}$



(d) No. 10: $t_{W,in} = 40.4\text{ }^\circ\text{C}$, $\dot{L} = 210.2\text{ kg/h}$



(e) No. 11: $t_{W,in} = 45.4\text{ }^\circ\text{C}$, $\dot{L} = 231.6\text{ kg/h}$



(f) No. 12: $t_{W,in} = 50.3\text{ }^\circ\text{C}$, $\dot{L} = 267.8\text{ kg/h}$

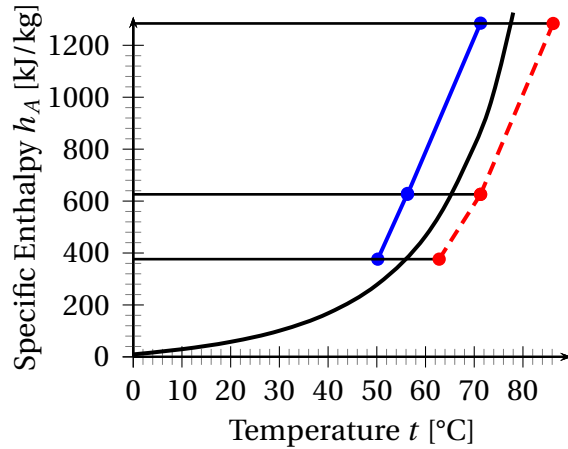


Figure 6.5: $h_A - t$ Diagram with Operating Lines of Humidifier and Dehumidifier of Two-Stage Closed-Air HD System, $\dot{Q}_{ext} = 4.7\text{ kW}$, $TBT_{set} = 85\text{ }^\circ\text{C}$, Overview of Measurement Data see Tab. 5.4, p. 82

6.3.3 Number of Transfer Units and Height of one Transfer Unit

The 1-D numerical simulation tool is used for the dimensioning of the humidifier and dehumidifier columns. A commonly used approach to determine the height of a column is defined in chapter 4.5.2.

The number of transfer units describes the ‘difficulty’ of the heat and mass transfer process [69]. Heat and mass transfer conditions can be visualized in the known manner by applying the graphical concept of the operating lines and further analyzing the number of transfer units NTU and the height of one transfer unit HTU as described in chapter 4.5.1.

The accuracy of the measurement values of the feed water temperatures $t_{W,1}$, $t_{W,2}$ and $t_{W,3}$ (x-coordinate) is high as the water temperature is obtained from measurements within tubes. In contrast, the accuracy of the value for the brine temperature $t_{W,4}$ is reduced as the measurements involve a thermocouple overflowed with brine. Time variations during the draining can affect the measurement accuracy. These uncertainties during the determination of $t_{W,4}$ are reflected by indicating the operating line of the humidifier as a dashed line.

The temperature difference $t_{W,4} - t_{W,1}$ is approximated with the temperature difference $t_{W,3} - t_{W,2}$. This follows from an energy balance on the overall system whereby the specific enthalpy of the condensation mass flow is deemed to be similar to the specific enthalpy of the brine water flow and the specific heat capacities are the same.

An increasing NTU corresponds to higher demands for the transport process as the driving potential decreases. The visualization of the heat and mass transfer processes with the operating lines, tie lines and consideration of NTU and HTU show that the $NTUs$ are not large because the operating lines approach the saturation line. However, these low $NTUs$ involve large temperature differences Δt_{23} leading to small performance ratios.

NTU increases extremely for conditions in which the transfer takes place at a small driving potential that is created when the operating line becomes tangent to the saturation line or both lines converge. The HTU increases

for larger quantities of fluids to be separated (proportional to \dot{G}) and for smaller separation column efficiency, i.e. smaller transfer surface and smaller transport coefficients.

With graphic visualization of the operating lines it is possible to detect disadvantageous transfer conditions in the humidifier and dehumidifier. The approach of the saturation line with the operating line can be avoided by adjusting the operational lines according to the temperature dependent slope of the saturation line.

The slope of the operating line incorporates the mass flow \dot{G} of dry air, which is derived from the energy and mass balance of the condensate and the difference of the absolute humidity ΔX . Consequently, the slope indicates an average value of \dot{G} that changes over height due to the cross flow created by the removal of the separation wall between humidifier and dehumidifier. The intersection point of the operating line with the water temperature $t_{W,2}$ results in the enthalpy $h_{A,2}$ of humid air. The exact operating line would be (slightly) curved as the denominator of \dot{L}/\dot{G} changes over the column height of humidifier and dehumidifier. Measurement of the feed water temperatures can be done with a higher accuracy than air temperatures within the system.

As shown for a multi-stage HD in Fig. 6.5, the operating line is bent according to the number of stages. The produced condensate flow in the bottom stage is low because of the low absolute humidity in air in this temperature region. The flat slope of the operating line results from a higher air velocity.

The approach of the operating lines towards the saturation line can be counter-steered by reducing the temperature difference t_{12} and aiming simultaneously to reduce the temperature difference t_{23} to achieve a high performance ratio PR_{HD} . This is easier to accomplish in lower temperature regions (up to 50 °C) as the curvature of the saturation line is smaller than in the higher temperature regions.

Tab. 6.2 indicates the slope $\dot{L}/\dot{G} \cdot c_{p,W}$, NTU_G and HTU_G for the each the experimental data as shown in Tab. 5.4. It also includes the effectively transferred enthalpy flow rate \dot{H}_{int} according Eq. (6.1). The enthalpy flow rate slightly decreases with increasing feed water inlet temperature $t_{W,in}$ for both

Table 6.2: *NTU* and *HTU* Analysis of Experimental Data of Single-Stage and Two-Stage HD Dehumidifier, Values based on Experimental Data given in Tab. 5.4, page 82

No.	\dot{L} [kg/h]	$t_{w,1}$ [°C]	\dot{H}_{int} [kW]		$\dot{L}/\dot{G} \cdot c_{p,W}$ [kJ/(kg · K)]		NTU_G [-]		HTU_G [m]		
			St. 1	St. 2	St. 1	St. 2	St. 1	St. 2	St. 1	St. 2	
Single-Stage	1	181.9	26.6	7.87	15.26	3.48	0.20				
	2	191.3	30.5	7.72	18.45	3.45	0.20				
	3	209.8	35.0	7.59	21.00	3.18	0.22				
	4	230.1	39.3	7.61	23.83	3.14	0.22				
	5	254.3	43.4	7.71	29.32	2.86	0.24				
	6	283.7	47.9	7.57	34.98	2.65	0.26				
Two-Stage	7	163.1	25.5	2.09	4.83	12.57	23.81	2.01	2.51	0.17	0.14
	8	183.5	30.9	2.27	4.93	15.73	29.83	1.82	2.38	0.19	0.15
	9	199.3	36.1	2.20	4.82	18.66	33.31	2.47	2.62	0.14	0.13
	10	210.2	40.4	2.04	4.61	23.29	35.98	1.78	2.32	0.20	0.15
	11	231.6	45.4	1.91	4.52	28.17	39.16	1.33	2.05	0.26	0.17
	12	267.8	50.3	1.88	4.67	41.47	43.95	1.51	1.91	0.23	0.18

configurations. This also corresponds to a decrease of the performance ratio PR , according to Eq. (6.4). The external heat input is approximately constant. It becomes evident for the two-stage configuration that the first stage transfers less than 50% of the enthalpy flow rate \dot{H}_{int} of the second stage. As previously noted, both stages have equal transfer surfaces.

Fig. 6.6 depicts the HTU for the single-stage and each stage of the two-stage configuration. The $HTUs$ are large due to the small specific surface and the small transfer coefficients. The operating lines adjust to the conditions that are determined by the transfer ability of the apparatus, indicated by HTU , and lead to the corresponding NTU .

The product of NTU and HTU is the same for humidifier and dehumidifier, as the product is the total height of the columns (700 mm). Consequently, the positions of the two operating lines are automatically adjusted on both sides of the saturation line according to the transfer conditions in the humidifier and dehumidifier.

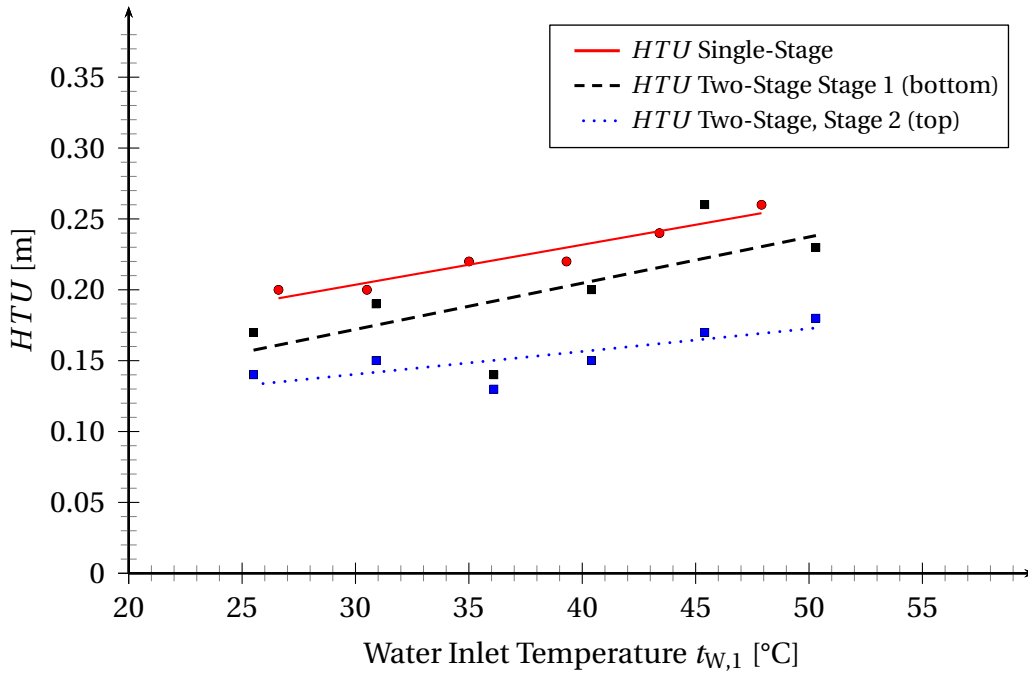


Figure 6.6: HTU for Increasing Feed Water Inlet Temperatures $t_{W,1}$ and Feed Water Mass Flow Rates \dot{L} for a Single-Stage and Two-Stage HD System, $TBT = 85^\circ\text{C}$

6.4 Summary

A sufficiently large air flow rate \dot{G} requires a large temperature range of the circulating water. Operation in the lower temperature regions has the disadvantage that heat and mass transfer is unfavourable due to the high ratio of NCG.

The experimental results can be interpreted as follows: A high performance ratio PR_{HD} is achieved when the temperature difference Δt_{12} of the feed water flow in the dehumidifier is large compared its temperature difference Δt_{23} in the external heater. The temperature difference Δt_{23} determines the driving force, which has to be larger for adverse heat and mass transfer conditions. Increasing the water inlet temperature $t_{W,in}$ at constant \dot{Q}_{ext} and constant top brine temperature TBT leads to an increase of the water mass flow \dot{L} as the temperature difference Δt_{23} decreases inverse proportional to \dot{L} . But it can also be observed that Δt_{12} decreases almost proportionally with Δt_{23} . Consequently, PR_{HD} remains almost constant.

From the results with the two-stage HD setup it can be concluded that the top stage transfers more than double the enthalpy flow \dot{H}_{int} than the bottom stage, for equal transfer surface areas. However, it is not sufficient to operate at only high temperatures, as it becomes evident from the experiments with the single-stage configuration. For a high performance ratio it is necessary to use a wide temperature region for the preheating of the feed water and a small driving temperature difference. This is achieved with large transfer surfaces, high transfer coefficients and the adjustment of the slope of the operating lines.

The low PR_{HD} of the studied HD system is caused by the relatively small column height Z and the small specific surface area a . Large specific surface areas a and high transport coefficients can be achieved with high packing densities $(1 - \epsilon)$ in the dehumidifier and humidifier. Increased packing densities create higher pressure losses, especially when air velocity is increased to improve the heat and mass transfer. This can be combined when forced convection is applied.

The following measures are recommended to increase the performance ratio:

1. Increase height respectively volume of HD columns.
2. Increase specific active surface area a of the packing.
3. Harmonize distance between operating line and saturation line.
4. Improve heat and mass transfer conditions.
5. Improve thermal insulation.

To achieve the desired high performance ratios the imposed restrictions due to natural convection should be resolved by applying forced convection. To generate a decent natural convection flow, internals with high porosity are required in the humidifier and dehumidifier to minimize pressure losses. Through increasing the parameters for heat and mass transfer (α, β, A) , the water mass flow \dot{L} can be increased for a given external heat input \dot{Q}_{ext} . Consequently, Δt_{23} is reduced and the performance ratio can increase.

However, small pressure losses diminish heat and mass transfer. Fig. 6.7a shows such a configuration with forced convection with a set air flow rate \dot{G} . The driving potential can become very small as the operating line approaches

the saturation line. The circled areas highlight the positions where the operating line approaches the saturation line, i.e. there are no driving potential differences ($NTU \rightarrow \infty$). Therefore, the performance ratio remains low.

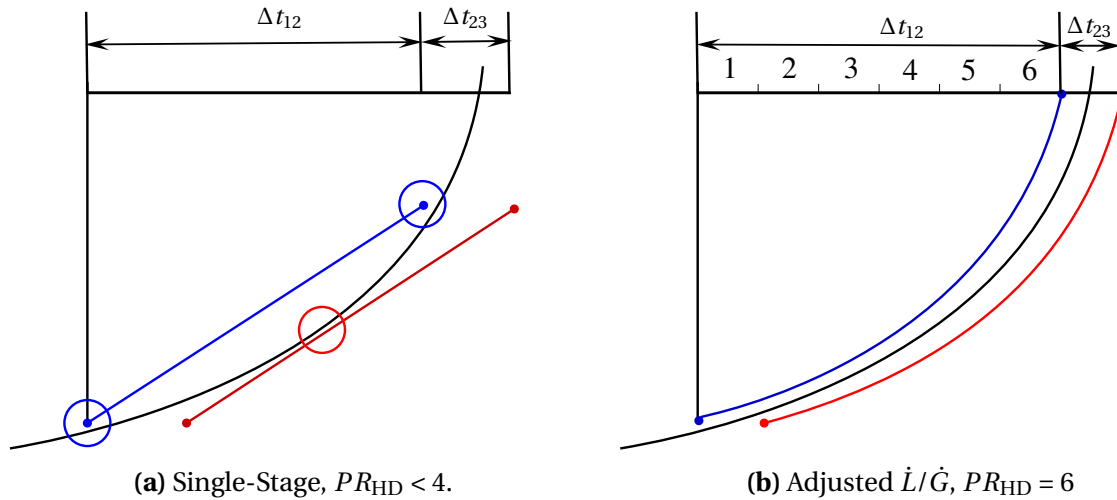


Figure 6.7: $h_A - t$ Diagrams of Single-Stage HD without (a) and with (b) adapted \dot{L}/\dot{G} ratio

Fig. 6.7b shows a HD system with adjusted slope of the operating lines by adjusting the air flow rate. Larger values for the performance ratio can be achieved by optimizing the form and location of the operating lines, in particular through continuous adaptation of the slope of the operating lines by adjusting the air mass flow rate along the column height Z .

7 Conclusions

The scope of this thesis is to investigate compact humidification-dehumidification (HD) desalination systems with natural convection through applying experimental and analytical methods to contribute towards performance improvements for HD systems.

Conclusions from literature are limited because of the complex interlinked heat and mass transfer processes, especially for natural convection. This work combines methods to simulate and visualize the heat and mass transfer correlations and to interpret the experimental results. These methods are used to evaluate the influence of the water inlet temperature, the main process parameter for the chosen setups on a single- and two-stage HD configuration.

The analysis of the performance of HD systems is usually based on the condensate mass flow rate \dot{M}_{Cond} . The determination of this value is associated with high measurement inaccuracies and long measurement intervals, especially in the case of small systems, which hinders its applicability. Therefore, an *adapted performance ratio* PR_{HD} is derived, requiring only a ratio of water temperature differences. The input values can be constantly measured with high accuracy. The differences based on the definitions of both performance ratios are small compared to the measurement inaccuracies for the conventional performance ratio. Thus, the adapted performance ratio PR_{HD} is the *key indicator for performance improvements*.

To create *higher feed water inlet temperatures*, brine water is recirculated. As the mean water temperature and the mean air temperature rises, heat and mass transfer processes take place in regions with higher vapor concentration. The feed water mass flow rises as the temperature difference between the feed water inlet and the constant top brine temperature is reduced and the external heating power is kept constant. These effects seem to increase the condensate mass flow rate. However, experiments show that the performance ratio decreases slightly. Further investigations concern the concept of multi-staging for HD with natural convection, which strives to create optimal air

mass flow rates within each stage. The experimental results show that the improvements in the upper stage are at the expense of the performance of the lower stage so that the overall performance is not improved.

An *unexpected observation is dropwise condensation* on the polypropylene tubes in the dehumidifier even after years of operation of the HD system. Whilst very high condensation rates are reported in literature for dropwise condensation of pure vapor, the main reason for low condensation rates in the experiments is explained by the high concentration of carrier gas. A simple mathematical approach is derived to account for this phenomenon.

To analyse and visualize the occurring heat and mass transfer processes the *concept of operating lines* is applied. This is combined with *analytical modeling* of the humidification and dehumidification process. Computation of heat and mass transfer along the height of the humidifier and dehumidifier columns considers the temperature at the interface between water and air. The *interface temperature* is essential to numerically determine the heat and mass transfer in water and air.

The performance ratio PR of the investigated HD system with natural convection is limited to relatively low values. The cause for the low performance ratio is mainly due to the small transfer surfaces, transfer coefficients and the unsatisfactory slope of the operating lines along the height of the system. Compact HD setups with natural convection face the principal limitation that the air flow is self regulated according to system configurations and process conditions.

Future research should focus on HD systems *operating in forced convection* and the ability to *continuously adjust the air flow rate* to optimize the operating lines. The analytical models and methodologies presented in this work can be applied to HD systems with forced convection to improve the performance ratio.

HD technology is already today used for a *range of applications*, such as the production of drinking water or the concentration of industrial liquids. It is predestined for the integration with solar water-heaters or *solar-thermal power-plants* which provides opportunities for further deployment.

Bibliography

- [1] H. B. Bacha, M. Boutguedna, M. S. Abid, and A. Y. Maalej. “Modelling and simulation of a water desalination station with solar multiple condensation evaporation cycle technique”. In: *Renewable Energy* 18 (1999), pp. 349–365.
- [2] H. B. Bacha, M. Bouzguenda, T. Damak, M. S. Abid, and A. Y. Maalej. “Study of a water desalination station using the SMCEC technique: Production optimisation”. In: *Renewable Energy* 21 (2000), pp. 523–536.
- [3] H. D. Baehr. *Thermodynamik*. 10th ed. Springer-Verlag Berlin, Heidelberg, 2000.
- [4] H. D. Baehr and K. Stephan. *Wärme- und Stoffübertragung*. 4th ed. Springer-Verlag Berlin, Heidelberg, 2004.
- [5] W. Beitz and K.-H. Grote. *Dubbel - Taschenbuch für den Maschinenbau*. 19th ed. Springer-Verlag Berlin, Heidelberg, 1997.
- [6] F. Bošnjaković. *Technische Thermodynamik II*. Steinkopf Verlag Dresden, Leipzig, 1965.
- [7] K. Bourouni, M. Chaibi, and L. Tadriss. “Water desalination by humidification and dehumidification of air: State of the art”. In: *Desalination* 137 (2001), pp. 167–176.
- [8] K. Bourouni, R. Martin, L. Tadriss, and H. Tadriss. “Experimental investigation of evaporation performances of a desalination prototype using the aero-evapo-condensation process”. In: *Desalination* 114 (1997), pp. 111–128.
- [9] T. Brendel. *German Patent: DE 10215079B5 - Verfahren zum Destillieren oder Entsalzen von Flüssigkeiten*. 2006.
- [10] T. Brendel. “Solare Meerwasserentsalzungsanlagen mit mehrstufiger Verdunstung”. PhD thesis. Ruhr Universität Bochum, 2003.
- [11] V. P. Carey. *Liquid-Vapor Phase-Change Phenomena: An Introduction to the Thermophysics of Vaporization and Condensation Processes in Heat Transfer Equipment*. Series in Chemical, Mechanical Engineering, Taylor, and Francis, 1992.
- [12] E. Chafik. “A new seawater desalination process using solar energy”. In: *Desalination* 153 (2002), pp. 25–37.
- [13] K. Chehayeb and J. H. Lienhard V. “Effect of Feed Salinity on the Performance of Humidification Dehumidification Desalination”. In: *The IDA World Congress on Desalination and Water Reuse*. 2016.

- [14] A. Cipollina, G. Micale, and L. Rizzuti, eds. *Seawater Desalination - Conventional and Renewable Energy Processes*. Springer-Verlag Berlin, Heidelberg, 2009.
- [15] H. Czichos and M. Hennecke, eds. *HÜTTE – Das Ingenieurwissen. Die Grundlagen der Ingenieurwissenschaften*. 33rd ed. Springer-Verlag Berlin, Heidelberg, 2008.
- [16] Y. J. Dai, R. Z. Wang, and H. F. Zhang. “Parametric analysis to improve the performance of a solar desalination unit with humidification and dehumidification”. In: *Desalination* 142 (2002), pp. 107–118.
- [17] Y. J. Dai and H. F. Zhang. “Experimental investigation of a solar desalination unit with humidification and dehumidification”. In: *Desalination* 130 (2000), pp. 169–175.
- [18] B. Dawoud, Y. H. Zurigat, B. Klitzing, T. Aldoss, and G. Theodoridis. “On the possible techniques to cool the condenser of seawater greenhouses”. In: *Desalination* 195 (2006), pp. 119–140.
- [19] H. T. El-Dessouky. “Humidification-dehumidification desalination process using waste heat from a gas turbine”. In: *Engineering Journal of Qatar University* (1989), pp. 203–221.
- [20] H. T. El-Dessouky and H. M. Ettouney. *Fundamentals of Salt Water Desalination*. Elsevier, New York, USA, 2002.
- [21] H. T. El-Dessouky and H. M. Ettouney. “Plastic/compact heat exchangers for single-effect desalination systems”. In: *Desalination* 122 (1999), pp. 271–289.
- [22] L. L. Diezel. “Untersuchung der Leistungssteigerung des MVC-Prozesses zur Meerwasserentsalzung über die Erzielung von Tropfenkondensation mittels Ionenimplantation”. PhD thesis. Friedrich-Alexander-Universität Erlangen-Nürnberg, 2011.
- [23] J. A. Duffie and W. A. Beckman. *Solar Engineering of Thermal Processes*. John Wiley and Sons, Inc., Hoboken, New Jersey, 2006.
- [24] H. Emmons. “The mechanism of drop condensation”. In: *Transactions, American Institute of Chemical Engineers* 35 (1939), pp. 109–125.
- [25] G. Al-Enezi, H. M. Ettouney, and N. Fawzy. “Low temperature humidification dehumidification desalination process”. In: *Energy Conversion and Management* 47 (2006), pp. 470–484.
- [26] S. Ergun. “Fluid flow through packed columns”. In: *Chemical Engineering Progress* 48 (1952), pp. 89–94.
- [27] A. Eucken. *Lehrbuch der chemischen Physik, Band 2/2 Kondensierte Phasen und Heterogene Systeme*. Akademische Verlagsgesellschaft, 1949.
- [28] M. M. Farid and A. W. Al-Hajaj. “Solar desalination with humidification-dehumidification cycle”. In: *Desalination* 106 (1996), pp. 427–429.
- [29] M. M. Farid, S. Parekh, J. R. Selman, and S. Al-Hallaj. “Solar desalination with a humidification-dehumidification cycle: Mathematical modeling of the unit”. In: *Desalination* (2003), pp. 153–164.

- [30] I. Garaway and G Grossmann. “Investigation of a solar-powered desalination system employing regeneration”. In: *Desalination* 197 (2006), pp. 63–74.
- [31] L García-Rodríguez. “Renewable energy applications in desalination: state of the art”. In: *Solar Energy* 75 (2003), pp. 381–393.
- [32] H. P. Garg, R. S. Adhikari, and R. Kumar. “Experimental design and computer simulation of multi-effect humidification (MEH)-dehumidification solar distillation”. In: *Desalination* 153 (2002), pp. 81–86.
- [33] P. Grassmann. *Physikalische Grundlagen der Verfahrenstechnik*. 2nd ed. Verlag Sauerländer, Aarau und Frankfurt am Main, 1970.
- [34] D. W. Green, ed. *Perry's Chemical Engineers Handbook*. 8th ed. McGraw-Hill, New York etc., 2007.
- [35] U. Grigull. *Technische Thermodynamik*. Sammlung Goeschen 2170. Walter de Gruyter, Berlin, 1977.
- [36] H. Groeber, S. Erk, and U. Grigull. *Grundgesetze der Wärmeübertragung*. 3rd ed. Springer-Verlag Berlin, Heidelberg, 1962.
- [37] K.-H. Grote and J. Feldhusen. *Dubbel - Taschenbuch für den Maschinenbau*. 23rd ed. Springer-Verlag Berlin, Heidelberg, 2011.
- [38] W. N. Grune, R. A. Collins, and T. L. Thompson. “Forced convection, multiple effect solar still for desalting sea and brackish waters”. In: *Proceedings of the United Nations Conference on New Sources of Energy* E35–S14 (1961), pp. 1–26.
- [39] S. Al-Hallaj, M. M. Farid, and A. R. Tamimi. “Solar Desalination with humidification–dehumidification cycle: performance of the unit”. In: *Desalination* 120 (1998), pp. 273–280.
- [40] A. H. Hassabou. “Experimental and numerical analysis of a PCM-supported humidification-dehumidification solar desalination system”. PhD thesis. Technische Universität München, 2012.
- [41] R. Hauenschild. “Übereinstimmung zwischen Theorie und Praxis bei Merkel-Zahl nachgewiesen”. In: *Brennstoff-Wärme-Kraft* (1986), pp. 1–5.
- [42] M. Hermann, J. Koschikowski, and M. Rommel. “Corrosion-free solar collectors for thermally driven seawater desalination”. In: *Solar Energy* 75 (2002), pp. 415–426.
- [43] O. Heschl and R. Sizman. “Solar Desalination with Recovery of Heat of Condensation”. In: *Tagungsbericht 5 - Internationales Sonnenforum, Berlin* (1984), p. 375.
- [44] C. N. Hodges and W. L. Collins. “Solar Desalination Experience of University of Arizona – Summary: General”. In: *Circum-Pacific Energy and Mineral Resources* A175 (1976), p. 73.
- [45] C. N. Hodges, J. E. Grob, and T. T. Lewis. “Solar Powered Humidification Cycle Desalination”. In: *Proceedings of the First International Symposium on Water Desalination*. 1965, pp. 429–455.

- [46] C. N. Hodges, T. L. Thompson, J. E. Groh, and D. H. Frieling. “Solar Distillation Utilizing Multiple-Effect Humidification”. In: *University of Arizona, Tuscon, Arizona* (1966).
- [47] C. N. Hodges, T. L. Thompson, J. E. Groh, and W. D. Sellers. “The Utilization of Solar Energy in a Multiple-Effect Desalinization System”. In: *Journal of Applied Science* 3 (1964), pp. 505–512.
- [48] S. Hou. “Two-stage solar multi-effect humidification dehumidification desalination process plotted from pinch analysis”. In: *Desalination* 222 (2008), pp. 572–578.
- [49] S. Hou, S. Ye, and H. Zhang. “Performance optimization of solar humidification–dehumidification desalination process using pinch technology”. In: *Desalination* 183 (2005), pp. 143–149.
- [50] S. Hou, D. Zeng, S. Ye, and H. Zhang. “Exergy analysis of the solar multi-effect humidification-dehumidification desalination process”. In: *Desalination* (2007), pp. 403–409.
- [51] *Human Development Report 2015: Work for Human Development*. UN Development Programme (UNDP), 2015.
- [52] S. Kalogirou. “Solar Thermal collectors and application”. In: *Energy and Combustion Science* 30 (2004), pp. 231–295.
- [53] S. Kalogirou. “Use of parabolic trough solar energy collectors for sea-water desalination”. In: *Applied Energy* 60 (1998), pp. 65–88.
- [54] A. B. Kananeh. “Experimental study of dropwise condensation on ion implanted horizontal single tubes and tube bundles”. PhD thesis. Universität Erlangen-Nürnberg, 2005.
- [55] M. Khedr. “Techno-Economic investigation of an air humidification-dehumidification desalination process”. In: *Chemical Engineering & Technology* 16 (1993), pp. 270–274.
- [56] F. Kiefer, F. Schummer, A. Praebst, M. Spinnler, and T. Sattelmayer. “Optimization of Multi-Effect Vacuum Membrane Distillation Systems for Highly Concentrated Aqueous Electrolyte Solutions in Liquid Desiccant Air Conditioning and Zero Liquid Discharge”. In: *Desalination for the Environment Clean Water and Energy*. 2016.
- [57] J. F. Klausner and R. Li Yi. and Mei. “Evaporative heat and mass transfer for the diffusion driven desalination process”. In: *Heat and Mass Transfer* 42 (2006), pp. 528–536.
- [58] J. F. Klausner, Y. Li, M. Darwish, and R. Mei. “Innovative diffusion driven desalination process”. In: *Journal of Energy Resources Technology* 126 (2004), pp. 219–225.
- [59] J. C. Kloppers and D. G. Kröger. “The Lewis factor and its influence on the performance prediction of wet-cooling towers”. In: *International Journal of Thermal Sciences* 44 (2005), pp. 879–884.
- [60] A. Kolb. *Theoretische und experimentelle Untersuchungen an einem neuen solaren Luftkolektor mit durchströmtem Absorber*. Reihe 6: Energietechnik, Nr. 356. VDI Verlag Düsseldorf, 1997.

-
- [61] A. Leipertz. *Wärme- und Stoffübertragung*. ESYTEC, 2008.
- [62] Y. Li, J. F. Klausner, R. Mei, and J. Knight. “Direct contact condensation in packed beds”. In: *International Journal of Heat and Mass Transfer* 49 (2006), pp. 4751–4761.
- [63] G. O. G. Löf. *Demineralization of saline water with solar energy*. Saline Water Conversion Program, Research and Development Progress Report No. 4. US Dep. of Interior, 1954.
- [64] J. Maćkowiak. *Fluidodynamik von Füllkörpern und Packungen*. Springer-Verlag Berlin, Heidelberg, 2009.
- [65] J. Maćkowiak. “Modellierung des flüssigkeitsseitigen Stoffüberganges in Kolonnen mit klassischen und gitterförmigen Füllkörpern”. In: *Chemie Ingenieur Technik* 80 (2008), pp. 57–77.
- [66] M. Mehrgoo and M. Amidpour. “Constructal design and optimization of a direct contact humidification–dehumidification desalination unit”. In: *Desalination* 293 (2012), pp. 69–77.
- [67] A. B. Meinel and M. P. Meinel. *Applied Solar Energy - An Introduction*. Addison-Wesley Publishing Company, Reading etc., 1979.
- [68] F. Merkel. *Verdunstungskühlung*. VDI Forschungsheft Nr. 275. VDI-Verlag, Düsseldorf, 1925.
- [69] A. Mersmann. *Thermische Verfahrenstechnik. Grundlagen und Methoden*. Springer-Verlag Berlin, Heidelberg, 1980.
- [70] A. M. I. Mohamed and N. A. S. El-Minshawy. “Humidification–dehumidification desalination system driven by geothermal energy”. In: *Desalination* 249 (2009), pp. 602–608.
- [71] H. Müller-Holst. “Mehrfacheffekt–Entfeuchtluftdestillation bei Umgebungsdruck – Verfahrensoptimierung und Anwendungen”. PhD thesis. Technische Universität München, 2002.
- [72] H. Müller-Holst. “Solar thermal desalination using the multiple effect humidification (MEH) method”. In: *Solar Desalination for the 21st Century: A Review of Modern Technologies and Researches on Desalination Coupled to Renewable Energies*. Ed. by L. Rizzuti, Ettourney H.M., and A. Cipollina. Springer-Verlag Berlin, Heidelberg, 2007, pp. 215–225.
- [73] A. S. Nafey, H. E. S. Fath, S. O. El-Helaby, and A. Soliman. “Solar desalination using humidification-dehumidification processes. Part II. An experimental investigation”. In: *Energy Conversion and Management* 45 (2004), pp. 1263–1277.
- [74] A. Nafey, H. Fath, S. El-Helaby, and A. Soliman. “Solar desalination using humidification dehumidification processes. Part I. A numerical investigation”. In: *Energy Conversion and Management* 45 (2004), pp. 1243–1261.

- [75] G. P. Narayan, R. K. McGovern, J. H. Lienhard V, and S. M. Zubair. “Helium as Carrier Gas in Humidification Dehumidification Desalination Systems”. In: *Proceedings of the ASME 2011 International Mechanical Engineering Congress and Exposition IMECE, Denver, USA* (2011).
- [76] G. P. Narayan, R. K. McGovern, J. H. Lienhard V, and S. M. Zubair. “Variable pressure humidification dehumidification desalination system”. In: *Proceedings of the ASME / JSME 8th Thermal Engineering Joint Conference AJTEC, Honolulu, Hawaii, USA* (2011), pp. 1–11.
- [77] G. P. Narayan, R. K. McGovern, G. P. Thiel, J. A. Miller, J. H. Lienhard V, M. H. Sharqawy, S. M. Zubair, and M. A. Antar. “Status of humidification dehumidification desalination technology”. In: *IDA World Congress on Desalination 366* (2011).
- [78] G. P. Narayan, M. H. Sharqawy, S. Lam, S. K. Das, and J. H. Lienhard V. “Bubble columns for condensation at high concentrations of noncondensable gas: Heat-transfer model and experiments”. In: *AIChE Journal* 59 (2013), pp. 1780–1790.
- [79] G. P. Narayan, M. H. Sharqawy, J. H. Lienhard V, and S. M. Zubair. “Thermodynamic analysis of humidification dehumidification desalination cycles”. In: *Desalination and Water Treatment* 16 (2010), pp. 339–353.
- [80] G. P. Narayan, M. H. Sharqawy, E. K. Summers, J. H. Lienhard V, S. M. Zubair, and M. A. Antar. “The potential of solar-driven humidification-dehumidification desalination for small-scale decentralized water production”. In: *Renewable and Sustainable Energy Reviews* 14 (2010), pp. 1187–1201.
- [81] N. K. Nawayseh, M. M. Farid, S. Al-Hallaj, and A. R. Al-Timimi. “Solar desalination based on humidification process – I. Evaluating the heat and mass transfer coefficients”. In: *Energy Conversion Management* 40 (1999), pp. 1423–1439.
- [82] N. K. Nawayseh, M. M. Farid, A. A. Omar, and A. Sabirin. “Solar desalination based on humidification process. II computer simulation”. In: *Energy Conversion Management* 40 (1999), pp. 1441–1461.
- [83] N. K. Nawayseh, M. Farid, A. Omar, and S. Al-Hallaj. “A simulation study to improve the performance of a solar humidification-dehumidification desalination unit constructed in Jordan”. In: *Desalination* 109 (1997), pp. 277–284.
- [84] S. Parekh, M. M. Farid, J. R. Selman, and S. Al-Hallaj. “Solar desalination with humidification-dehumidification cycle – a comprehensive technical review”. In: *Desalination* 160 (2004), pp. 167–186.
- [85] W. I. Ratzel. “Kunststoffe in der Solartechnik”. In: *Proceedings 2nd International Solar Forum, Deutsche Gesellschaft für Sonnenenergie, München 1* (1978), pp. 181–193.
- [86] M. Rausch. “Grundlegende Untersuchungen zur Ursache von Tropfenkondensation an durch Ionenimplantation modifizierten Metalloberflächen”. PhD thesis. Friedrich-Alexander-Universität Erlangen-Nürnberg, 2010.

-
- [87] M. Rommel, M. Köhl, W. Graf, C. Wellens, and F. Brucker. “Corrosion-free collectors with selectively coated plastic absorbers”. In: *Desalination* 109 (1997), pp. 149–155.
- [88] T. Sattelmayer. *Technische Thermodynamik - Energielehre und Stoffverhalten*. Lehrstuhl für Thermodynamik, 2012.
- [89] E. Schmidt, W. Schurig, and W. Sellschopp. “Versuche über die Kondensation von Wasserdampf in Film-und Tropfenform”. In: *Forschung im Ingenieurwesen* (1930), pp. 53–63.
- [90] B. Seifert, A. Kroiss, M. Spinnler, and T. Sattelmayer. “About the History of Humidification-Dehumidification Desalination Systems”. In: *The IDA World Congress on Desalination and Water Reuse*. 2013.
- [91] B. Seifert, P. Schaufuss, M. Spinnler, and T. Sattelmayer. “CFD Simulation of a Humidification-Dehumidification Desalination Plant for Transient Solar Irradiation”. In: *The IDA World Congress on Desalination and Water Reuse*. 2009.
- [92] B. Seifert, M. Wenzel, R. Gobitz-Pfeiffer, M. Spinnler, and T. Sattelmayer. “CFD Simulation of a HDH-Desalination Plant for Transient Solar Irradiation”. In: *The IDA World Congress on Desalination and Water Reuse*. 2011.
- [93] S. M. Soufari, M. Zamen, and M. Amidpour. “Performance optimization of the humidification-dehumidification desalination process using mathematical programming”. In: *Desalination* 237 (2009), pp. 305–317.
- [94] M. Spinnler, J. Blumenberg, W. Moik, H. Müller-Holst, and H. U. Krispler. “Small-scale systems for solar-thermal desalination of sea and brackish water”. In: *India Narosa Publishing House, Renewable Energy Technologies* Millenium Int. Conference on Renewable Energies (2000), pp. 179–189.
- [95] S. G. Talbert, J.A. Eibling, and G.O.G. Loeff. “Manual on solar distillation of saline water”. In: *Office of Saline Water, Reseach and Development Report* Report No. 456 (1970).
- [96] G. N. Tiwari and A. K. Tiwari. *Solar Distillation Practice for Water Desalination Systems*. Anshan Pub., 2008.
- [97] R. E. Treybal. *Mass-Transfer Operations*. McGraw-Hill Book Co, 1952.
- [98] E. Tzen and R. Morris. “Renewable energy sources for desalination”. In: *Solar Energy* 75 (2003), pp. 375–379.
- [99] VDI-Gesellschaft, ed. *VDI-Wärmeatlas (German Edition)*. 10. Edition. Springer-Verlag Berlin, Heidelberg, 2006.
- [100] *Water Desalination Technologies in the ESCWA Member Countries*. United Nations, 2001.
- [101] I. Watson, O. J. Moarin, and L Henthorne. *Desalting Handbook for Planners*. 3. United States Department of the Interior, 2003, p. 310.
- [102] D. Wernicke. *Methoden und Strategien zur Beurteilung von Abnahmeversuchen an Naßkühltürmen*. Forschungsheft Nr. 367. VDI Verlag Düsseldorf, 1997.

Bibliography

- [103] C. Yamall and I. Solmus. “A solar desalination system using humidification-dehumidification process: experimental study and comparison with the theoretical results”. In: *Desalination* 220 (2008), pp. 538–551.
- [104] M. Zamen, M. Amidpour, and S. M. Soufari. “Experimental investigation of a two-stage solar humidification dehumidification desalination process”. In: *Proceedings of ECOS, Italy* (2012).

List of Figures

1.1	Schematic Setup CA-WH HD-Configuration	2
1.2	t_A -X Diagram of Humid Air for Various Relative Humidity Values	4
2.1	Proposed HD Classifications	7
2.2	Closed-Air Water-Heated HD System Overview	8
2.3	Multi-Stage Configurations of HD Systems	17
3.1	Temperature-Entropy Diagram of Pure Water	21
3.2	Film and Dropwise Condensation on Tubes	25
3.3	Dropwise Condensation in Absence of NCG	26
3.4	Contact Angle and Surface Tensions Droplet	27
3.5	Characteristic Density Profile in HD	31
4.1	Evaporation Conditions of Water and Air Flow in Humidifier . .	37
4.2	Control Volumes Humidifier	39
4.3	Control Volumes Humidification	41
4.4	Computational Chart of 1-D Model for HD	42
4.5	Example 1-D Simulation Temperature Profile Humidifier	43

4.6	Schematic Humidifier for Integral Energy Balance	44
4.7	Operating Line for Humidifier	45
4.8	Schematic Dehumidifier for Integral Energy and Mass Balance .	46
4.9	Schematic Overview Energy Transfer in HD	48
4.10	Differential Control Volume Dehumidifier at Interface	48
4.11	Heat and Mass Transfer Dehumidification	49
4.12	Film Condensation With and Withouth NCG	51
4.13	Pressure Profile in Dehumidifier (Humid Air Side)	52
4.14	Heat and Mass Transfer Surfaces Dropwise Condensation	52
4.15	Modelling of Dropwise Condensation	53
4.16	Operating Line and Tie Line for Humidifier	56
4.17	Example Tie Line 1-D Simulation	57
5.1	Photos Experimental Setups	62
5.2	Experimental Test Setup	63
5.3	Field Test Single-Stage HD System, Greece	67
5.4	Humidifier Packing (Hewitech NC20)	69
5.5	Distribution System	70
5.6	Experimental Setup Dehumidifier for Single-Stage	71
5.7	Foto of Dropwise Condensation on Plastic Tubes	75
5.8	Experimental Temperature Profiles Single-Stage	79
5.9	Experimental Temperature Profiles Two-Stage	80
5.10	Example Condensate Mass Flow	81

6.1	Overview Mass and Heat Flows in HD	84
6.2	PR_{HD} Comparison Single Stage and Two Stage HD System	88
6.3	Overview Operating Lines Single-Stage and Two-Stage	93
6.4	$h_A - t$ Diagram Single-Stage CA HD System	94
6.5	$h_A - t$ Diagram Two-Stage CA HD System	95
6.6	HTU Plot	99
6.7	$h_A - t$ Diagram Overview	101

Appendix

A Performance Ratio PR versus Gained Output Ratio GOR

The performance ratio should not be substituted with the gained output ratio GOR . Large-scale thermal desalination plants, such as multi-stage flash (MSF) or multi-effect distillation (MED), use pressurized high temperature steam (from power plants) as external heat source. The GOR characterizes the multi-effectiveness of a desalination plant as it relates the produced condensate mass flow \dot{M}_{Dist} to the amount of required heating steam mass flow \dot{M}_{Steam} :

$$GOR \equiv \frac{\dot{M}_{Dist}}{\dot{M}_{Steam}}. \quad (A.1)$$

The GOR relates masses or mass flows to express multi-effectiveness whereby the PR relates energies. Translating the mass flows into energy flows based on the stored energy in each mass flow ultimately results to an equation similar to the performance ratio. Therefore, the nominal value of GOR is similar to PR but should only be used for systems which require heating steam as external heat source.

B Experimental Equipment

Table B.1: Overview Experimental Equipment as indicated in Fig. 5.2

ID Number	Description	Specifics
01	Casing (Height x Width x Depth)	1.1 m x 0.8 m x 1.1 m
02	Humidifier	1.1 m x 0.26 m x 1.1 m
03	Dehumidifier	1.1 m x 0.54 m x 1.1 m
04	External Heater	0 ... 9 kW
05	Distribution System	> 500 holes with \varnothing 5 mm
10	Brine Tank	80 l
11	Feed Water Tank	160 l
12	Condensate Tank	80 l
20	Control Valve	
21	Pump	SHURflo (2088-313-145)
22	Electric Power Control	
23	Data Logging, Control	Vis. & Labview©
50	Brine Flow	
51	Feed Water Flow	
52	Water Flow	
53	Hot Water Flow	
54	Brine Flow	
55	Condensate Flow	
56	Feed Water	
TIR 01	Temperature in Brine Heat Recovery Tank	Type T (CuCu-Ni)
TIR 02	Temperature in Feed Water Tank	Type T (CuCu-Ni)
TIR 03	Temperature Inlet Dehumidifier	Type T (CuCu-Ni)
TIR 04	Temperature Outlet of Dehumidifier	Type T (CuCu-Ni)
TIR 06	Temperature Inlet Humidifier	Type T (CuCu-Ni)
TIR 10 - 19	Temperature of Humid Air Humidifier	at various locations
TIR 20 - 39	Temperature Water Humidifier	at various locations
TIR 50 - 79	Temperature Water Dehumidifier	various locations
TIC 01	Temperature at Valve linked to (20)	10 ... 60 °C
TIC 02	Top Brine Temperature linked to (21)	< 99 °C
MIR 01	Mass of Condensate	Kern (FKB60K2A)
FR 01	Flow of feed water	
EC 01	Electric Control of Heater	0 ... 9 kW

C Heat and Unidirectional Mass Transfer in the HD Humidifier

The molecular mass transfer (diffusion) of vapor in the air can be described with the concept of a laminar boundary layer which is adherent to the interface between water and air. For equimolar countercurrent diffusion, this phenomenon is described by the first Fick's law e.g. [33, p. 232] which defines a diffusion coefficient D for the molecular transport along the y -coordinate:

$$\dot{n}_V = -D \cdot \frac{d\tilde{\rho}_V}{dy} = -\frac{D}{\tilde{R}T} \cdot \frac{dp_V}{dy}. \quad (\text{C.1})$$

The diffusive molar mass flow density \dot{n}_V of vapor is proportional to the gradient of the partial molecular density $\tilde{\rho}_V$ of vapor within the humid air in the adherent layer which is proportional to the partial pressure p_V if the ideal gas law is valid. For evaporative diffusion, water is transported into the air phase but there is no (or only negligibly small) transport of the inert gas (air) into the water, defined as unidirectional¹ diffusion (index u) [36, p. 350 ff].

As the diffusive molecular transfer \dot{n}_G of dry air towards the interface can not enter the liquid phase (cp. Fig. 4.1), a convective compensating flow, called 'Stefan flow' is created. The convective flow transports water vapor according to the concentration ratio respectively the pressure ratio p_V/p_G . The total molar mass flux $\dot{n}_{V,u}$ for the unidirectional configuration is the sum of the diffusional part (Fick's law) and the convective part being transferred with the Stefan flow [69, p. 119, 36, p. 352]:

$$\dot{n}_{V,u} = -\frac{D}{\tilde{R} \cdot T} \cdot \frac{dp_V}{dy} - \frac{D}{\tilde{R} \cdot T} \cdot \frac{dp_V}{dy} \cdot \frac{p_V}{p_G}. \quad (\text{C.2})$$

Integrating Eq. (C.2) over the thickness of the boundary layer y_b results [69, p. 120] in

$$\dot{n}_{V,u} = \frac{D}{y_b} \cdot \frac{p}{\tilde{R}T} \cdot \ln \left(\frac{p - p_{V,\infty}}{p - p_{V,I}} \right). \quad (\text{C.3})$$

¹ German translation: 'einseitige Diffusion' [4, p. 82] or 'Diffusion an halbdurchlässiger Wand' [36, p. 350 ff].

This can be approximated from a series expansion for the logarithmic expression:

$$\dot{n}_{V,u} \approx \dot{n}_V \cdot \frac{1}{1 - p_{V,m}/p}. \quad (\text{C.4})$$

Hereby, the partial pressure $p_{V,m}$ is the arithmetic mean value of $p_{V,I}$ and $p_{V,\infty}$. For equimolar mass transfer problems, the mass transfer coefficient β is applied which is related to the concentration differences between interface and bulk air flow respectively to the partial density differences $\rho_{V,I} - \rho_{V,\infty}$ [69, p. 116] with vapor as ideal gas:

$$\dot{m}_V = \beta \cdot (\rho_{V,I} - \rho_{V,\infty}) = \beta \cdot \frac{p_{V,I} - p_{V,\infty}}{R_V \cdot T}. \quad (\text{C.5})$$

The mass transfer coefficient β corresponds to the heat transfer coefficient α in heat transfer correlations, as described in chapter C. For unidirectional transfer, the ‘Stefan flow’ increases the molar transfer of the vapor approximately with the factor $1/(1 - p_{V,m}/p)$. According to Eq. (C.4) the mass transfer coefficient for evaporation is:

$$\dot{m}_{V,u} = \beta_u \cdot \frac{p_{V,I} - p_{V,\infty}}{R_V \cdot T} \approx \beta \cdot \frac{p_{V,I} - p_{V,\infty}}{R_V \cdot T \cdot (1 - p_{V,m}/p)}. \quad (\text{C.6})$$

The analogy between heat and mass transfer is given due to the similar differential equations for heat and equimolar mass transfer, if the boundary conditions are identical. The heat transfer equation for a dependency only in y-direction can be written [36, p. 344] as

$$\dot{q} = \alpha \cdot (T_1 - T_2) = -a \cdot \frac{d(\rho \cdot h)}{dy}, \quad (\text{C.7})$$

with the heat transfer coefficient α and the thermal diffusivity $a = \lambda/(\rho \cdot c_p)$. The corresponding mass transfer equation according to first Fick’s law for equimolar countercurrent flow is

$$\dot{m} = \beta \cdot (\rho_1 - \rho_2) = -D \cdot \frac{d\rho}{dy}. \quad (\text{C.8})$$

C.1 Dimensionless Numbers

Results from studies and experiments on heat or mass transfer can be described using dimensionless numbers, the Nusselt number Nu for heat transfer and the Sherwood number Sh for mass transfer [4, p. 94 and p. 370 ff.]:

$$Nu \equiv \frac{\alpha \cdot L}{\lambda}, \quad (\text{C.9})$$

$$Sh \equiv \frac{\beta \cdot L}{D}. \quad (\text{C.10})$$

The dimensionless numbers Nu and Sh are preferably described as power functions, valid for the relevant configurations. These power functions of the Reynolds number Re , Schmidt number Sc and Prandtl number Pr can then be transformed from the heat to a mass transfer problem or vice versa². The functions are consequently of identical form.

Therefore, from the analogy between heat and mass transfer, formulas for α/β are derived which are again a power function in the form of [69, p. 128, 36, p. 347]

$$\frac{\alpha}{\beta} = \frac{\lambda}{D} \cdot \left(\frac{D}{a}\right)^n. \quad (\text{C.11})$$

The Lewis number Le is the ratio between the thermal diffusivity coefficient a and the molecular diffusivity D .

$$Le \equiv \frac{a}{D} = \frac{\lambda}{\rho \cdot c_p \cdot D} = \frac{Sc}{Pr}. \quad (\text{C.12})$$

Kloppers [59] investigated the Lewis numbers for wet cooling towers and suggested the use of consistent values of Lewis numbers instead of general simplifications³. The Lewis number for the diffusion of water vapor in air is 0.87 for 0 °C [4, p. 95]. This value corresponds to the rounded values given by Grigull [36, p. 417] for temperatures between 0 to 100 °C for high dilutions. The so called ‘Lewis Relation’ describes the case for $Le = 1$, i.e., $a = D$, and gives an

² Grigull [36, p. 349] points out the limits of these correlations. Especially for unidirectional flows, the mass transfer problems can not be directly applied for the heat transfer problems. He derives a more accurate relation for β_u . The given approximation of this relation is used in Eq. (C.6).

³ For standard cooling tower configurations, Le is mostly set to 1 with adequate precision.

indication of the ratio between heat and mass transfer [69, p. 128]:

$$\beta = \frac{\alpha}{\rho \cdot c_p}. \quad (\text{C.13})$$

This transformation leads to the mass transfer coefficient β for the for the equimolar mass transfer. For unidirectional mass transfer, as it is the case for humidification and dehumidification, the correction factor needs to be included according to Eq. (C.6).

C.2 Lewis Factor $Le_{f,u}$ for Unidirectional Transport

The numerical calculations can be simplified by combining the relations for heat and mass transfer. The Lewis Factor Le_f is applicable for this calculation as it relates the heat and mass transfer can be derived from Eq. (C.11) [69, p. 128]:

$$Le_f = \frac{\alpha}{\beta \cdot \rho \cdot c_p} = Le^{1-n}. \quad (\text{C.14})$$

For evaporation processes, Lewis Factor Le_f is calculated according to the correlations for the unidirectional flow using the correlation for β_u according to Eq. (C.6):

$$Le_{f,u} = \frac{\alpha}{\beta_u \cdot \rho \cdot c_p} = Le^{1-n} \cdot \left(1 - \frac{p_{V,m}}{p}\right)^{-1}. \quad (\text{C.15})$$

A common definition of the Lewis Factor $Le_{f,u}$ for unidirectional mass transfer uses the evaporation coefficient σ_{evap} instead of β_u . Hauenschild [41] gives the relation between σ_{evap} and β_u . The mass transfer rate \dot{m}_V is proportional to β_u and also to the partial density difference of water vapor in humid air $\Delta\rho_V$ and to σ_{evap} and ΔX ,

$$\sigma_{\text{evap}} = \beta_u \cdot \frac{p}{R_G \cdot T_m} \cdot \left(1 - \frac{p_{V,m}}{p}\right). \quad (\text{C.16})$$

with the mean temperature of humid air T_m , the arithmetic mean of the water and air temperature. The conversion of β_u to σ_{evap} is shown in Annex C.3. The unidirectional Lewis Factor $Le_{f,u}$ can be expressed as:

$$Le_{f,u} = \frac{\alpha}{\sigma_{\text{evap}} \cdot c_p} \cdot \left(1 - \frac{p_{V,m}}{p}\right). \quad (\text{C.17})$$

The Lewis Factor $Le_{f,u}$ is used for the derivation of the temperature t_I of the interface I, as shown in Eq. (4.15).

C.3 Correlations for β , β_u and σ_{evap}

As discussed in chapter C.2, the unidirectional Lewis Factor $Le_{f,u}$ can be expressed with the unidirectional mass transfer coefficient β_u or the evaporation coefficient σ_{evap} . Eq. (C.16) expresses σ_{evap} as a function of β_u and can be derived as follows:

$$\dot{m}_V = \beta_u \cdot \left(\frac{1}{R_W \cdot T_m} \right) \cdot (p_{V,I} - p_{V,\infty}). \quad (\text{C.18})$$

$$\dot{m}_V = \sigma_{\text{evap}} \cdot (X_I - X_\infty) = \sigma_{\text{evap}} \cdot \frac{\tilde{M}_W}{\tilde{M}_G} \cdot \left(\frac{p_{V,I}}{p - p_{V,I}} - \frac{p_{V,\infty}}{p - p_{V,\infty}} \right). \quad (\text{C.19})$$

$$\sigma_{\text{evap}} = \left[\beta_u \cdot \frac{1}{R_W \cdot T_m} \cdot \frac{R_W}{R_G} \right] \cdot \frac{(p_{V,I} - p_{V,\infty}) \cdot (p - p_{V,I}) \cdot (p - p_{V,\infty})}{p_{V,I} \cdot (p - p_{V,\infty}) - p_{V,\infty} \cdot (p - p_{V,I})}. \quad (\text{C.20})$$

$$\sigma_{\text{evap}} = \beta_u \cdot \frac{p}{R_G \cdot T_m} \cdot \left(1 - \frac{p_{V,I}}{p} \right) \cdot \left(1 - \frac{p_{V,\infty}}{p} \right). \quad (\text{C.21})$$

$$\text{with } T_m = 0.5 \cdot (T_I - T_\infty) \quad \text{and} \quad \frac{R_G}{R_W} = \frac{\tilde{M}_W}{\tilde{M}_G} = 0.622. \quad (\text{C.22})$$

The unidirectional mass transfer coefficient β_u can be expressed with the mass transfer coefficient β for equimolar mass flow and a correction factor. This coefficient β can be determined from analogies between heat, mass and momentum transfer [36, p. 350 ff.]⁴:

$$\beta = \frac{\beta_u}{p} \cdot \frac{p_{V,I} - p_{V,\infty}}{\ln \frac{p - p_{V,\infty}}{p - p_{V,I}}} = \frac{\beta_u}{p} \cdot \frac{p_{G,\infty} - p_{G,I}}{\ln \frac{p_{G,\infty}}{p_{G,I}}}. \quad (\text{C.23})$$

The logarithmic mean partial pressure of the carrier gas \dot{G} between interface I and the bulk (index ∞) flow can be approximated for small pressure differences to $p_{V,I}$ [36, p. 354 ff.] leading to a simplified relation for the (unidirec-

⁴ Grigull [36] labels β_h as the mass transfer coefficient for unidirectional diffusion at the semipermeable wall.

tional) evaporation coefficient σ_{evap} :

$$\beta \approx \beta_u \cdot \frac{p_{G,I}}{p} = \beta_u \cdot \left(1 - \frac{p_{V,I}}{p}\right). \quad (\text{C.24})$$

$$\sigma_{\text{evap}} \approx \beta \cdot \frac{p}{R_G \cdot T_m} \cdot \left(1 - \frac{p_{V,\infty}}{p}\right). \quad (\text{C.25})$$

The controlling mass transfer coefficient β_h and the Lewis Factor Le_f were previously introduced.

Due to the difference between the temperature of the bulk water flow \dot{L} and its interface (index I) in the humidifier, heat is transferred from the water to the interface, which can be described principally as convective heat transfer [6]:

$$\dot{Q}_{\text{conv,W}} = \alpha_W \cdot (T_{W,\infty} - T_I) \cdot A_\alpha. \quad (\text{C.26})$$

In the gaseous phase, heat is transferred from the interface to the bulk air flow:

$$\dot{Q}_{\text{conv,A}} = \alpha_A \cdot (T_I - T_{A,\infty}) \cdot A_\alpha. \quad (\text{C.27})$$